GEOMORPHOLOGY AND GEOCHRONOLOGY OF SAND RAMPS ADJOINING THE CORAL PINK SAND DUNES, KANE COUNTY, UTAH

by

Kerri E. Spuller

A thesis

submitted in partial fulfillment

of the requirements for the degree of

Master of Science in Geoscience

Boise State University

December 2019

BOISE STATE UNIVERSITY GRADUATE COLLEGE

DEFENSE COMMITTEE AND FINAL READING APPROVALS

of the thesis submitted by

Kerri E. Spuller

Thesis Title: Geomorphology and Geochronology of Sand Ramps Adjoining the Coral Pink Sand Dunes, Kane County, Utah

Date of Final Oral Examination: 06 November 2019

The following individuals read and discussed the thesis submitted by student Kerri E. Spuller, and they evaluated the student's presentation and response to questions during the final oral examination. They found that the student passed the final oral examination.

David Wilkins, Ph.D.	Chair, Supervisory Committee
Jennifer Pierce, Ph.D.	Member, Supervisory Committee
Tammy Rittenour, Ph.D.	Member, Supervisory Committee
Richard L. Ford, Ph.D.	Member, Supervisory Committee

The final reading approval of the thesis was granted by David Wilkins, Ph.D., Chair of the Supervisory Committee. The thesis was approved by the Graduate College.

ACKNOWLEDGEMENTS

I would like to thank my advisor, Dr. David Wilkins, and committee members, Dr. Jennifer Pierce, Dr. Tammy Rittenour, and Dr. Richard L. Ford, for their support and enthusiasm throughout this research; the Utah State University Luminescence Laboratory for the use of their lab, in particular Dr. Tammy Rittenour (Lab Director), Michelle Summa-Nelson (Lab Manager), and Carlie Ideker (Assistant Lab Manager) for their OSL help and guidance; and the Coral Pink Sand Dunes State Park for access to the study site.

ABSTRACT

Projected climate change is expected to have widespread impacts on arid regions of the world. Inland, continental dune fields are sensitive to changes in climate and the surrounding environment and are an important source for understanding interactions between Earth's surface, atmosphere, and biosphere in drylands. Reconstructing past periods of aeolian activity from dune fields can provide insights into how landscapes have responded to previous changes in climate. However, the nature of aeolian systems to recycle older deposits leads to a preservation bias towards only the youngest deposits. Targeting geomorphic settings that are conducive to preserving older records is critical to reconstructing longer and more complete records of landscape change.

This MS thesis is divided into three chapters. Chapter One describes the geomorphology and geochronology of sand ramps adjacent to the lower dune field in the Coral Pink Sand Dunes, Utah. Chapter Two is written as a manuscript to be submitted as a Brief Research Report to Frontiers in Earth Science - Quaternary Science, Geomorphology and Paleoenvironment Section. Chapter Two discusses the results of the first chapter in the context of regional paleoclimate and geomorphic records to identify drivers of aeolian activity. Chapter Three is a summary of major findings and discusses suggestions for future work.

Chapter One investigates sand ramps in the Coral Pink Sand Dunes (CPSD), Utah, a fault-bound dune field located on the northwestern Colorado Plateau. Sand ramps are topographically-controlled features composed of alluvial, fluvial, and aeolian

sediments, and therefore have the potential to store long records of past landscape change. Sand ramp stratigraphy is described in the CPSD from natural exposures where ephemeral streams have incised through the sand ramps. Deposits are characterized as either aeolian, fluvial, or alluvial based on grain size, sorting, and primary bedding structures. Five aeolian units were sampled and analyzed using optically stimulated luminescence (OSL) to constrain timing of aeolian activity. Luminescence dating estimates the last time sediment was exposed to sunlight, providing a way to date past periods of aeolian activity. Stratigraphic positions of dated aeolian deposits are used to reconstruct the geomorphic history of the sand ramps. Results show that the CPSD sand ramps formed during the end of the last glacial (MIS 6) through MIS 5d/e (OSL ~149 ka to OSL ~114 ka) until at least the late Pleistocene-Holocene transition (OSL ~12.5 ka), filling the accommodation space at the base of the Sevier Normal Fault scarp. CPSD dune geochemistry is distinct from nearby dune fields, indicating that aeolian sediments are sourced locally, rather than transported long distances.

Chapter 2 compares the CPSD aeolian chronology to other regional dune chronologies, geomorphic records, and paleoclimate reconstructions to identify possible climatic and environmental controls on aeolian activity. Topographic and structural (i.e., fault scarp) controls present in the CPSD sand ramp system have preserved the first evidence of aeolian activity during Marine Isotope Stages (MIS) 6 on the Colorado Plateau. Aeolian activity during the late Pleistocene-Holocene transition (MIS2/1; ~12.5 ka) occurred under conditions that were relatively wetter and cooler than present. Dune activity during the MIS 6 and MIS 5 (~149 to ~114 ka) spans a range of climate conditions during a period of rapid and abrupt change. Rather than a response to any

specific climate regime, the late Pleistocene aeolian chronology may instead record changes in sediment supply under variable climate conditions.

TABLE OF CONTENTS

LIST OF TABLES

LIST OF FIGURES

LIST OF ABBREVIATIONS

BLM	Bureau of Land Management
CPSD	Coral Pink Sand Dunes
D_E	equivalent dose
D_R	environmental dose rate
ICP-AES	inductively coupled plasma atomic emission spectroscopy
ICP-MS	inductively coupled plasma mass spectrometry
ISB	Intermountain Seismic Belt
MASL	meters above sea level
MIS	Marine Isotope Stage
OSL	optically stimulated luminescence
REE	rare earth elements
USULL	Utah State University Luminescence Laboratory

CHAPTER ONE: SAND RAMP GEOMORPHOLOGY AND GEOCHRONOLOGY

1.1 Introduction

1.1.1 Importance of Work

Drylands currently cover approximately 45% of the Earth's land surface (Prăvălie, 2016) and are expected to expand under projected climate change (Huang, Yu, Guan, Xu, & Oldfield, 2016). Inland, continental dune fields are sensitive to change and are therefore an important source for understanding interactions between Earth's surface, atmosphere, hydrosphere, and biosphere in drylands (Lancaster, 2008; Ewing & Kocurek, 2010). Dune activity is driven by sediment supply, wind transport capacity, and the availability of sediment, which is controlled by surface conditions such as effective moisture and vegetation cover (Kocurek & Lancaster, 1999). Each of these factors are influenced by global and regional climate, as well as local geologic and hydrologic conditions. Because of this complex relationship, climatic controls on aeolian processes are not well constrained. More work is needed to understand how climate change, both now and in the past, influences these vulnerable landscapes.

Reconstructing spatial and temporal patterns of past phases of dune activity can be used to identify thresholds, frequency, and magnitude of erosion, which can provide insights into the climatic, environmental, and geomorphic drivers of aeolian activity (Singhvi & Porat, 2008). Luminescence dating estimates the last time sediment was exposed to sunlight (Huntley, Godfrey-Smith, & Thewalt, 1985), providing a way to date

past periods of aeolian activity (Duller, 2008). By directly dating mineral grains, luminescence dating is particularly useful in drylands where organic material for radiocarbon dating is rarely preserved (Thomas & Burrough, 2012). Recent advances in optically stimulated luminescence (OSL) dating techniques have improved the accuracy and resolution of geomorphic records (e.g., Murray & Wintle, 2000), increasing the availability of field data from drylands around the world (Lancaster et al., 2016). Global and regional dune chronologies can identify paleowind directions and atmospheric circulation patterns, validate earth system and paleoclimate models (Pelletier et al., 2015), and help to identify drivers of activity (e.g., Mayer & Mahan, 2004; Chase & Thomas, 2006).

Despite their importance in understanding landscape response to climate change, dunes and other types of aeolian features are particularly prone to preservation bias toward younger deposits (Lancaster et al., 2016). While many aeolian features, such as migrating dunes and sand sheets, have low preservation potential, sand ramps are protected by topography and therefore have the potential to preserve longer records of aeolian activity (e.g., Kumar, Srivastava, & Meena, 2017). Sand ramps are depositional features composed of hillslope, aeolian, and fluvial sediments that accumulate at the base of topographic features (Lancaster & Tchakerian, 1996). Sand ramps form where there is adequate accommodation space, a viable aeolian sediment source upwind, and gravity-driven hillslope or fluvial deposition, and therefore exist on the spectrum between purely aeolian features (e.g., climbing or falling dunes) and purely hillslope features (e.g., colluvium and alluvial fans) (Rowell, Thomas, Bailey, & Holmes, 2018). Sand ramps are common features in the deserts of the southwestern United States (e.g., Lancaster &

Tchakerian, 1996; Bateman, Bryant, Foster, Livingstone, & Parsons, 2012) and in drylands around the world (e.g., Bertram, 2003; Telfer, Mills, & Mather, 2014). Targeting geomorphic settings that are conducive to preserving older records is important for reconstructing longer and more complete records of landscape change.

1.1.1.1. Sand ramps adjoining the Coral Pink Sand Dunes, Utah

This study investigates sand ramps in the Coral Pink Sand Dunes (CPSD) State Park, Kane County, Utah. The CPSD is composed of two distinct dune fields separated by the steeply dipping Sevier Normal Fault (Sevier fault) (Hayden, 2013). The sand ramps are situated along the base of the Sevier fault scarp in the lower dune field (Figure 1.1). Except for basic surficial mapping at a 1:24,000 scale (Hayden, 2013), the stratigraphy, age, and characteristics of the sand ramp system were not yet previously investigated. The CPSD sand ramps are considered relict features because their surfaces are stabilized and vegetated, they are actively being incised by fluvial activity, and they are no longer accreting aeolian or hillslope sediment. In this study, we investigate why these relict sand ramps situated adjacent to an active dune field and what information about past landscape change is stored within these features.

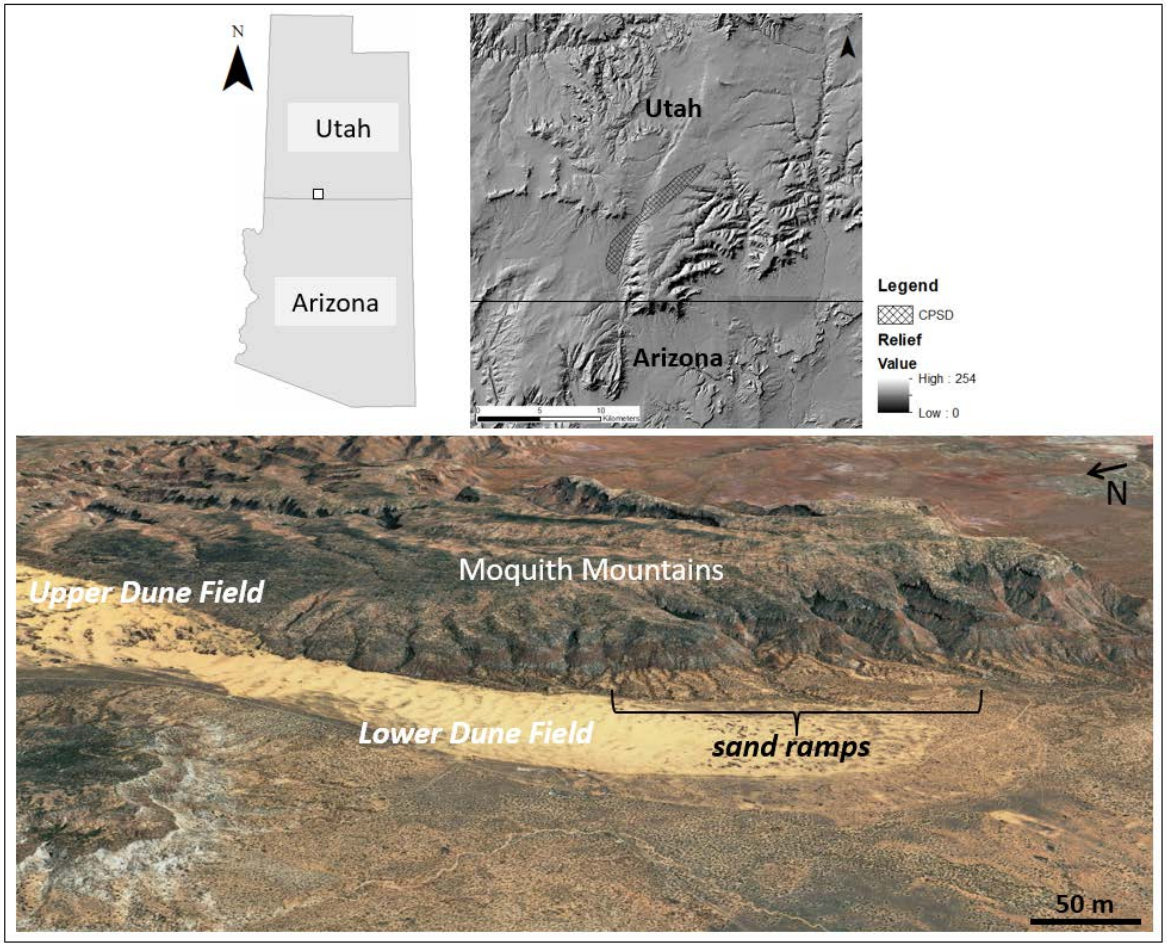

Figure 1.1 View looking east across the Coral Pink Sand Dunes at the sand ramps along the base of the Moquith Mountains. The sand ramps are the focus of this study because of their potential to store long records of aeolian activity. Image Source: Google Earth.

1.1.2. Previous Work

1.1.2.1 Coral Pink Sand Dunes

The Coral Pink Sand Dunes were first described by Gregory during his field expeditions in the 1930s (Gregory, 1950) and the CPSD have since been an active area of research for dune geomorphology (e.g., Wilkins, Ford, Clement, & Nicoll, 2005; Wilkins & Ford, 2007; Ford, Gillman, Wilkins, Clement, & Nicoll, 2010; Rozar, 2015) and ecology (e.g., Bowers, 1984; Knisley & Hill, 2001; Gowan & Knisley, 2014). Previous work shows that the CPSD dunes have responded to changes in climate and effective moisture, which affects vegetation cover and sediment availability. OSL work in the active region of the lower dune field has identified at least three distinct phases of aeolian activity starting around 4 ka that correspond to periods of regional drought (Wilkins, Ford, Clement, & Nicoll, 2007) and also generally coincide with activity in dune fields across the Colorado Plateau in New Mexico (Chaco Dune Field; Wells, McFadden, & Schultz, 1990), Arizona (Tusayan Dunes; Stokes & Breed, 1993), and Colorado (Great Sand Dunes; Forman et al., 2006). The CPSD dunes stabilized with the onset of relatively cooler and wetter conditions during the Little Ice Age (Wilkins, Ford, Clement, & Nicoll, 2005). Tree rings from ponderosa pines in the southern dune field record wet and dry cycles over the past 200 years since the end of the Little Ice Age, including short-term, but severe droughts in the late 19th century, 1930s, and 1950s that correspond to dry conditions across the southwestern United States (Wilkins, Ford, Clement, & Nicoll, 2007). Gregory (1950) noted a high degree of activity in the southern dune field during his 1937 fieldwork and observed aeolian sediment entering the dune fields from the southwest. Wilkins & Ford's (2007) nearest neighbor analysis of dune crest spacing over

time from repeat aerial photography shows that the northern section of the lower dune field is more clustered compared to the southern section. This difference is attributed to influxes of sediment during drought conditions from 1931 to 1961 that have since been working through the system, redistributing the sediment across the dune field (Wilkins & Ford, 2007).

1.1.2.2 Dune Activity on the Colorado Plateau

In recent decades, stabilized sand sheets and dunes on the Colorado Plateau have been reactivated in response to multi-decadal drought (Draut, Redsteer, & Amoroso, 2012) and increased wind power (Bogle, Redsteer, & Vogel, 2015). The Colorado Plateau physiographic province is located in the dry interior of the southwestern United States; low effective moisture, strong winds, and variable climate limit perennial vegetation cover, making its landscapes highly susceptible to wind erosion (Redsteer, Bogle, & Vogel, 2011). Projections for the southwestern United States predict drier and more variable conditions (Kerr, 2008). Under projected conditions, dune fields in this region are expected to continue to remobilize (Munson, Belnap, & Okin, 2011). While direct observations of modern dune mobility captures responses to short-term climate variability on annual to decadal time scales, reconstructing past phases of dune activity can help to quantify the magnitude, frequency, and thresholds of activity and therefore help to illuminate the role wind plays in shaping these landscapes.

Aeolian landforms on the Colorado Plateau were first described by Hack (1941) who recognized that different dune morphologies result from specific wind regime, vegetation cover, and sediment supply conditions. Dune chronologies have been developed for several dune fields on the Colorado Plateau, although there has been

relatively little work in this region compared to other regions of North America (Halfen, Lancaster, & Wolfe, 2016). Chaco Dune Field, in northwestern New Mexico, was active from 16 to 12 ka and experienced several phases of reactivation throughout the mid to late Holocene (Wells, McFadden, & Schultz, 1990). Reactivation of previously stabilized dunes during the late Holocene has also been recorded in northern Arizona (Stokes & Breed, 1993; Ellwein, Mahan, &, McFadden, 2015) and southern Utah (Reheis et al., 2005; Wilkins, Ford, Clement, & Nicoll, 2005).

Topographically-controlled dune deposits have preserved a much different record of activity in this region compared to chronologies derived solely from active sand sheets and dune fields. Sand ramps and falling dunes on the Black Mesa were formed primarily before the end of the last glacial from 30 to 16 ka (Ellwein, Mahan, &, McFadden, 2015). While migrating dune forms and sand sheets record phases of dune reactivation, topographically-controlled aeolian deposits are not prone to reactivation and therefore preserve a record of initial sand emplacement. Unlike the late Holocene record, late Pleistocene dune activity occurred under relatively cool and wet glacial climates (Reheis et al., 2005; Ellwein, Mahan, &, McFadden, 2015). Currently, pre-Holocene records of dune activity on the Colorado Plateau are sparse in the literature, demanding more work to define the spatial and temporal distribution of Pleistocene aeolian deposits across the Colorado Plateau (Halfen, Lancaster, & Wolfe, 2016).

1.1.3 Research Questions

The CPSD have responded rapidly to changes in temperature and effective moisture throughout the late Holocene and historic times (Wilkins, Ford, Clement, & Nicoll, 2005; 2007). While OSL ages of shallow aeolian exposures in the active core of the dune field extends to about 4 ka, the topographically-controlled sand ramps have the potential to preserve a longer record of aeolian activity. We investigate aeolian deposits preserved in topographically-controlled sand ramps in the CPSD to answer the following questions:

1) When were the Coral Pink Sand Dunes sand ramps active in the past? When did they become dissected from the main dune field?

2) Is the aeolian sand source local or far-traveled? Has the source changed over time?

3) What can the sand ramps tell us about past landscape change on local (i.e., within the CPSD system) and regional (i.e., in the context of the Colorado Plateau and southwestern deserts) scales?

Sand ramp stratigraphy is described from natural exposures in fluvial channels incised through the features. Deposit types are classified according to grain size, bedding, and primary structures. Aeolian deposits preserved within the sand ramps are dated with optically stimulated luminescence (OSL) for age control on past periods of aeolian activity. We investigate relationships between deposit age and geomorphic setting to define physical characteristics of the sand ramps and to develop a conceptual model for the CPSD sand ramp development to determine how these features formed and when they became dissected from the main dune field. Rare and trace element concentrations are used to identify possible changes in sediment source over time rom. The CPSD aeolian

chronology is compared to other dune chronologies, geomorphic records, and paleoclimate proxies from the Colorado Plateau to identify climatic and environmental drivers of activity.

1.2 Study Area

1.2.1 Geographic Location and Physical Setting

The Coral Pink Sand Dunes (CPSD) are located approximately 15 kilometers west of the City of Kanab, Utah near the Utah-Arizona border on the northern Colorado Plateau (Figure 1.2). The dune field is approximately 14 km^2, averaging about 13 km on its long axis and about 1.1 km wide. The dune field trends northeast to southwest and is divided into two separate (upper and lower) regions where the Sevier fault crosses the dune field. The lower dune field exists within Sand Canyon and is bounded on the eastern side by the 50 to 180-meter-tall, steeply dipping Sevier fault scarp. The upper dune field starts where climbing dunes migrate northeast over the Sevier fault scarp. The lower dune field is located within CPSD State Park and the upper dune field is managed by the Bureau of Land Management (BLM). The dune field ranges in elevation from 1,700 to 2,000 meters above sea level (MASL), and the highest elevation of the adjacent Moquith Mountains to the east extend to 2100 MASL. The entire study area is located within the Utah Geological Survey Yellowjacket Canyon Quadrangle, Kane County, Utah and Mohave County, Arizona (Hayden, 2013).

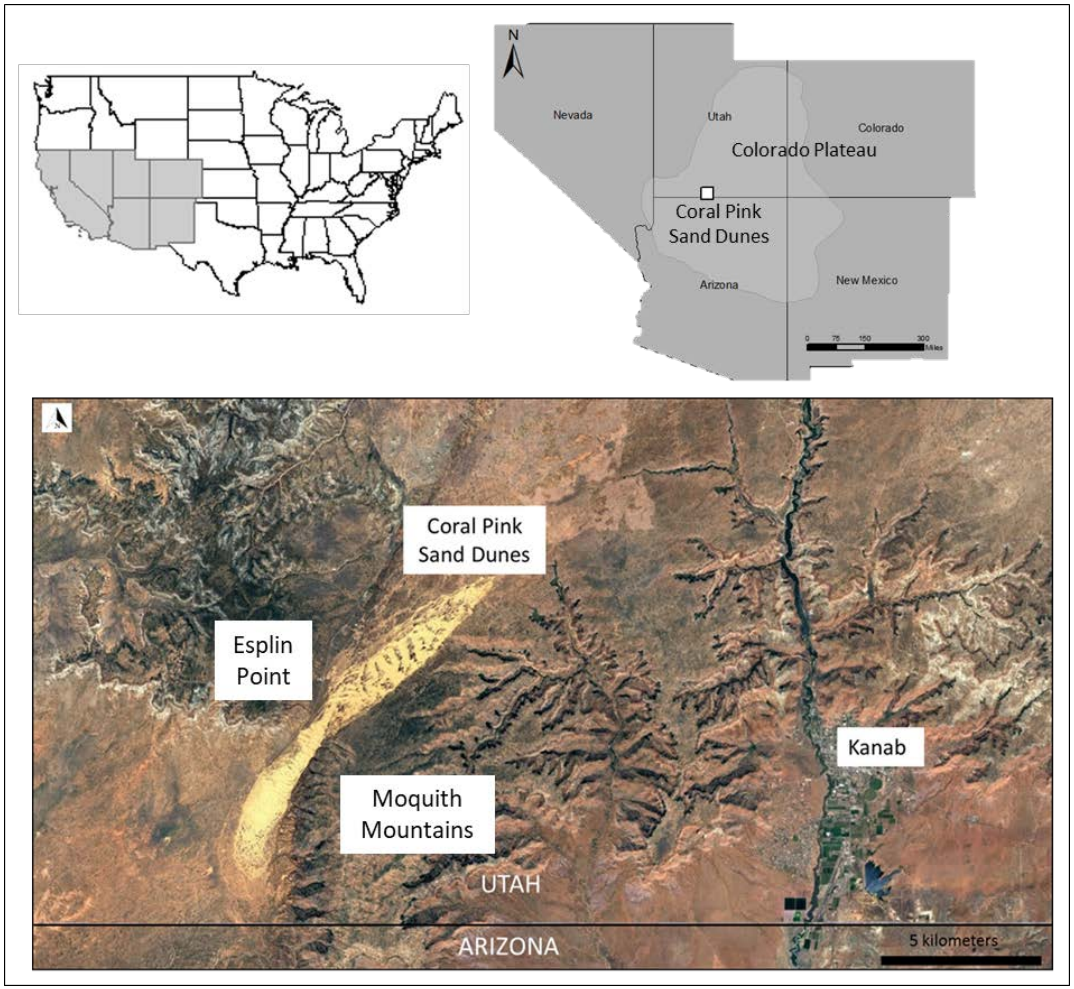

Figure 1.2 The Coral Pink Sand Dunes are located in Kane County, Utah, on the western Colorado Plateau, approximately 15 kilometers west of the City of Kanab, Utah. The CPSD trend northeast-southwest within Sand Canyon, between the Moquith Mountains and the White Cliffs.

1.2.2 Geology

1.2.2.1 Bedrock geology

The CPSD are located on the Vermillion Cliffs section of the Grand Staircase. Bedrock is mainly Mesozoic sedimentary rocks, primarily the Jurassic sedimentary units of the Glen Canyon Group overlying Triassic formations, influenced by Cenozoic uplift and faulting. The largest bedrock exposure in the dune field is Navajo sandstone, a high-angle cross-bedded aeolianite interbedded with lenses of limestone and dolostone. Varying levels of carbonate cementation result in three unique members with different erodibilities; the Lower and Upper members are both cliff-forming units and are more resistant than the Middle, slope-forming member (Hayden, 2013). The lower Navajo sandstone unit caps the Moquith Mountains to the east, and the upper unit makes up the bedrock beneath the dune field and the base of Esplin Point to the west. Esplin Point is capped by Temple Cap Sandstone and Co-op Creek limestone; this sandstone to limestone sequence represents the transition from an inland sand erg to a shallow marine depositional environment during the Jurassic epoch (Hayden, 2013). Cenozoic volcanic cones and large basalt flows are scattered across Kane County, but are not present in the CPSD.

1.2.2.2 Structural Setting

CPSD is located in the structural transition zone between the Great Basin and the Colorado Plateau structural provinces. The Colorado Plateau structural province is characterized by thick, sedimentary bedrock that was uplifted during the early Cenozoic with little deformation (Dumitru, Duddy, & Green, 1994). Aside from localized zones of contraction and plutonism, the Colorado Plateau has been relatively inactive since the

Cenozoic uplift compared to the adjacent Great Basin Province (Rowley, Anderson, Williams, & Fleck, 1978). The Great Basin structural province is characterized by surface expression of fault block tectonism from repeated periods of extension and contraction, and current extension in the Great Basin has been occurring since the Early Miocene (Parsons, 1995). The 100-kilometer-wide transition zone displays characteristics of both structural provinces, including heat flow properties, upper mantle velocities, and surface expression of fault block tectonism similar to the eastern Basin and Range, as well as the thick, uplifted sedimentary bedrock of the Colorado Plateau (Wannamaker et al., 2001). The Sevier Normal Fault, part of the Sevier /Toroweap fault system, exhibits typical basin and range extensional faulting. The Sevier fault divides the CPSD into two distinct upper and lower fields (Figure 1.3). Within the lower dune field, the main fault strikes at about N30°E and dips 75°W, and is composed of braided fault segments (Hayden, 2013). The eastern edge of the southern dune field is bounded by the 50 to 180 meter west-facing faultline scarp, and the upthrown block forms the flattop block mesas of the Moquith Mountains to the east. Total offset from the top of the Moquith Mountains to the lower dune field is about 475 meters (Anderson & Christenson, 1989). The Lower Dune Field exists within a structurally controlled graben bound by a series of shallow, east-dipping antithetic faults running parallel to the main fault (Rozar, 2015).

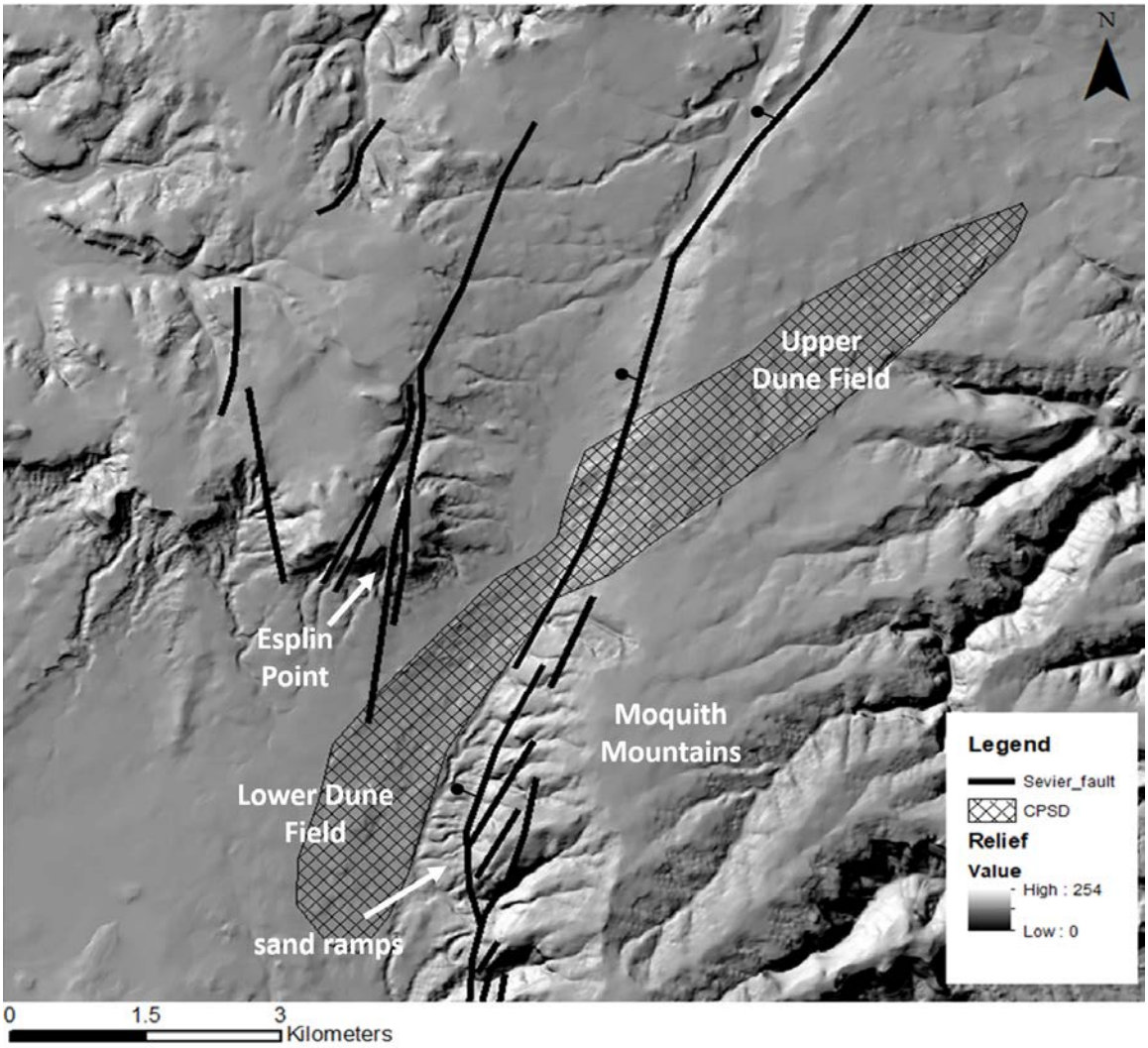

Figure 1.3 The Sevier fault runs through the CPSD, dividing the dune field into two separate dune fields. The upper dune field sits on the upthrown block. The lower dune field is housed within a graben, bound by the Sevier fault scarp on the east and smaller, antithetic faults to the west.

1.2.2.2.1 Sevier Normal Fault activity

The Sevier fault is part of the Intermountain Seismic Belt (ISB), a zone of seismicity that extends from southern Nevada to northwest Montana. The southern portion of the ISB is characterized by typically low magnitude earthquakes (<4 magnitude), however, several large events in this region were recorded in the 1900s. One of the largest recorded events on the Colorado Plateau was the Kanab-Fredonia earthquake in 1957, which was a magnitude 5.7. Historically no events have resulted in

surface ruptures, but earthquake activity suggests that the Sevier fault is still experiencing extensional strain (Brumbaugh, 2008).

In the region of the CPSD, current fault activity has likely transitioned away from the large surface-rupturing events that formed the fault block landscape features to local aseismic fault creep (Anderson & Christenson, 1989). Surficial deposits within the CPSD do not exhibit offset, but some structural features are suggestive of Quaternary deformation. The fault scarp along the Moquith Mountains abruptly changes in character from the rounded upper slope to the lower cliff-forming section, forming several steps in the profile. Anderson & Christenson (1989) hypothesize that these steps were created by Pleistocene movement, rather than by differential erosion. Also Clay Flat, a small (~1 km^2) closed depositional basin, has formed where there is a large (2.5 kilometer) left en-echelon step in the fault a few kilometers north of the dune field (Figure 1.4). Recent fault movement and subsidence are most likely necessary to sustain this localized depositional basin (Anderson & Christenson, 1989). Hazard assessments estimate the lower section of the Sevier fault has a slip rate of 0.1 mm/year (Lund, Knudsen, & Vice, 2008) and surface rupturing events have an estimated minimum recurrence interval of 30,000 years (Hayden, 2013). Low-magnitude earthquake activity, the stepped scarp profile, and the existence of Clay Flat suggest that the Sevier fault is active in the CPSD region.

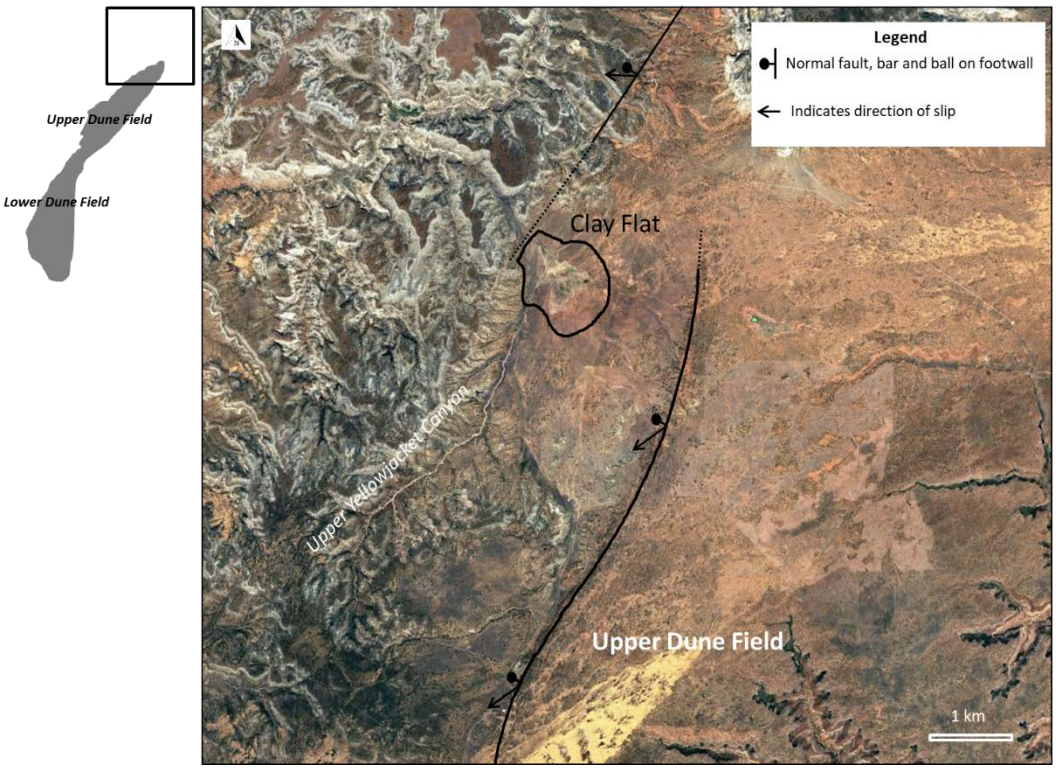

Figure. 1.4 Upper Yellowjacket Canyon drains into Clay Flat, a deposition pull-apart basin created by a left en echelon step in the Sevier fault about 5 kilometers north of the CPSD. Figure adapted from Lund, Knudsen, & Vice, 2008.

1.2.2.3 Dune field geomorphology and surficial deposits

Extensive Quaternary surficial units mantle the Mesozoic bedrock throughout the region, including aeolian sand sheets and dunes, fluvial, and alluvial deposits. Surficial aeolian dune deposits are mapped into seven units based on morphology (Figure 1.5) (Ford, Gillman, Wilkins, Clement, & Nicoll, 2010; Hayden, 2013).

The upper dune field sits on the up-thrown block of the Sevier fault. Dune sediments are sourced from the lower dune field from climbing dunes (Qedc) that transport sand over the fault scarp. The majority of the dune field is composed of large parabolic dunes (Qedp) that migrate to the northeast over shallow Navajo sandstone bedrock, and bedrock is exposed in interdune areas. The western margin is covered in partially stabilized sand sheets (Qeds).

The lower dune field trends northeast-southwest within the fault-bounded Sand Canyon and is a depositional sink for both external and locally-derived aeolian, alluvial, and fluvial sediments. The dune field transitions from stabilized sand sheets (Qess) at its southern extent to partially stabilized sands (Qeds) and eventually into a series of migrating dune forms (Qedt) in its active core. There are large ponderosa pine trees that grow in the partially stabilized sand sheets in between the stabilized sand sheets and active dunes. The active core of the dune field is dominated by transverse ridges and barchanoid ridges, two types transverse dunes that form asymmetric ridges positioned perpendicular to prevailing winds and migrate to the northeast. Barchanoid ridges on the eastern margin migrate into the bedrock cliffs of the Moquith Mountains and form echo dunes. Smaller parabolic dunes (Qedpm) cover the western margin of the field. Sand ramps (Qes), the focus of this study, are found along the eastern margin of the dune field.

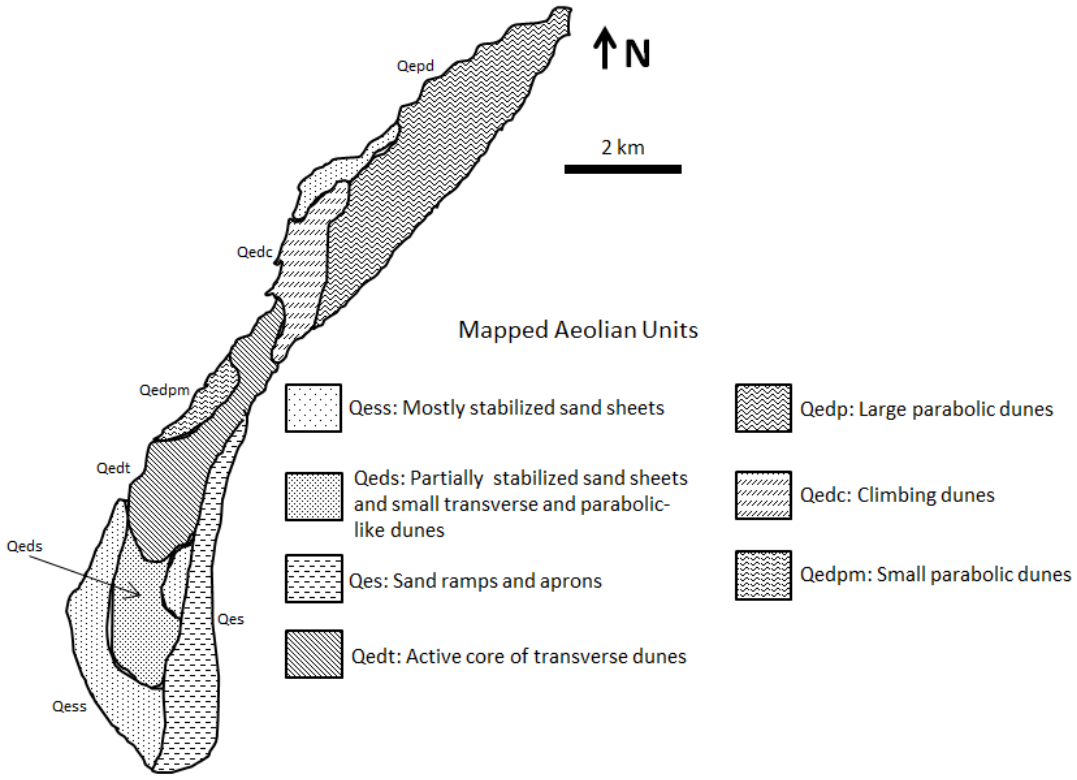

Figure 1.5 CPSD surficial dune and sand sheet deposits are mapped into seven distinct morphologies (Ford et al. 2010; Hayden, 2013). Sections of the southern, southwestern, and eastern edge of the lower dune are covered in sand sheets (0-15 meters thick) stabilized by a shallow water table, scrubs, and grasses (Qess). The south central region of the lower dune field is covered in partially stabilized sand sheets and small transvers and parabolic-like dunes and vegetated with large ponderosa pine trees (Qeds). The majority if the central region of the lower dune field is covered in active transverse dunes and ridges and barchanoid ridges (Qedt). A small section along the northwestern margin of the lower dune field is covered in small, vegetated parabolic dunes (Qedpm). The eastern margin along the base of the Sevier fault scarp is covered in sand aprons and ramps (Qes). Climbing dunes transport sand from the lower dune field, over the Sevier fault scarp and into the upper dune field (Qedc). The majority of the upper dune field covered in large parabolic dunes (Qedp) and the southwestern region is stabilized sand sheets (Qess).

1.2.3 Climate and Wind Regime

The CPSD are located within a high elevation, semi-arid steppe environment. Modern average annual minimum and maximum temperatures are 4°C and 21°C, respectively. Average monthly highs reach 34°C in July and lows of -6°C in January. Predominant precipitation occurs during the winter and summer; the spring and fall are typically dry. Summer precipitation occurs as convective storms. Total annual precipitation is 35 cm and total snowfall is 57 cm. In the summer winds are predominantly southwesterly and in the winter months northeasterly storms can reverse the wind regime (Western Regional Climate Center accessed July 2018).

1.2.4 Vegetation

Vegetation varies across the dune field with elevation and differences in geology and hydrology (Figure 1.6). A shallow water table and springs in the dune field sustain vegetation growth in stabilized regions of the dune field. Interdune swales are vegetated with grass (*Stipa hymenoides* R&S), forbs (*Sophora stenophylla* Gray, *Psoralidium lanceolatum* Rybd, *Reverchonia arenaria* Gray, *Dicoria brandegei* Gray, *Eriogonum*), and subshrub species (*Wyethia scabra* Hook, *Chrysothamnus* sp.) (Knisley & Hill, 2001). Partially stabilized sand sheets in the upper dune field and eastern and southern extent of the lower dune field have ponderosa pines (*Pinus ponderosa*) that date as far back as the 16th century C.E. (Wilkins, Ford, Clement, & Nicoll, 2005). Ponderosa pines on the Colorado Plateau typically grow between 2,100 to 2,500 MASL (Betancourt, 1990), making this stand of low-elevation ponderosas a unique feature. The stabilized sand ramps along the base of the Moquith Mountains are forested with pinyon-juniper

woodlands (*Juniperus osteosperma*, *Pinus edulis*) and sagebrush (*Artemesia*) and rabbitbrush (*Chrysothamnus nauseosus*).

Figure 1.6 Image looking east across the lower dune field. Pinyon-juniper woodlands in the foreground with Sparse grass, forbs, and shrubs in the foreground. Ponderosa pines in partially stabilized sand sheets along the margin of the active dune field. Pinyon-juniper woodlands on the sand ramps along the base of the Moquith Mountains. Photo Credit: D. Wilkins

1.2.5 Hydrology

A drainage divide north of the CPSD diverts surface water north into Yellowjacket Canyon, part of the Virgin River watershed, or south toward Sand Canyon and into the CPSD. In the upper dune field spring-fed wetlands line the northeastern margin and ephemeral ponds form in low-laying areas throughout the dune field. On the eastern margin of the lower dune field, Sand Canyon Wash is a deeply incised ephemeral channel with several large tributaries sourced from bedrock fractures in the Moquith Mountain canyons above. Sand Canyon Wash drains into a tributary to Kanab Creek south of the City of Kanab, which eventually drains to the Colorado River (Figure 1.7).

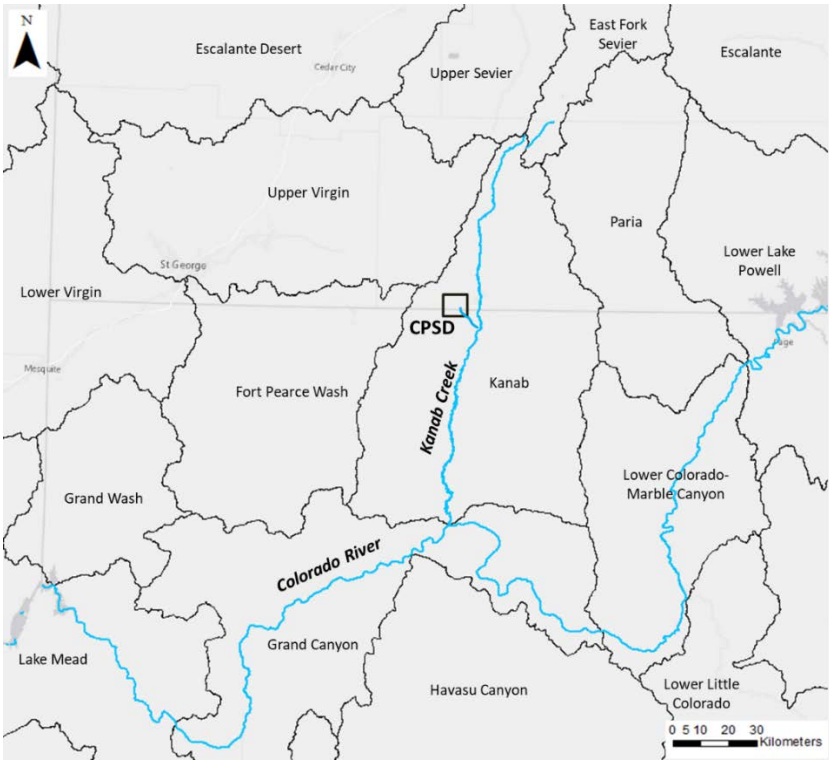

Figure 1.7 Map of watershed boundaries (HUC 8) and major rivers in the study region. Sand Wash is an ephemeral stream in CPSD fed by springs from the canyons of the Moquith Mountains. It flows into a tributary to Kanab Creek south of the City of Kanab, Utah, and eventually to the Colorado River.

1.3 Methods

This study investigates topographically-controlled sand ramps in the Coral Pink Sand Dunes, Utah. Field work completed during 2017-2018 includes stratigraphic descriptions of vertical exposures within the sand ramps, classification of deposits, and sampling for grain size analysis and OSL analysis. A total of five aeolian deposits were identified in the CPSD sand ramps and dated by optically stimulated luminescence (OSL) to provide age control on periods of past activity. One fluvial sand unit was also analyzed for comparison. The OSL samples were analyzed at Utah State University Luminescence Laboratory (USULL).

1.3.1 Sand ramp stratigraphy

Sand ramp stratigraphy is described from natural exposures in ephemeral fluvial channels incised through the sand ramps. Profiles were cleared with a shovel and each stratigraphic unit is described noting the texture, composition, bedding structure, and color. When applicable soil formation is described according to Birkeland, Machette, & Haller (1991). The entire stratigraphic profile was tested for calcium carbonate content with dilute hydrochloric acid (HCl) and, if applicable, the stage of pedogenic carbonate formation is classified according to Birkeland, Machette, & Haller (1991). Units are classified as aeolian, fluvial, or alluvial based on grain size and primary sedimentary structures. Aeolian units were identified in the field as homogenous, well-sorted sand units with primary bedding structures. Five aeolian units are identified in natural exposures within the sand ramps. Paleocurrent or dip direction (crossbeds) were measured for four of the aeolian units.

Samples were taken from different deposit types for grain size analysis. In the lab, samples were analyzed by laser light diffraction with a Malvern Mastersizer 2000 and grain sizes classified according to Wentworth (1922) methods. Samples were dry sieved to exclude grains >2 mm, sonicated in water for one minute to disperse aggregates, and analyzed three times following a standard operating procedure provided by Utah State University Luminescence Laboratory (USULL). The GRADISTAT program (Blott & Pye, 2001) was used to plot grain size distributions and calculate statistics by the Folk & Ward (1957) and moments methods.

1.3.2 Optically stimulated luminescence (OSL) dating

Luminescence dating works on the premise that quartz and feldspar are able to store energy within their crystal structure. While sediment is buried it is exposed to ionizing radiation from radiogenic decay of rubidium (Rb), uranium (U), thorium (Th), and potassium (K) in the surrounding sediments and cosmic radiation (Figure 1.8). The adsorption of ionizing radiation evicts electrons from their valence bands into higher energy levels, where they can become trapped in defects in the crystal lattice. Electrons can be released from high energy level 'traps' back to their valence state upon exposure to either sufficient sunlight or heat (referred to as 'bleaching' events). The release of an electron from a high to low energy state emits energy as a photon, producing a luminescence signal. The luminescence signal of a grain can be stimulated either by light, optically stimulated luminescence (Huntley, Godfrey-Smith, & Thewalt, 1985; Aitken, 1998), or by heat, thermoluminescence (Aitken, 1985).

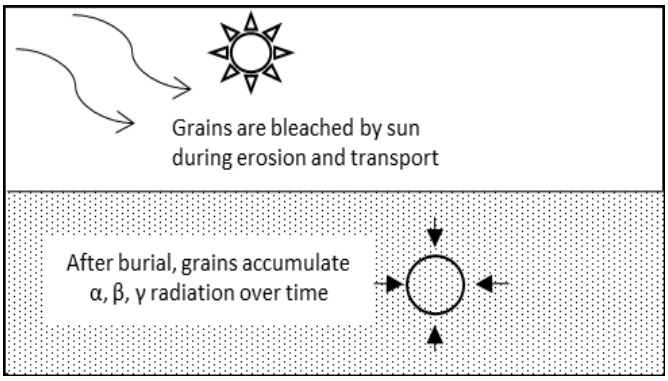

Figure 1.8 Quartz and feldspar are able to store energy within their crystal lattice. Exposure to sunlight during transport removes stored energy, bleaching the luminescence signal to zero. After burial, grains are subject to ionizing radiation from surrounding sediment and cosmic rays that rebuild its luminescence signal. Luminescence dating measures the signal of a buried grain to determine when it was last exposed to sunlight.

Luminescence dating measures the signal of a buried grain to determine when it was last exposed to sunlight. The equivalent dose (D_E) is the amount of laboratory radiation needed to induce a luminescence signal equal to the natural luminescence signal of the sample. The D_E is assumed to be approximately equivalent to the 'natural dose,' which is the amount of radiation the sample received in nature. The environmental dose rate (D_R), which is the rate at which the grains absorbed radiation during burial, is derived from concentrations of radioisotopes from surrounding sediment. An OSL age is estimated from the ratio of D_E (units of Grays) to D_R (units of Grays per ka) to yield an age (ka) (Equation 1). Luminescence dating assumes that grains were fully bleached prior to burial and therefore the luminescence signal being measured has been acquired since burial. Because grains are typically fully-bleached within seconds of aeolian transport during daylight conditions, luminescence dating is particularly well-suited to investigate aeolian activity. (Godfrey-Smith, Huntley, & Chen, 1988).

Equation 1. $$\text{Age (ka)} = \frac{DE\ (Gy)}{DR\ (\frac{Gy}{ka})}$$

1.3.2.1 OSL sample collection

OSL samples were collected following procedures described in Nelson et al. (2015). D_E samples were taken by pounding an opaque metal tube (8-inch-long by 2-inch diameter) horizontally into the outcrop with a rubber mallet until full. The ends of the tube were sealed with aluminum foil and tape to prevent exposure to sunlight. Samples were taken from the lower part of each deposit and at least 30 cm away from erosional unconformities to avoid disturbances and post-depositional mixing. For each D_E sample, one homogenized D_R sample was taken within a 15-cm radius surrounding the D_E sample location (Figure 1.9). A sediment sample to measure in-situ water content was taken from the same location as the D_E sample, stored in an airtight container, and measured as soon as possible in the laboratory.

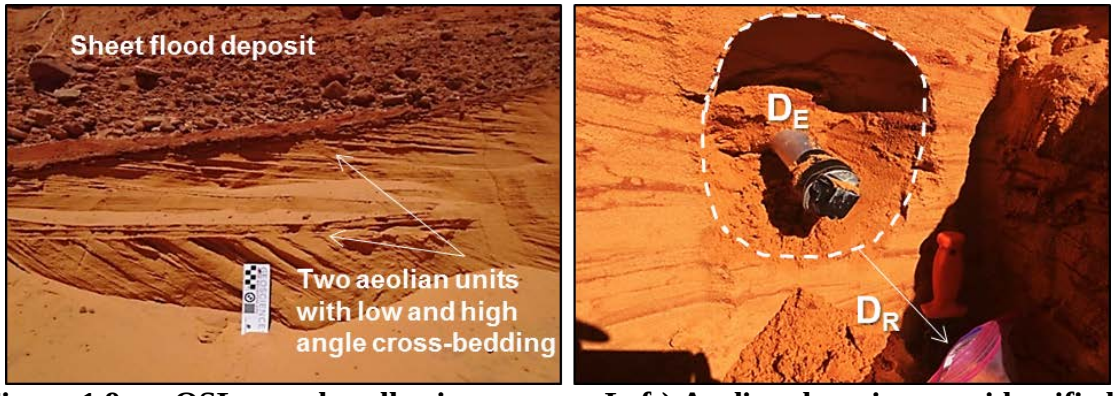

Figure 1.9 OSL sample collection process. Left) Aeolian deposits were identified based on field and laboratory observations (primary structures and grain size). In this photograph, two distinct aeolian units are capped by a sheet flood deposit. Right) A D_E sample is collected by pounding an opaque metal tube horizontally into an outcrop. D_R is collected from a 15 cm radius surrounding the D_E sample and stored in a Ziploc bag.

1.3.2.2 D_E sample preparation and measurement

D_E samples were prepared at USULL under dim, amber light. After discarding 2 cm of sand from each end of the sample, the remaining sediment was extracted and prepared for analysis. Samples were wet sieved to isolate the desired target grain size fraction of 90 to 150 µm. Carbonates were removed with 10% hydrochloric acid (HCl) solution and organics were removed with bleach. No samples had reactions to either of these steps, meaning that there was little to no carbonate or organics present in the samples. Quartz grains were isolated with sodium polytungstate with a density of 2.7 g/cm^3 to remove heavier minerals. The remaining quartz fractions were then etched three times with 47% hydrofluoric acid (HF) for 30 minutes each, for a total of 90 minutes. HF removes feldspar and other minerals and etches the outermost surface that is prone to alpha radiation, which is not included in the D_E calculation. After the final HF treatment, the quartz was placed in a 37% HCl solution for 30 minutes to remove feldspar grains and prevent precipitation of fluorite. Infrared (IR) simulations were used to check for the presence of feldspar that may not have been removed during processing and any aliquots (i.e., sub-samples) that showed presence of feldspar were not used in final age calculation. The remaining quartz fraction was placed into an oven to dry. A single layer of dry sand grains was attached onto 1-cm stainless steel disks with silicone spray using 2-mm-diameter masks.

Optical measurements were made on a Risø TL/OSL DA-20 reader at USULL. The luminescence signal was stimulated with blue-green (470-nm wavelength) light emitting diodes at 90% power at 125ºC for 40 seconds. The resulting luminescence signal was filtered with a UV filter (280 to 380 nm) and measured in units of photon counts per

channel. For each sample, D_E was statistically estimated from aliquot measurements using the single-aliquot regenerative (SAR) protocol for quartz sand (Murray & Wintle, 2000). SAR estimates the D_E by comparing the natural luminescence signal of each aliquot to signals from the same sample after a series of regenerative laboratory doses are applied (Figure 1.10).

For each aliquot, repeated luminescence measurements at known laboratory doses bracket the natural dose, and points are fit with a saturating exponential growth curve. Each aliquot is bleached by measuring the natural luminescence signal, which resets the samples luminescence signal to zero. Next, known doses of laboratory radiation below D_E, at D_E, and above D_E (R1, R2, and R3, respectively) from a calibrated 90Sr/90Y beta source are applied to regenerate a luminescence signal. A regenerative dose of zero irradiation (R4) is applied to check for recuperation. R5 is a duplicate regenerative dose equal to R1. Aliquots that exhibit a high recycling ratio (R5:R1) or high recuperation (R4) are not included in final D_E calculation. D_E was calculated based on the Central Age Model by Galbraith & Roberts (2012) using a minimum of 20 aliquots per sample.

SAR Sequence:

1. Measure natural (L_N) or give dose (R1, R2, R3, R4, or R5)
2. Preheat to 240°C for 10 seconds
3. Stimulate for 40 seconds at 90% LED power, measure regenerative dose luminescent signal (L_i)
4. Apply test dose
5. Cut-heat to 160°C for 100 seconds
6. Stimulate 90% LED power for 40 seconds, measure test dose luminescence signal (T_i)
7. Repeat from Step 1

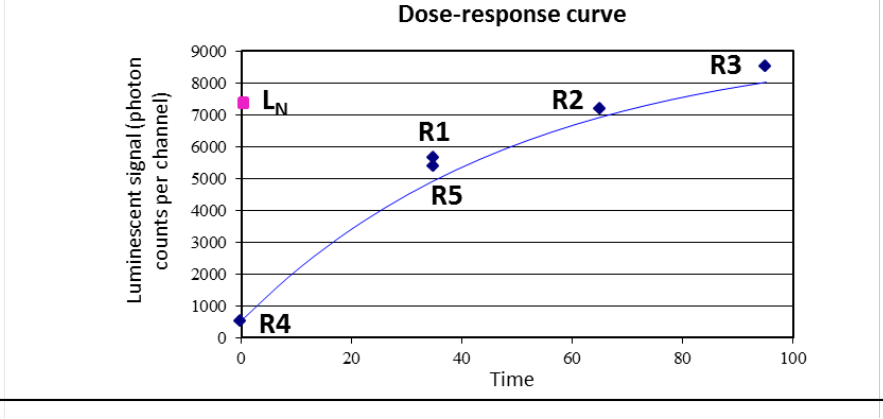

Figure 1.10 The list of steps used to measure DE with the SAR procedure (Murray & Wintle, 2000). The relationship between luminescence signal intensity (measured in photon counts per channel) versus laboratory dose (measured in Grays) is non-linear and varies for each sample. The natural dose (LN), the luminescence signal with no dose applied, is measured first, followed by a series of laboratory doses. The equivalent dose is interpolated from the dose response curve.

1.3.2.3 D_E estimates and error calculation

Standardized D_E estimates and standard error for each aliquot are displayed on radial plots (Figure 1.11). Differences in D_E measurements between aliquots of a single sample can be caused by instrument error and natural sources of variability. Natural sources of variability include incomplete bleaching of grains during transport, post-depositional mixing of grains, or in-situ dose heterogeneity during burial (Mayya, Morthekai, Murari, & Singhvi, 2006; Lomax, Hilgers, Twidale, Bourne, & Radtke,

2007). Error due to intra- and inter-grain variability was limited by careful field sampling methods, as well as additional laboratory steps to detect and correct for variability. Test doses were applied to detect and correct for sensitivity, which is a grain's ability to consistently store and emit known doses of radiation given in the laboratory. Sensitivity is measured by testing the difference between the natural or regenerative dose response signal and its corresponding test dose. Test doses were applied after every SAR step and aliquots with high test dose scatter were rejected from final D_E calculation. Because energy stored in shallow traps results in highly variable D_E measurements, a pre-heat plateau test measured the response of aliquots to increasing pre-heat temperatures and was used to choose an appropriate preheat temperature range for a given sample to release unstable electrons from shallow traps prior to measurement.

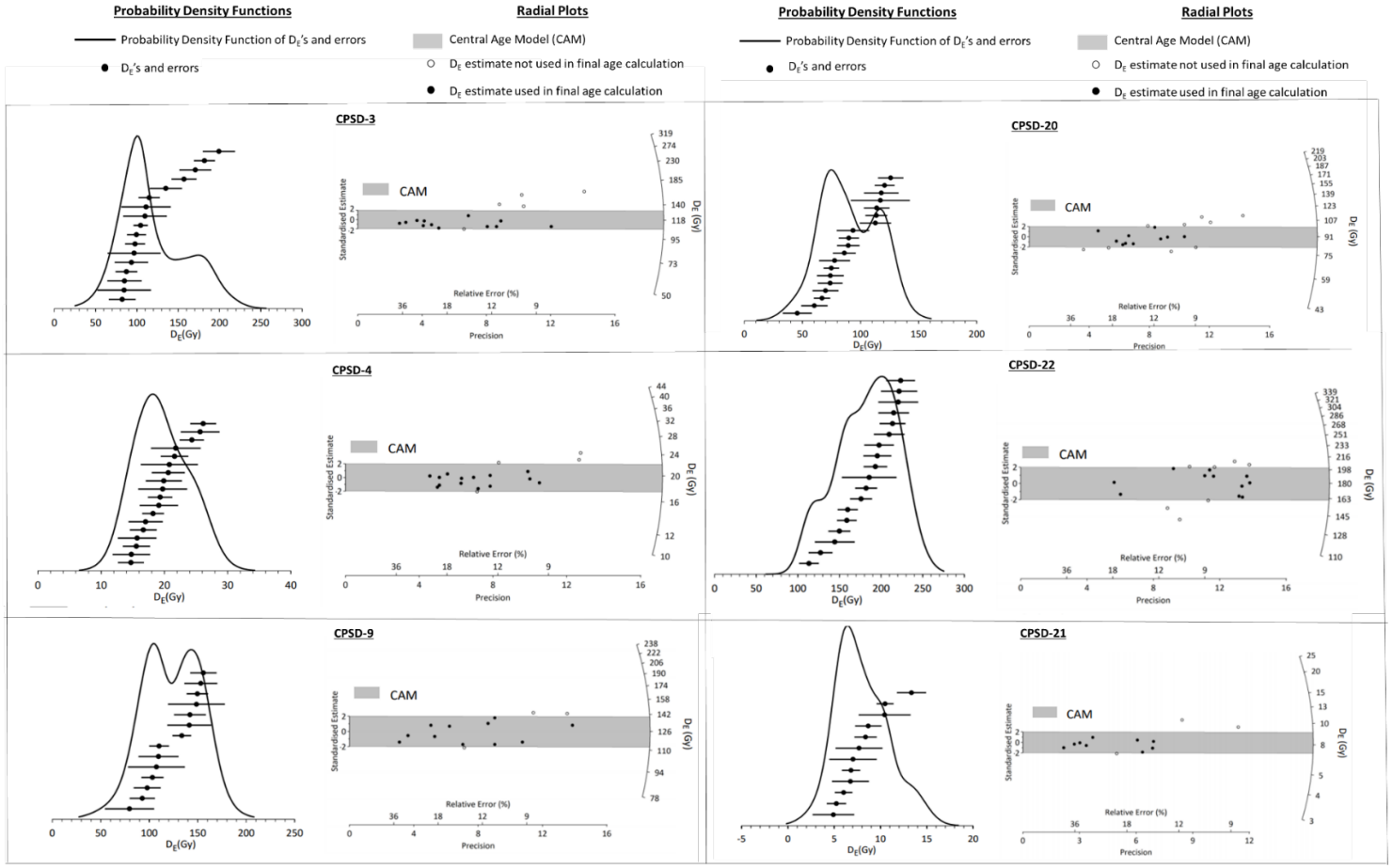

Figure 1.11 Probability Density Functions (PDF) and radial plots of aeolian deposits (CPSD-3, 4, 9, 20, 22) and fluvial deposit (CPSD-21). Radial plots are scatter plots of the standardized estimates on the left vertical axis (within 2 sigma error) plotted against standard error (reciprocal of standard error is precision) on the horizontal axis (Galbraith, 1988). The 95% confidence interval, calculated with CAM, is highlighted in gray. DE estimates are shown on the right with a radial axis, and read by extending a line from the origin through the point. Radial plots display different relative errors (and precision) for aliquots within a single sample, which is difficult to display with other plot types.

1.3.2.4 D_R calculation

The environmental dose rate (D_R) is the rate at which the grains acquired radiation while buried. Sources of radiation include alpha, beta, and gamma radiation from surrounding sediment and cosmogenic radiation. Each D_R sample was pre-processed at USULL where it was dried, homogenized, and split into a 50-gram representative sub-sample. Sub-samples were then sent to ALS Chemex Laboratory for analysis by inductively coupled plasma mass spectrometry (ICP-MS) and inductively coupled plasma atomic emission spectroscopy (ICP-AES) to determine concentrations of radioisotopes. Concentrations of K, Rb, Th, and U were used in D_R Calculation (Table 1.1). One dose rate value for each sample was calculated from the concentrations of radioisotope concentrations converted to radiation dose (Guérin, Mercier, & Adameic, 2011) and the cosmogenic contribution to total dose rate is estimated from altitude, latitude, and depth below ground surface (Prescott & Hutton, 1994). D_R values were then corrected for estimated burial history water content because moisture attenuates the rate at which grains acquire radioactive decay.

Table 1.1 Dose rate information

D_R is derived from concentrations of radioisotopes (K, Rb, Th, U) converted with factors from Guérin, Mercier, & Adameic (2011) and cosmic dose rate, which is estimated based on altitude, latitude, and depth below surface of the sample (Prescott & Hutton, 1994). The D_R estimate is corrected for water content because pore moisture attenuates the rate at which radioactive decay move through sediment.

Site ID	Grain size fraction (um)	In-situ H_2O (%)[1]	K (%)[2]	Rb (ppm)[2]	Th (ppm)[2]	U (ppm)[2]	Cosmic dose rate (Gy/ka)
Site 3	150-250	1.7	0.85±0.02	26.0±1.0	0.8±0.2	0.2±0.1	0.15±0.01
Site 4	150-250	3.9	1.34±0.03	39.4±1.6	1.0±0.2	0.3±0.1	0.21±0.02
Site 9	150-250	3.7	0.58±0.01	19.0±0.8	0.9±0.2	0.3±-0.1	0.22±0.02
Site 20	150-250	0.3	0.44±0.01	13.3±0.5	0.6±0.2	0.2±0.1	0.24±0.02
Site 21	150-250	0.1	0.22±0.01	6.9±0.3	0.7±0.2	0.2±0.1	0.26±0.03
Site 22	150-250	1.6	0.92±0.02	29.1±1.2	1.0±0.2	0.2±0.1	0.24±0.02

[1] Measured in-situ water content. Assumed 5.0% for all samples as moisture content over burial history.
[2] Radioelemental concentrations determined by ALS Chemex using ICP-MS and ICP-AES techniques.

1.3.3 Sediment geochemistry

This study applies several trace element and rare earth elements (REE) geochemical relationships that have shown to be useful in studies of dune provenance (e.g., Muhs et al., 2008; Hao, Guo, Qiao, Xu, & Oldfield, 2010; Muhs, 2017). Trace elements and rare earth elements (REEs) are relatively stable, and are therefore useful fingerprints of sediment source. Elemental concentrations were available from ICP-MS and ICP-AES analyses for each dated aeolian deposit as part of the OSL process (Table 1.2). One additional sample from the surface of the main dune field was collected and analyzed. CPSD dune sediments are also compared to the chemistry of the Kanab Dunes, which are located about 10 kilometers downwind of the CPSD, for a more complete understanding of regional sand transport pathways (Kanab Dunes data provided by H. Cornacchione of Utah State University).

Table 1.2 Trace elements and REE concentrations

Trace element and REE concentrations from CPSD used in sediment source analyses. Concentrations measured by ICP-MS and ICP-AES at Chemex ALS Laboratory.

		Major Element	**Trace Elements**					**Rare Earth Elements**	
Site ID	**Deposit Type**	**K (%)**	**Ba (ppm)**	**Zr (ppm)**	**Rb (ppm)**	**U (ppm)**	**Th (ppm)**	**La (ppm)**	**Sc (ppm)**
3	aeolian	0.85	170	13.3	26	0.2	0.76	2.6	0.6
4	aeolian	1.34	240	16.9	39.4	0.3	0.97	3.4	0.6
9	aeolian	0.58	120	13.5	19	0.3	0.88	2.7	0.5
20	aeolian	0.44	100	11.4	13.3	0.2	0.61	1.9	0.4
21	fluvial	0.22	50	10.4	6.9	0.2	0.73	1.9	0.3
22	aeolian	0.92	180	18.7	29.1	0.2	0.96	3.1	0.7
N/A[1]	aeolian	0.73	160	12.5	21.17	0.2	0.67	2.2	0.37

[1] Additional sample taken from surface of active dune field to represent modern dune sand.

1.4 Results

1.4.1 Sand ramp chronostratigraphy

Topographic and structural (i.e., fault scarp) controls present in the CPSD sand ramp system have preserved periods of dune activity during the end of the last glacial (MIS 6) through MIS 5d/e (OSL ~149 ka to OSL ~114 ka) and during the late Pleistocene-Holocene (LPH) transition (OSL ~12.5 ka) (Table 1.3). Five aeolian units (CPSD-3, 4, 9, 20, and 22) and one fluvial sand deposit (CPSD-21) were identified in natural exposures within the sand ramps and dated with OSL (Figure 1.12). The CPSD sand ramps are composed primarily of alluvial and fluvial sediments interbedded with aeolian units (Figure 1.13). The five aeolian units are unconsolidated, moderately well-sorted to moderately sorted medium- to fine-grained sand with some silt and clay (Table 1.3; additional data in Appendix A). All aeolian units were capped and stabilized by alluvial or fluvial deposits (Figure 1.13). While each of the overlaying fluvial and alluvial units had weakly developed pedogenic carbonate coatings, none of the aeolian units had evidence of soil formation or secondary mineral accumulations (Table 1.4).

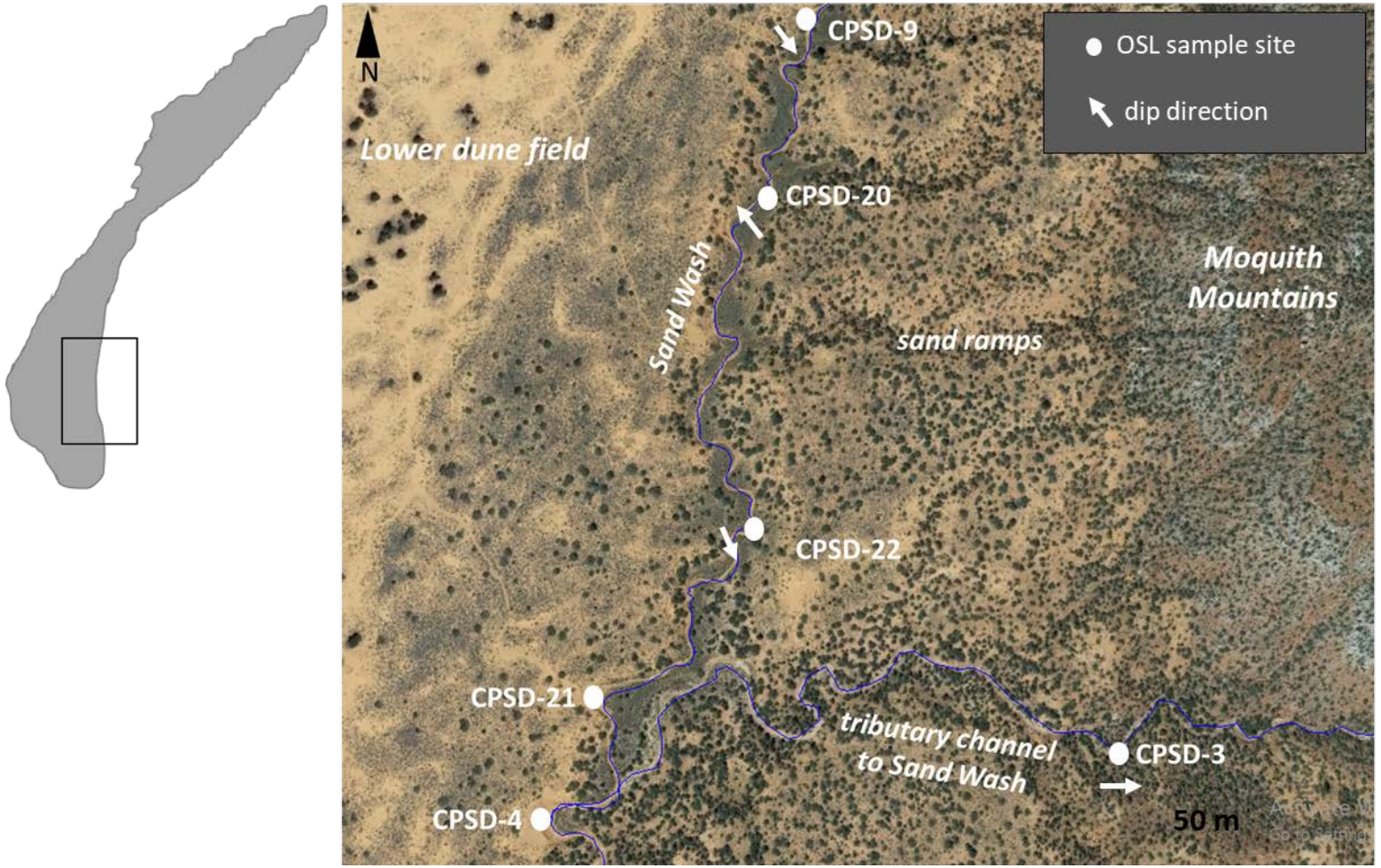

Figure 1.12 Locations of 6 OSL sampling sites. Samples were taken from natural exposures in Sand Wash and a tributary channel. Arrows shows the general dip direction of sampled aeolian deposit that are used to infer dune type (e.g., climbing dune, migrating dune).

Table 1.3 OSL Age Estimates and Deposit Characteristics

Final age estimates are reported at two sigma standard deviation of the age uncertainty D_E measurements. D_E, D_R, and error calculations were completed by USULL.

	Aeolian					Fluvial
Site ID	**CPSD-3**	**CPSD-4**	**CPSD-9**	**CPSD-20**	**CPSD-22**	**CPSD-21**
OSL measurements						
# aliquots[1]	17 (26)	18 (27)	14 (21)	19 (26)	18 (22)	12 (23)
D_R (Gy/ka)	1.04 ± 0.05	1.59 ± 0.07	0.88 ± 0.05	0.74 ± 0.04	1.21 ± 0.06	0.55 ± 0.04
D_E[2] **± 2σ (Gy)**	118.98 ± 17.56	19.74 ± 1.76	125.69 ± 12.92	90.46 ± 10.08	180.76 ± 16.05	8.09 ± 1.46
OD[3] **(%)**	25.3 ± 6.1	13.2 ± 4.3	13.8 ± 4.7	20.4 ± 4.6	16.3 ± 3.6	23.2 ± 8.0
OSL age± 2σ (ka)	**114.7 ± 20.6**	**12.40 ± 1.65**	**142.7 ± 20.4**	**123.0 ± 18.6**	**149.8 ± 20.0**	**14.62 ± 3.07**
Deposit characteristics						
Dry Color[4]	5YR 5/6	5YR 6/8	5YR 5/8	5YR 6/8	5YR 6/8	5YR 6/8
Wet Color[4]	2.5YR 4/8	5YR 6/8	5YR 5/6	5YR 5/8	5YR 5/8	5YR 5/8
% Sand[5]	100	98.2	96.3	100	98	97.2
% Silt[5]	0	1.8	3.6	0	2	2.7
% Clay[5]	0	0	0.1	0	0	0.1
Dip Direction	090°	ND	150°	330°	155°	ND
Dip Angle	18°	ND	25°	22°	25°	ND
Inferred Dune Type[6]	climbing	NA	migrating	migrating	migrating	NA

[1] Age analysis using the single-aliquot regenerative-dose procedure of Murray & Wintle (2000) on 2mm small-aliquots of quartz sand. Number of aliquots used in age calculation and number of aliquots analyzed in parentheses.
[2] Equivalent dose (D_E) calculated using the Central Age Model (CAM) of Galbraith & Roberts (2012).
[3] Overdispersion represents variance in DE data beyond measurement uncertainties, value >20% may indicate significant scatter due to depositional or post-depositional processes.
[4] Color determined with Munsell Color Chart.
[5] Grain size analyses by laser light diffraction and results summarized with GRADISTAT, see Appendix A-C for full results.
[6] Dune type is inferred from orientation of paleocurrent direction relative to main dune field and Sevier fault scarp.

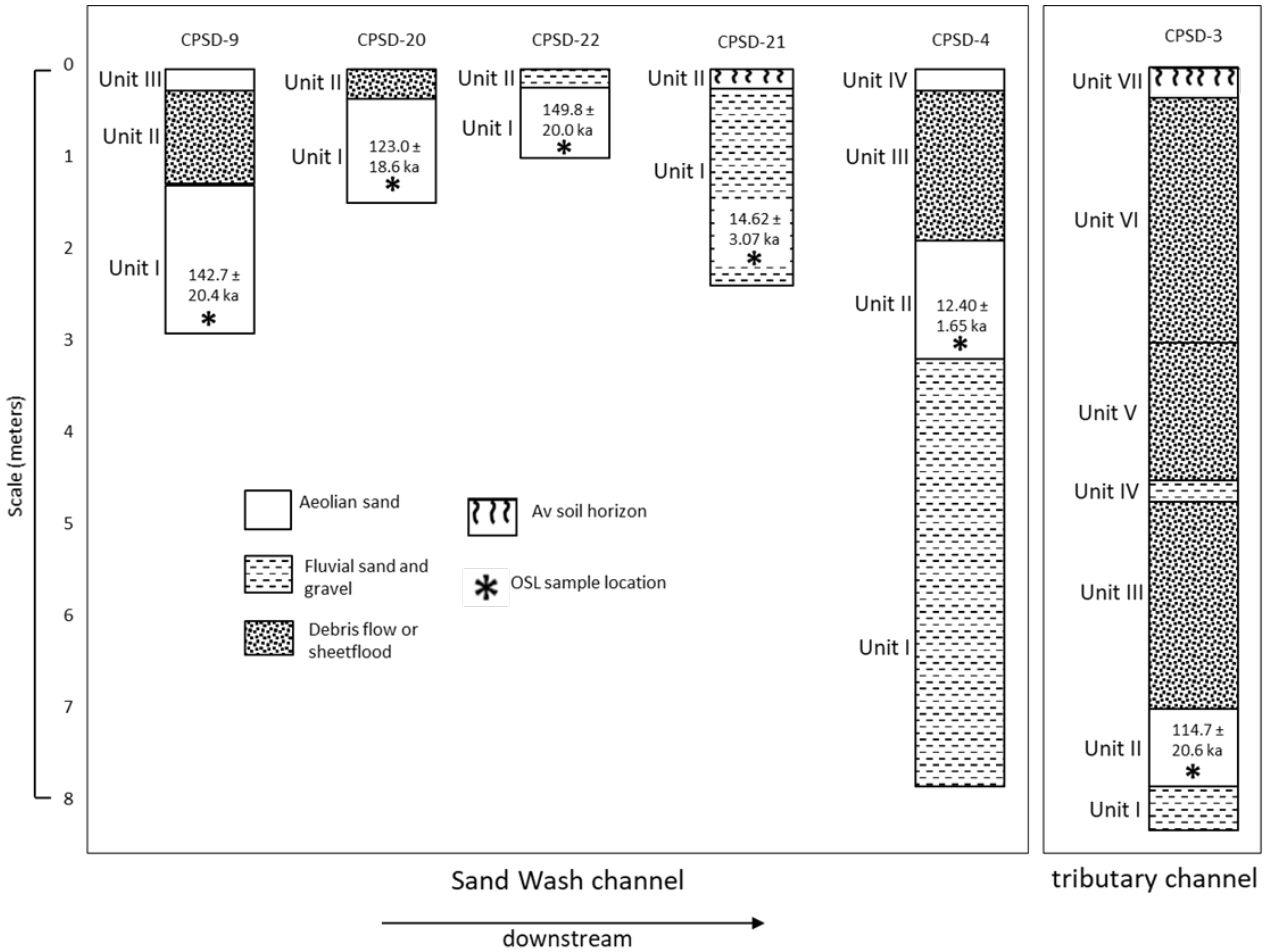

Figure 1.13 Simplified chronostratigraphic columns of topographically-controlled aeolian deposits within the sand ramps. Sand ramps stratigraphy is primarily fluvial and alluvial deposits interbedded with aeolian units. All OSL-dated aeolian units are capped and preserved by fluvial or alluvial deposits. Detailed descriptions are located in Table 1.4.

Table 1.4 Description and Inferred Depositional Setting of Stratigraphic Units

General description of stratigraphy of entire vertical profile at each site where an OSL sample was taken. Units are numbered from bottom-most exposed unit and divided based on differences in composition, bedding styles, and structures.

Unit	Depth (m)	Description (composition and bedding style/structures)	Depositional Environment
CPSD-3; Located in a main tributary east of Sand Canyon Wash (37.01899, -112.71660, elev 1768 m)			
VII	0.7	Weakly developed soil in sand and silt; Av horizon, capped with biogenic crust	Aeolian
VI	3.3	Angular, unsorted, boulders up to 1 meter diameter, clast supported, Stage 1 pedogenic carbonate	Colluvial
V	4.9	Angular, unsorted clast supported gravel	Colluvial
IV	5.1	Gravel lenses in sand	Fluvial
III	7.1	Angular unsorted sand to boulders, clast supported, interbedded with layers of sand and gravel	Alluvial
II	**7.8**	**High angle bedding, unconsolidated sand, dip direction 090°, dip angle 18°, no reaction to HCl**	**Aeolian***
I	8.1+	Gravel lenses interbedded in sand	Fluvial
CPSD-4; Located in Sand Canyon Wash main channel (37.01822, -112.72327, elev. 1729 m)			
IV	0.05	Modern dune sand	Aeolian
III	2.0	Imbricated sub-rounded to angular unsorted sand to boulder clasts (sheet flood couplets) with thin pedogenic carbonate coating, bottom of unit has a layer of red sand hardened with secondary silica precipitate	Alluvial
II	**3.0**	**High angle bedding, unconsolidated sand, dip angle 25°, no reaction to HCl**	**Aeolian***
I	7.0+	Sand interbedded with gravel lenses and fine grained mud layers	Fluvial

CPSD-9; Located in Sand Canyon Wash main channel (37.02726, -112.71993, elev 1755 m)			
III	0.05	Modern dune sand	Aeolian
II	1.3	Imbricated clast supported large cobbles and boulders interbedded with sand and gravel lenses, bottom of unit has a layer of red sand hardened with secondary silica precipitate	Alluvial
I	**2.8+**	**High angle bedding, unconsolidated sand, dip angle 25°, No reaction to HCl**	**Aeolian***
CPSD-20; Located in Sand Canyon Wash main channel (37.02526, -112.72074, elev 1752 m)			
II	0.15	Unsorted 50 % sand 50% pebbles with some pedogenic carbonate coating, but not cemented and no ped structure	Alluvial
I	**1.25+**	**High angle bedding, unconsolidated sand, dip direction 330°, dip angle 22°, no reaction to HCl**	**Aeolian***
CPSD-21; Located in Sand Canyon Wash Main channel (37.01914, -112.72270, elev 1731 m)			
II	0.1	Weakly developed soil in sand and silt (Av horizon)	Aeolian
I	**2.25+**	**Sand that grades into gravel 10 meters downstream, low angle bedding, 15 meters downstream of a fluvial anti-dune sand unit, no reaction to HCl**	**Fluvial***
CPSD-22; Located in Sand Canyon Wash main channel (37.02224, -112.72120, elev 1743 m)			
II	0.1	Unsorted, imbricated gravel with pedogenic carbonate coating	Fluvial
I	**1.0+**	**High angle bedding, unconsolidated sand, dip direction 155°, dip angle 25°**	**Aeolian***

*OSL sample taken from unit

1.4.1.1 Dune morphology affects age interpretation

Dune morphologies represent different types of activity and therefore influence the interpretation of deposit ages (Bateman, 2003). Dip direction was measured on four of the five aeolian deposits and used to interpret dune type (Figure 1.12 and Table 1.3). CPSD-9, 20, and 22 are interpreted as migrating dunes because their bedding dip directions are oriented parallel to the Sevier fault scarp. These deposits are all located in Sand Canyon Wash channel, along the margin of the main, active dune field and the relict sand ramps. Migrating dunes overwrite earlier periods of activity during continual re-exposure to sunlight, therefore, OSL ages of migrating dunes stabilized by overlaying alluvium indicate the last time that the was dune active and provide a minimum age on aeolian activity. The dip directions of the migrating dunes are bi-modal (they generally dip either northeast or southwest). This corresponds with modern wind data showing seasonal shifts in wind regime, with predominantly southwesterly winds in the summer and northeasterly storms reversing wind regime in the winter months (Western Regional Climate Center accessed July 2018). Also, wind is very sensitive to local topography (e.g., Jewell & Nicoll, 2011) and is likely influenced by the steep Sevier fault scarp along the margin of the dune field. The aeolian deposit at site CPSD-3, located about ten meters from the fault scarp, is interpreted to be a climbing dune because the dip direction is oriented perpendicular to the fault scarp. The Sevier fault scarp provides a strong structural control that inhibits remobilization of aeolian deposits along its base. Unlike migrating dunes, climbing dunes form by filling their accommodation space and are unlikely to remobilize (e.g., Ellwein, Mahan, &, McFadden, 2015).

1.4.1.2 Descriptions of exposures with dated aeolian deposits

Site CPSD-3 is located nearest to the Sevier fault scarp in a large tributary to Sand Canyon Wash (Figure 1.14). The exposure is greater than eight meters thick and is composed of seven units. The lowest exposed unit (Unit I) is fluvial sand and gravel. Unit II is a 70-cm-thick aeolian unit dated at OSL 114.7 ± 20.6 ka. This unit is interpreted to be a climbing dune because the beds dip perpendicular to the Sevier fault scarp. The overlying 6.4 meters are alluvial, fluvial, and colluvial deposits (Units III-VI). Unit VII, the uppermost unit is 70-cm-thick aeolian sand and loess with a vesicular, weakly formed soil horizon and stabilized by a biogenic crust. Unit VII was not dated with OSL because of pedogenic alteration.

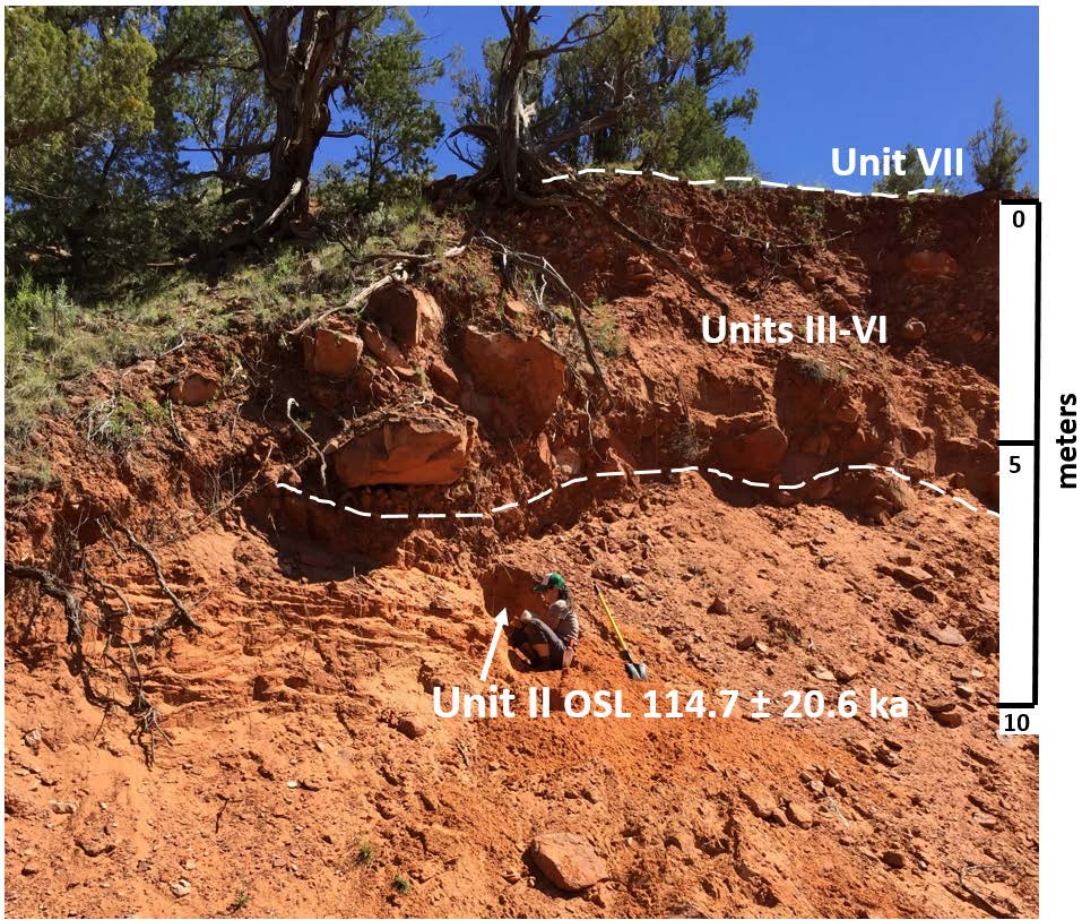

Figure 1.14 CPSD-3, located in a tributary of Sand Canyon Wash, is a climbing dune oriented perpendicular to the Sevier fault scarp. Units VI through III hillslope deposits are hillslope deposits over seven meters thick that cap Unit II, an aeolian unit dated at OSL 114.7 ± 20.6 ka. Unit I is a fluvial deposit (not pictured) and Unit VII is the modern surface, a thin mantle of aeolian sand.

The following four sites are all located in the main channel of Sand Canyon Wash, and are described moving from upstream to downstream. CPSD-9 is the farthest upstream site, located on the cutbank in a small meander in Sand Canyon Wash (Figure 1.15). Unit I is a high angle bedded, unconsolidated sand aeolian unit dated to OSL 142.7 ± 20.4 ka. Unit II is a ~1-meter alluvial deposit composed of clast-supported cobbles and boulders interbedded with a thick sand unit. The bottom of unit has a layer of red sand hardened with secondary silica precipitate. CPSD-20 is located in the main channel of Sand Canyon Wash (Figure 1.16). Unit I is a high angle bedded, unconsolidated aeolian

sand unit dated at OSL 123.0 ± 18.6 ka, and capped by a thin (15 cm) alluvial deposit composed of rounded to sub-angular pebbles and sand (Unit II). CPSD-22 is located in a cutbank in the main channel of Sand Canyon Wash (Figure 1.17). Unit I is the oldest dated aeolian unit at OSL 149.8 ± 20.0 ka, capped by a thin (10 cm) alluvial deposit composed of gravel (Unit II). CPSD-4 is located in an exposure on the cutbank of a large, deeply incised meander in the main channel of Sand Canyon Wash (Figure 1.18). The entire profile is 17 meters from the bottom of the channel. The lowest exposed unit is fluvial sand interbedded with gravel lenses and mud layers (Unit I). Unit II is a one meter aeolian migrating dune dated to OSL 12.40 ± 1.65 ka. The profile is capped by an alluvial package composed of sheet flood couplets (alternating layers of fine and coarse grains) (Unit III). Grains are imbricated sub-rounded to angular, sand to boulder-sized clasts that hold a vertical face. Clasts are covered in a thin pedogenic carbonate coating. The bottom of the unit (boundary with Unit II) is a layer of red sand hardened with secondary silica precipitates.

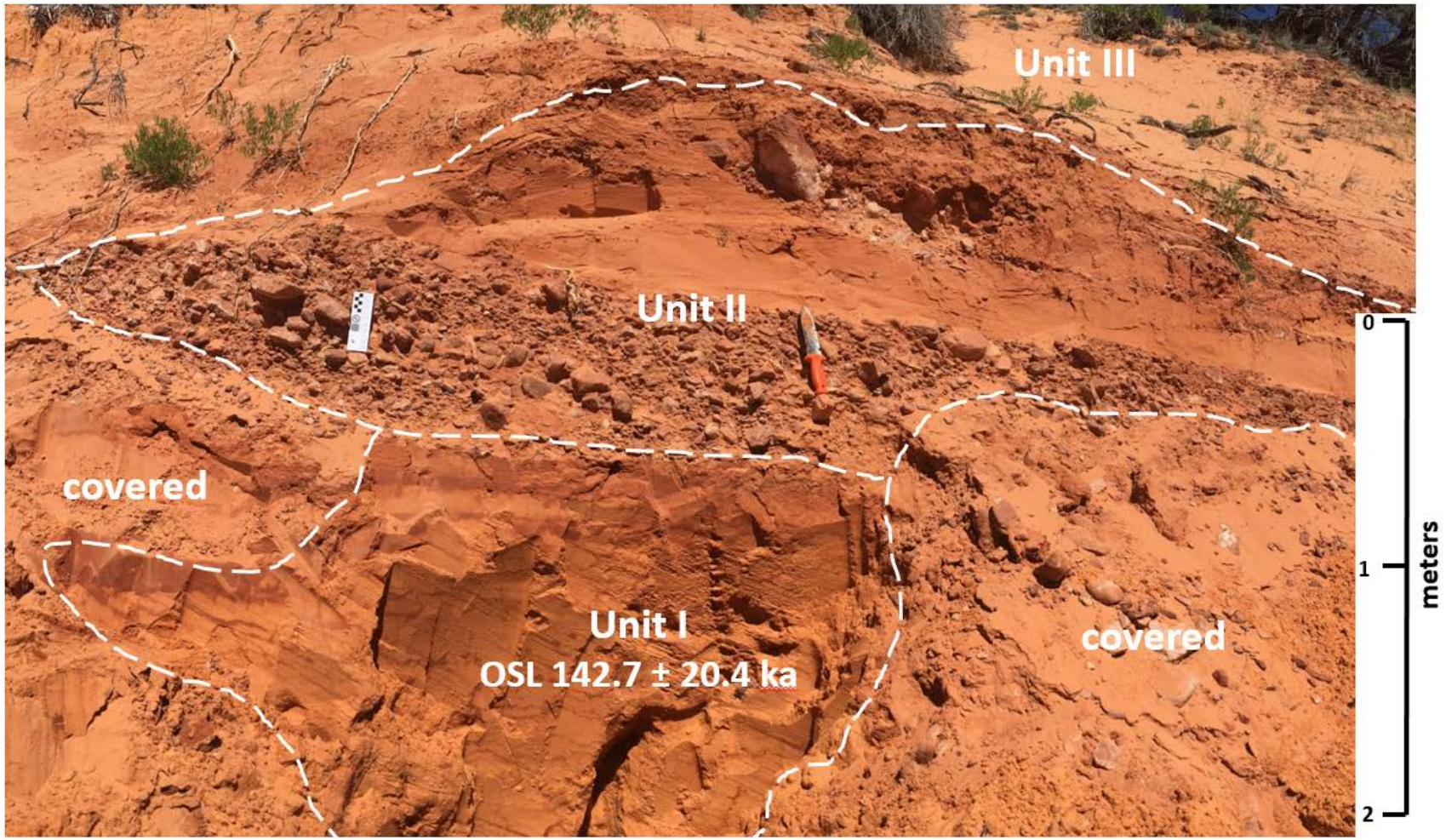

Figure 1.15 CPSD-9 is located the farthest upstream in the main channel of Sand Wash. Unit I, an aeolian unit dated at OSL 142.7 ± 20.4 ka, is capped by a debris flow deposit with a sand lens (Unit II).

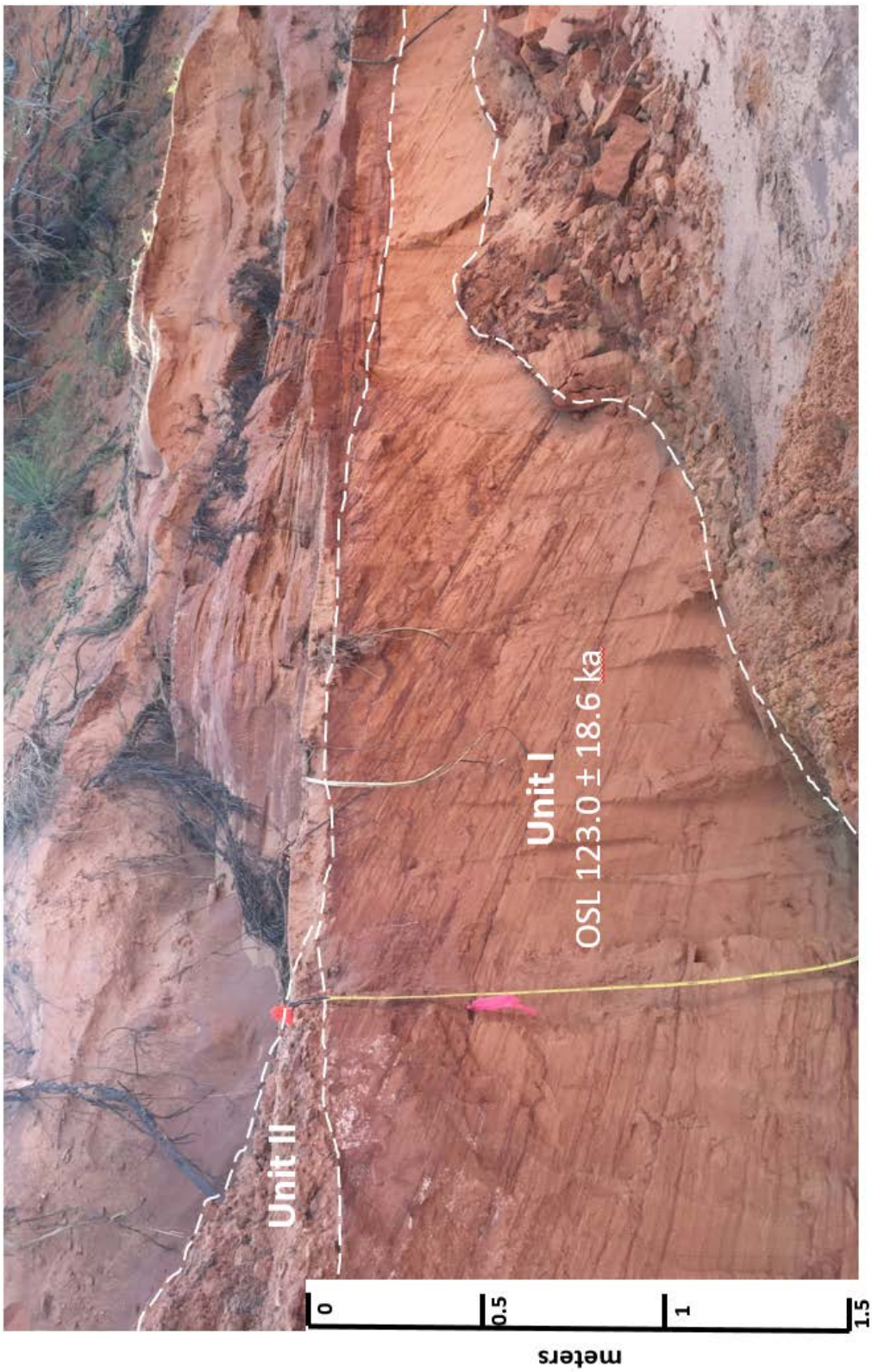

Figure 1.16 CPSD-20, exposed in a terrace in Sand Wash, is a high-angle crossbedded aeolian unit (OSL 123.0 ± 18.6 ka) capped by a gravel deposit with thick pedogenic carbonate coatings.

Figure 1.17 CPSD-22, located in the main channel of Sand Wash. Unit II, a fluvial deposit pedogenic carbonate coatings caps Unit I, an aeolian deposit. Unit I is the older dated deposit, 149.8 ± 20.0 ka.

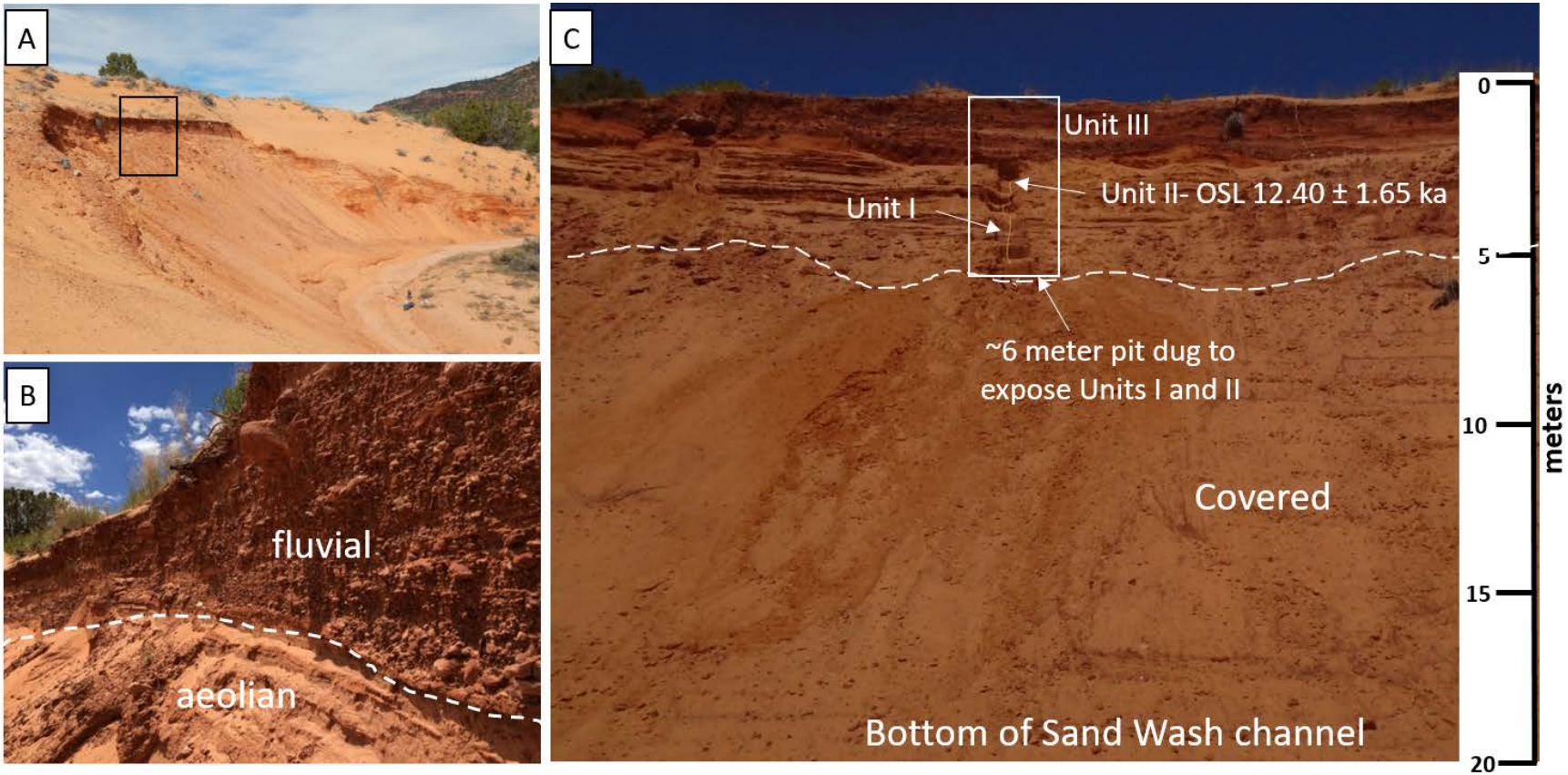

Figure 1.18 CPSD-4 is located in a large bend in Sand Wash. A seven pit was dug to expose Units I and II. Unit II is the youngest dated aeolian deposit (OSL 12.40 ± 1.65 ka).

1.4.1.3 Description of dated flood deposit

CPSD-21 is located in Sand Canyon Wash main channel, 300 meters upstream of CPSD-4 (Figure 1.19). Unit I is a thick (> 1 meter) flood deposit composed of low-angle dipping sand beds, and laterally grades into gravel about 10 meters downstream. This deposit is primarily sand with some clay and silt, but unlike the aeolian units it has a bi-modal grain size distribution (Appendix A). This fluvial sand deposit was dated at OSL 14.62 ± 3.07 ka, within error of aeolian deposition at CPSD-4 (12.40 ± 1.65 ka). Unit II is aeolian sand and loess with a vesicular, weakly formed A horizon. This unit was not dated with OSL because of pedogenic alteration.

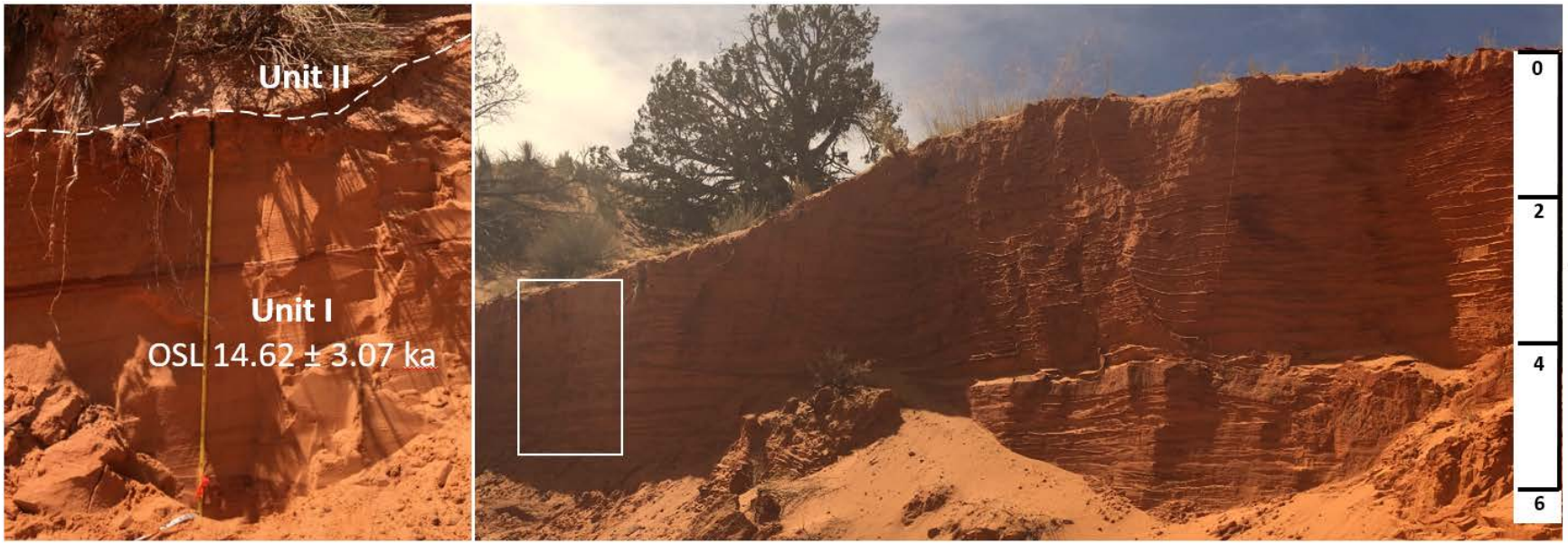

Figure 1.19 CPSD-21 is a flood deposit composed primarily of unconsolidated sand. This unit is different from aeolian units because of its low dip angle, bi-modal grain size distribution, and gravel lenses.

1.4.1.3 Sand Ramp Characteristics

The relationships between deposit type, age, and geomorphic setting were examined to understand how the sand ramps formed. In general, aeolian sediment was deposited farther from the fault scarp and at lower elevations over time as the sand ramps grew (Figure 1.20). The climbing dune (CPSD-3, OSL ~114 ka) is located closest to the Sevier fault scarp and at a higher elevation compared to other deposits. The three migrating dunes (CPSD-9, 20, 22; OSL ~120-150 ka) located in the main channel of Sand Wash all group together based on elevation and location from the Sevier fault scarp. The youngest deposit (CPSD-4; OSL ~12.5 ka) is located farthest from the fault scarp and at the lowest elevation. This is not an example of inverted ages with respect to topography; rather it shows that the sand ramps grew to fill their accommodation space, with aeolian sediment being deposited farther from the fault scarp over time as the features grew.

Longitudinal profiles in Figures 1.21 and 1.22 show cross sections of the sand ramps from north to south and from east to west, respectively. The sand ramps slope downward from north to south down-gradient with the base level of Sand Wash (Figure 1.21) and from east to west from the Sevier fault scarp to the main dune field (Figure 1.22). This shows that the CPSD sand ramps were built on complex, uneven terrain. Therefore, we do not cross-correlate ages between deposits based on elevation or position.

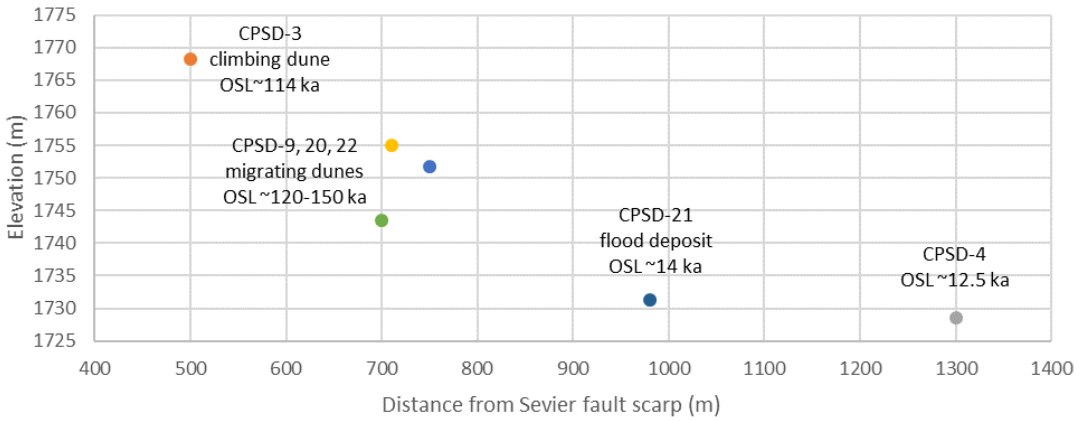

Figure 1.20 Relationship between elevation, deposit type, and distance from the Sevier fault scarp for each sample. CPSD-3, a climbing dune, is located nearest to the Sevier fault scarp compared to the other samples, Migrating dunes CPSD-9, 20, and 22 all group together location from the fault scarp and OSL age. The youngest deposit, CPSD-4, is located farthest from the fault scarp and at the lowest elevation. CPSD-21 is the flood deposit located about 300 meters upstream from CPSD-4 and at about the same elevation.

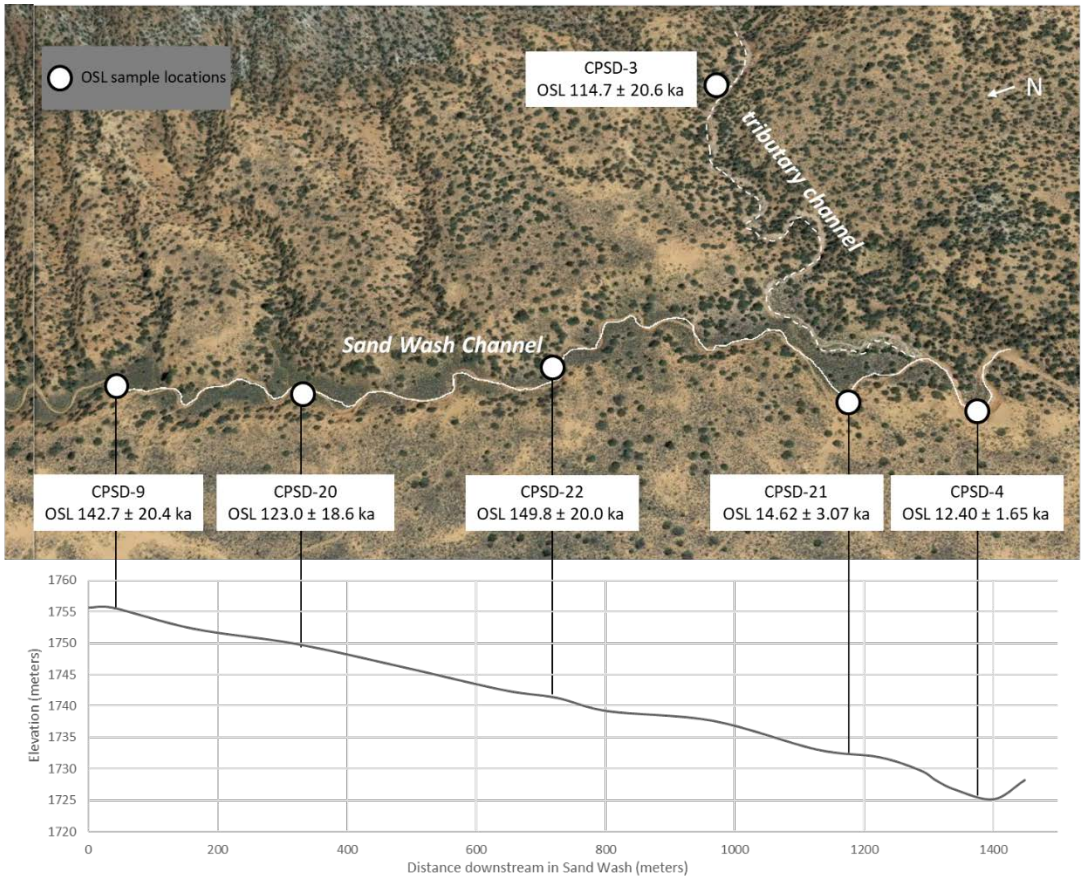

Figure 1.21 Longitudinal profile of Sand Canyon Wash channel noting location and ages of OSL sample sites. CPSD-4, 9, 20, 21, and 22 are located in the main channel of Sand Canyon Wash along the eastern margin of the lower dune field. CPSD-3 is located in a tributary to Sand Canyon Wash at the base of the Moquith Mountain.

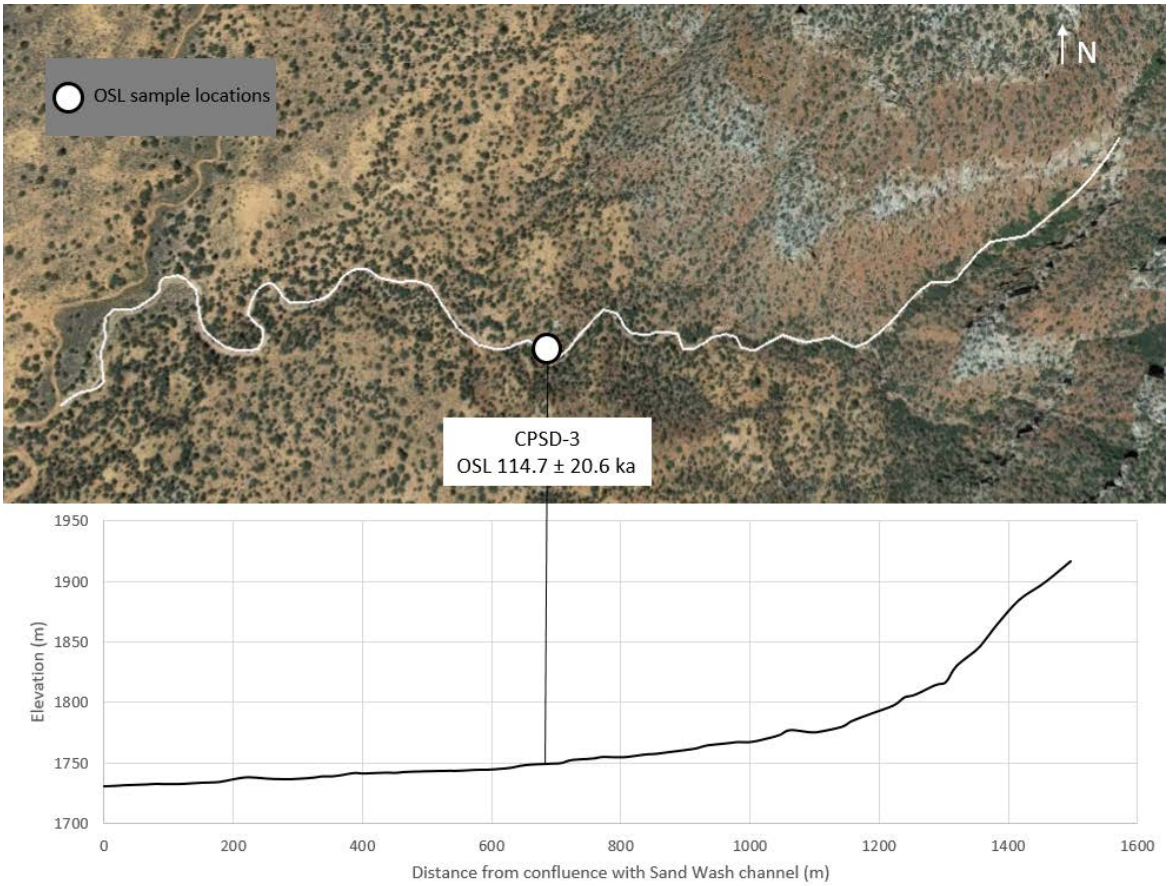

Figure 1.22 Longitudinal profile of the main tributary to Sand Wash, showing a cross section of the sand ramps. CPSD-3 is located nearest to the Sevier fault scarp in the tributary channel.

1.4.2 Sediment geochemistry

Concentrations of rare and trace elements are used to identify possible changes in sediment source over time, as well as differences in sediment source between the CPSD and the nearby Kanab Dune field (Figure 1.23). Over time, minerals become enriched with immobile and insoluble trace as relatively lighter or more soluble elements are lost or altered during weathering and transport (Bhatia & Crook, 1986). Immobile and insoluble trace elements are considered the most suitable for sediment source analysis because they reflect the chemical signature of the parent rock (Holland, 1978). This study applies several trace element and rare earth elements (REE) geochemical relationships that have shown to be useful in studies of dune provenance (e.g., Muhs et al., 2008; Hao, Guo, Qiao, Xu, & Oldfield, 2010; Muhs, 2017). Results show that aeolian deposits have remained geochemically similar over time, and CPSD and Kanab Dune field are geochemically distinct from each other.

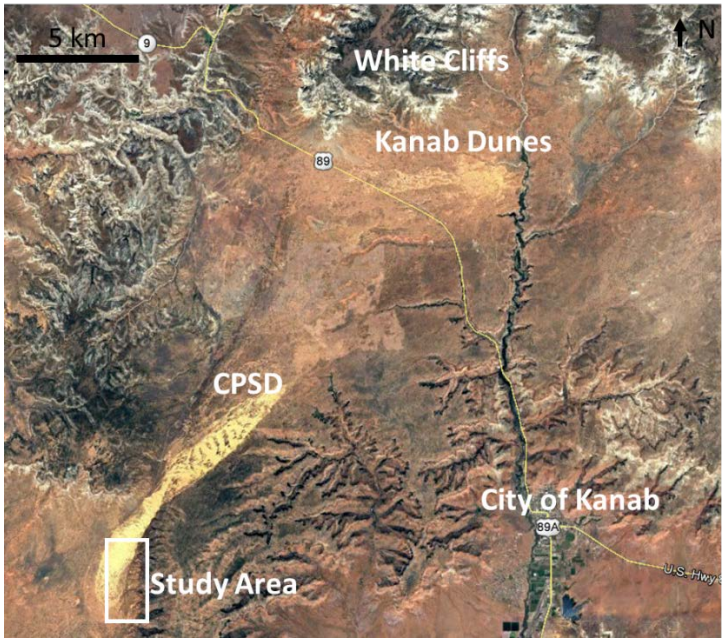

Figure 1.23 The Kanab Dunes are located about 10 kilometers northeast of CPSD, but dune geochemistry indicates different aeolian sediment sources.

1.4.2.1 La-Th-Sc and Zr-Th-Sc relative abundance

Immobile trace elements lanthanum (La), thorium (Th), scandium (Sc), and zirconium (Zr) are well-suited to provenance analysis because of their immobility during weathering, erosion, and digenesis (Holland, 1978). Relative abundances of these trace elements are plotted in La-Th-Sc (Taylor & McLennan, 1985; Bhatia & Crook, 1986) and Zr-Th-Sc (Bhatia & Crook, 1986) ternary diagrams (Figure 1.24). Developed to classify sediment sources of clastic sedimentary rocks, these relationships have been used successfully to discriminate aeolian deposits from different sources (Muhs et al., 2008; Hao, Guo, Qiao, Xu, & Oldfield, 2010).

CPSD and Kanab Dune sediments are clustered into two distinct groups on the La-Th-Sc ternary plot (Figure 1.24). CPSD sediments have lower La content, similar Th content, and higher Sc content as the Kanab Dunes. All samples from the Kanab Dunes and CPSD sediments plot closely on the Zr-Th-Sc ternary plot (Figure 1.24), containing greater than 90% Zr and less than 10% Th and Sc. While all samples plot closely, there is clustering of sediments from each dune field caused by higher abundance of Sc in CPSD sediments.

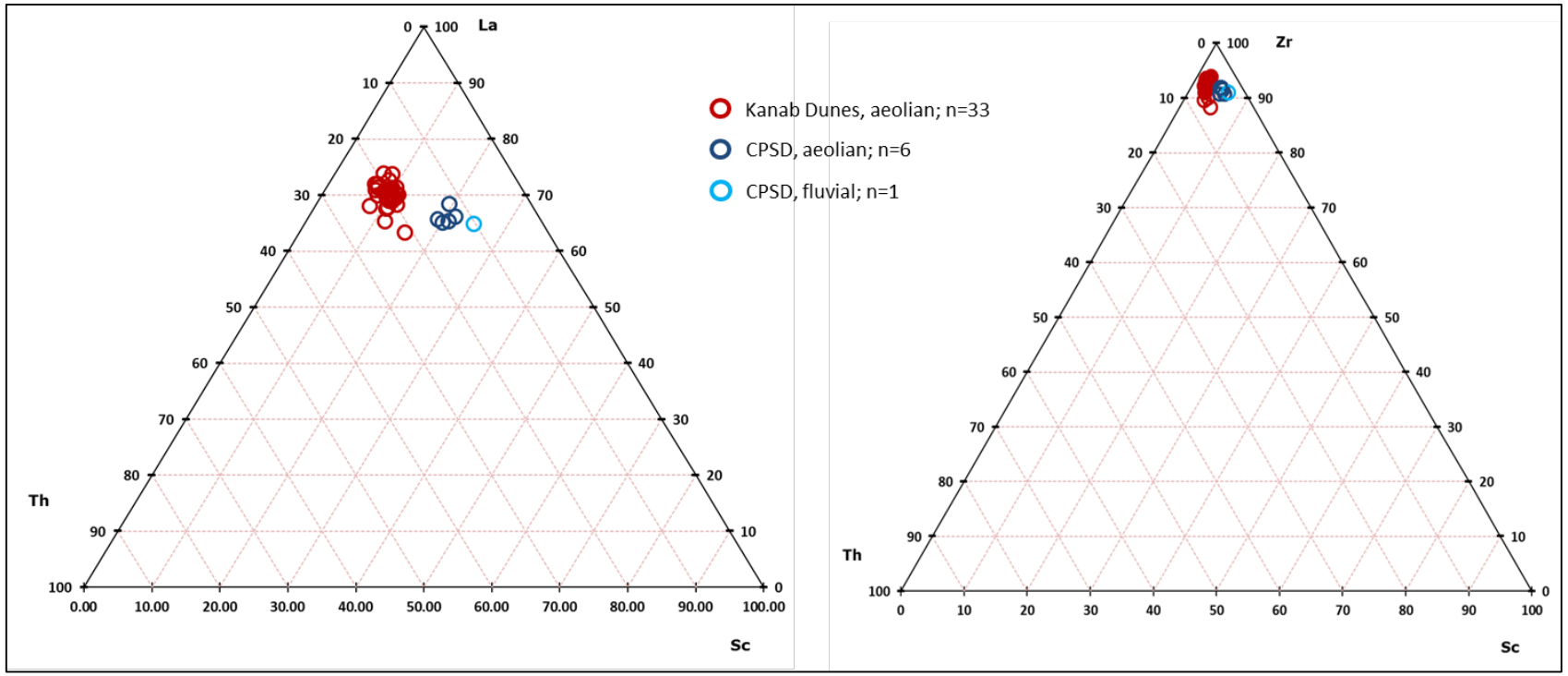

Figure 1.24 Relative abundances of trace elements in CPSD aeolian (n=6) and fluvial (n=1) sediments and Kanab Dune aeolian sediments. La-Th-Sc ternary plot shows that CPSD sediments have lower La content, similar Th content, and higher Sc content compared to the Kanab Dunes, and each dune field clusters into two distinct groups. Zr-Th-Sc ternary plot shows that Kanab Dunes and CPSD sediments all group around 90% Zr and less than 10% Th and Sc. While all samples plot closely, there is clustering of sediments from each dune field.

1.4.2.2 K/Ba and B/Rb ratios

Most North American dune fields are ultimately derived from sediments composed of a mix of rock types, including plutons, metamorphic rocks of varying grades, and sedimentary units partially composed of rock fragments from igneous and metamorphic sources that can result in unique geochemical fingerprints across different dune fields and regions. Muhs (2017) developed a simple geochemical tracer based on properties of potassium feldspar, found in most dune fields across North America. Trace elements rubidium (Rb) and barium (Ba) are found in potassium feldspars, and ratios of potassium (K) to Rb and Ba can be used to measure potassium feldspar composition and are effective discriminators for potassium feldspars derived from different source sediments across North American dune fields. The mixed source compositions of North American dune fields result in distinct K/Rb and K/Ba values that are also reflected in sediments, including alluvial and fluvial sediments that serve as sources for dune sediments as well as in dune sediments. Unlike individual element concentrations, element ratios such as K/Rb and K/Ba are insensitive to degree of mineral maturity, as long as at least some potassium feldspar has survived.

Major to trace element ratios are based on substitution geochemical properties of major rock-forming minerals (Goldschmidt, 1954). Trace elements can substitute for major elements in minerals, so ratios of trace elements compared to major elements can be used to signify parent rocks of sediment. The K/Ba ratio is based on the camouflage property of Ba^{+2}, which has a similar ionic radius as K, but with a higher charge, causing it to be captured by K-bearing minerals. The K/Rb ratio is based on the rule of admission, which is when a trace element is admitted into the crystal lattice of a mineral grain. This

can occur either when a trace element has a similar ionic radius, but lower charge than a major element or when the trace element has an identical charge, but larger ionic radius. Rb^+ has a larger ionic radius and identical charge to K^+, so it substitutes for K in potassium feldspar. In magma, Ba is captured by K-bearing minerals resulting in early formed minerals that are Ba-enriched. Minerals that form later and are more differentiated minerals are enriched in Rb. Therefore, within the same rock, potassium feldspar minerals will typically have low K and high Rb, and biotite minerals will have low K and high Rb.

Plots of K/Ba and K/Rb ratios of the CPSD are compared to other southwestern dune fields published in Muhs (2017) (Figure 1.25). CPSD and Kanab Dunes K/Rb to K/Ba values plot close to each other, but do not overlap. CPSD are more enriched in both Rb and Ba than the Kanab Dunes. CPSD K/Rb and K/Ba values range from 305 to 340 and 44 to 55, respectively. Kanab Dunes K/Rb and K/Ba values range from 237 to 300 and from 36 to 47, respectively. While these values are within similar ranges as other dune field across the southwestern U.S. (Muhs, 2017), both CPSD and Kanab Dunes plot separately from other dune fields in the southwestern United States.

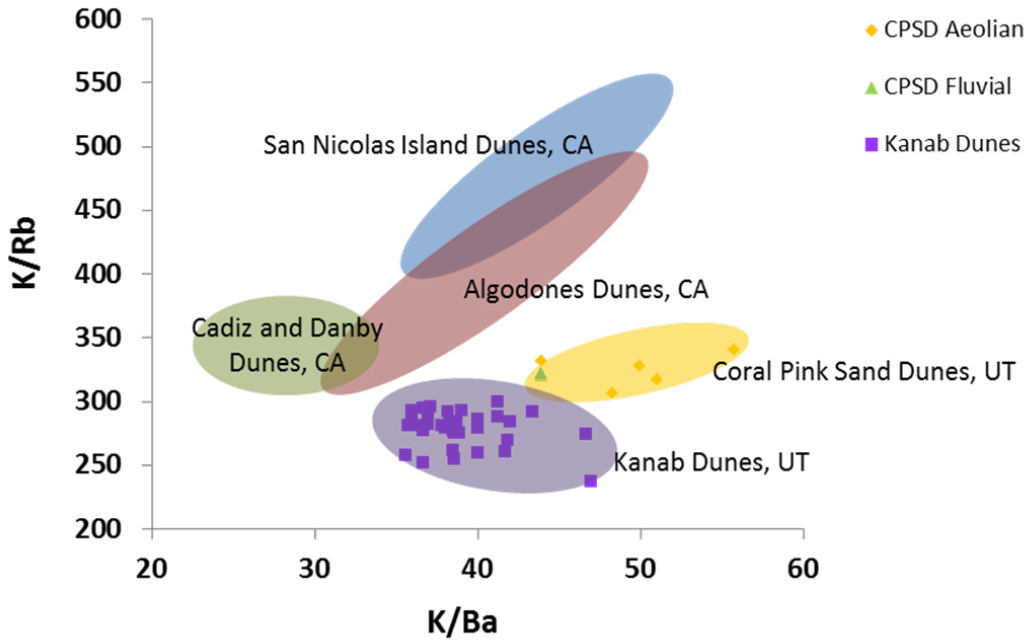

Figure 1.25 K/Rb and K/Ba values are a measure of K-feldspar composition, and have been shown to be effective discriminators for K-feldspars derived from different source sediments across North American dune fields (Muhs, 2017). CPSD and Kanab Dunes K/Rb:K/Ba values plot close to each other, but do not overlap. CPSD are more enriched in both Rb and Ba than the Kanab Dunes. CPSD K/Rb and K/Ba values range from 305 to 340 and 44 to 55, respectively. Kanab Dunes K/Rb and K/Ba values range from 237 to 300 and from 36 to 47, respectively. While these values are within similar ranges as other dune field across the southwestern U.S. (Muhs, 2017), both CPSD and Kanab Dunes plot separately from other dune fields. Ranges of values for Cadiz and Danby Dunes, San Nicolas Island Dunes, and Algodones Dunes are adapted from Muhs (2017).

1.5 Discussion of Results

The aeolian chronology presented in this study is constructed from five samples collected from a 2.5 km^2 area in sand ramps located in the CPSD. Here we develop a conceptual model for CPSD sand ramp formation based on the timing of aeolian deposition in different stratigraphic and geomorphic settings (Section 5.1) and identify local fluvial and alluvial inputs as the primary aeolian sediment source (Section 5.2). In Chapter 2 we compare the CPSD chronology to other regional dune chronologies, geomorphic records, and paleoclimate proxy records to identify spatial and temporal trends and to investigate climatic and environmental controls on aeolian activity.

1.5.1 Sand ramp formation

Stratigraphic positions of dated aeolian deposits are used to reconstruct the geomorphic history of the sand ramps. The aeolian chronostratigraphy presented in Section 4.1 shows that CPSD sand ramps were actively forming along the eastern margin of the lower dune field from ~150 ka until at least 12.5 ka. During this time hillslope material from the Moquith Mountains deposited directly onto the active dune field and preserved marginal dunes (CPSD-4, 9, 20, 22) and could have served as a local aeolian sediment source for the sand ramps (Rozar, 2015) (also see Section 5.2). The incision of Sand Canyon Wash occurred around ~12.5 ka (CPSD-4, OSL 12.40 ± 1.65 ka) and dissected the sand ramp system from the main dune field. Large-scale incision of Sand Canyon Wash channel produced an irreversible change in the morphology of the sand ramp system; the physical isolation of the sand ramps from the main dune field effectively separated it from its aeolian sediment source. Rather than migrate directly onto the sand ramps, aeolian sediments are now deposited into Sand Canyon Wash channel, where it is

stored until it is mobilized by ephemeral flows and ultimately removed from the CPSD system. The thick hillslope deposits have stabilized the surface of the sand ramps, allowing vegetation to establish. Figure 1.26 shows a conceptual model for sand ramp evolution over time.

Aeolian sediments preserved in different locations of the sand ramps represent two different modes of sand ramp formation. The aeolian deposits in the main channel of Sand Wash (CPSD-9, 20, and 22) located along the eastern margin of the active dune field indicate that the sand ramps formed on top of an older, larger active lower dune field. These deposits are migrating dunes, based on dip direction of beds that are generally parallel to the fault scarp and with modern parabolic dune dip directions. The deposits capping the aeolian units at these sites are fluvial and alluvial, but with generally smaller grains (pebbles to cobbles) compared to CPSD-3. CPSD-3 is in the tributary channel closer to the fault scarp, and the aeolian deposit is capped by alluvium and colluvium with much larger grain sizes (up to ~1 meter-diameter boulders). Higher energy mass movements occur closer to the fault scarp, and the sites farther from the fault scarp preserve relatively lower energy, distal deposits. The aeolian deposit at CPSD-3 is a climbing dune, with its dip direction is oriented perpendicular to the fault scarp. Unlike the migrating dues along the margin of the main dune field, this deposit most likely represents aeolian deposition directly onto the sand ramps, indicating coeval aggradation of alluvial, colluvial and aeolian units. Therefore, aeolian sediments preserved in different locations of the sand ramps represent two different modes of sand ramp formation: 1) the aeolian deposits in the main channel of Sand Wash indicate that the sand ramps capped and preserved the edges of a former, larger dune field, and 2) the

aeolian deposits located in the tributary channel closest to the Sevier fault scarp indicates coupled aggradation of sand ramps with coeval aeolian and hillslope deposition.

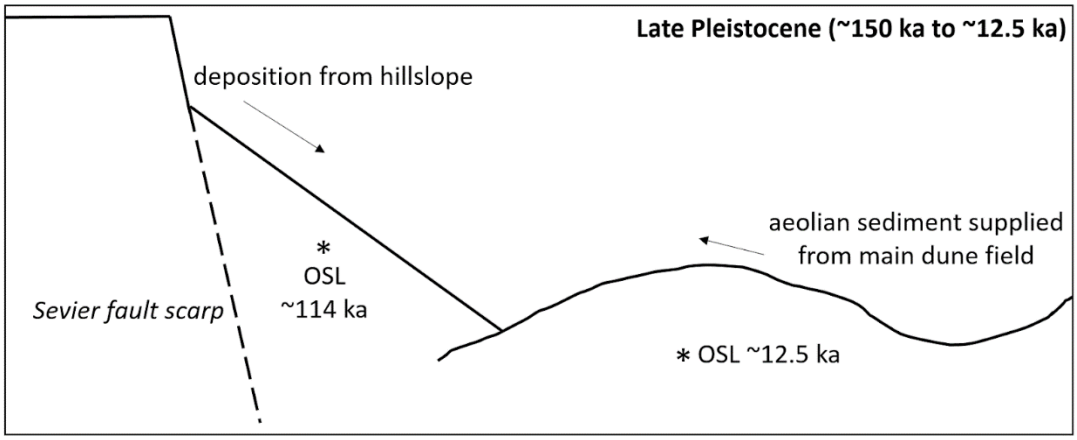

Figure 1.26 Conceptual model of sand ramp formation and dissection from the main dune field reconstructed from OSL dating of aeolian deposits preserved within the sand ramps. From 150 to 12.5 ka, aeolian sediments were deposited from the main dune field into the sand ramp system. Sometime after 12.5 ka Sand Wash incised, dissecting the sand ramps from the main dune field.

1.5.2 Sediment source

Several hypotheses have been proposed for the source of the aeolian dune sand. Gregory (1950) observed aeolian sediment entering the CPSD dune fields and identified the fault block mesas of the Moccasin Terrace as the likely aeolian sediment source supplied by the predominant southwesterly winds. Doelling, Davis, & Brandt (1989) proposes the highly erodible middle slope-forming “pink” member of the Navajo sandstone as the primary source, which is best developed and exposed to the west of the park near the Kane County boundary and the east in Johnson Wash Canyon (Figure 1.27). Ford, Gillman, Wilkins, Clement, & Nicoll (2010) also suggests that the main source is likely the middle member of the Navajo sandstone, but that it is supplied from fine-grained sand and gravel deposits that mantle the Moccasin Terrace along the base of the Moccasin Mountains to the southwest. These well-sorted sand grains are transported by the strong southwesterly prevailing winds, and the topographic expression of the Sevier fault scarp impedes the velocity of prevailing winds and sand is deposited along the scarp (Ford, Gillman, Wilkins, Clement, & Nicoll, 2010). Rozar (2015) suggests that, in addition to these previously mentioned sources, the alluvial and fluvial sediment that is eroded from the canyons of the Moquith Mountains and deposited directly into the dune field also serves as a local aeolian sediment source.

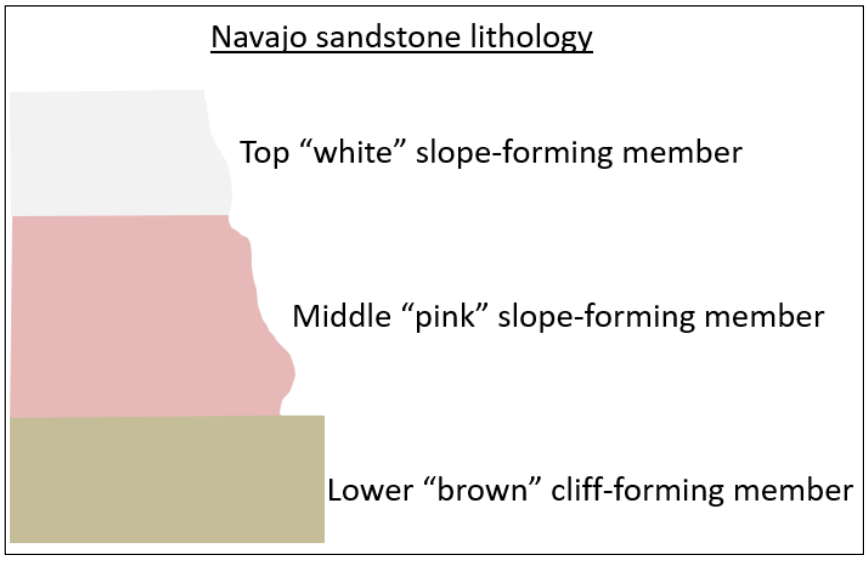

Figure 1.27 Navajo sandstone is classified into three distinct members based on color and erodibility (Doelling, 2008). The top “white,” slope-forming member forms the slope between the western edge of the dune field and Esplin Point. The middle “pink” slope-forming member is mostly covered by Quaternary aeolian deposits. The lowest part of the formation is the “brown” cliff-forming sandstone that caps the Moquith Mountains to the east of the dune field. Each of these three members outcrop near the Coral Pink Sand Dunes (Hayden, 2015). The lower “brown” member is exposed in the Sevier Fault scarp and caps the Moquith Mountains east of the CPSD dune field. The Kanab Dunes are located at the base of the White Cliffs, which is an exposure of the “white” member of Navajo sandstone. Differences in aeolian sediment chemistry may be due to these differences in lithology.

Plots of relative abundance of trace elements from the CPSD show little variability in aeolian sediment geochemistry over time and no difference between the sand ramp aeolian sediments and sediment from the surface of the active region of the lower dune field (Figure 1.24). Therefore, the CPSD aeolian sediment source has likely not changed over the past 150 ka. However, there are differences between the CPSD and the Kanab Dunes (Figures 1.24 and 1.25), showing that although these dune fields are only located approximately 10 kilometers apart, they are derived from different sources.

Differences in the geochemistry of the CPSD and Kanab Dune aeolian sediments suggests that these dune fields were formed from local sources, rather than via long

transport pathways. Local sources likely include nearby bedrock exposures and alluvial and fluvial deposits eroded from these exposures. Both the CPSD and Kanab dune fields are located at the base of cliffs carved into different formations of the Grand Staircase. The Kanab Dunes are located at the base of the White Cliffs, which is an exposure of the top “white” member of the Navajo sandstone. The lower “brown” member of the Navajo sandstone is exposed by the Sevier Fault scarp and caps the Moquith Mountains east of the lower CPSD dune field. The Sevier fault may also expose other bedrock lithologies (e.g., Kayenta Formation) beneath the Navajo sandstone that are covered by the sand ramps. Differences in aeolian sediment geochemistry may be due to these differences in lithology. Further work looking into geochemistry of local bedrock and alluvial and fluvial sediments would likely show that dune sediments are primarily derived from these nearby sources.

1.6 Conclusions

The CPSD sand ramps are primarily alluvial and fluvial depositional features, but have captured and preserved past periods of aeolian deposition as far as 150 ka. The CPSD sand ramps have preserved a record of aeolian activity that would have been erased in upper portion of the main, active dune field. The CPSD sand ramps formed from 150 ka to 12.5 ka, filling accommodation space at the base of the Sevier fault scarp. In addition to the structural control imposed by the Sevier fault scarp, overlaying hillslope deposits have also helped to preserved these older aeolian deposits. These features have remained stable during subsequent periods of climate change. Vegetation cover further stabilizes the surfaces and inhibits hillslope erosion and aeolian activity of the modern surfaces. CPSD dune geochemistry is distinct from nearby dune fields,

indicating that aeolian sediments are sourced locally, rather than transported long distances. This study provides the first evidence of aeolian activity during the last major glacial (MIS 6) on the Colorado Plateau and an opportunity to investigate hypotheses of landscape change during glacial-interglacial climate change. Chapter 2 compares the CPSD aeolian chronology to regional dune chronologies, geomorphic records, and paleoclimate proxy records from similar latitudes or elevations to understand how the landscapes of the Colorado Plateau were influenced by past climate change.

References

Aitken, M. J. (1985). Alpha particle effectiveness: numerical relationship between systems. *Ancient TL*, *3*(3), 22-25.

Aitken, M. J. (1998). *Introduction to optical dating: the dating of Quaternary sediments by the use of photon-stimulated luminescence*. Clarendon Press.

Anderson, R. E., & Christenson, G. E. (1989). Quaternary faults, folds, and selected volcanic features in the Cedar City 1 x 2 quadrangle. *Utah: Utah Geological and Mineral Survey Miscellaneous Publication*, 89-6.

Bateman, M. D., Thomas, D. S., & Singhvi, A. K. (2003). Extending the aridity record of the Southwest Kalahari: current problems and future perspectives. Quaternary International, 111(1), 37-49.

Bateman, M. D., Bryant, R. G., Foster, I. D., Livingstone, I., & Parsons, A. J. (2012). On the formation of sand ramps: A case study from the Mojave Desert. *Geomorphology*, *161*, 93-109.

Bhatia, M. R., & Crook, K. A. (1986). Trace element characteristics of graywackes and tectonic setting discrimination of sedimentary basins. *Contributions to mineralogy and petrology*, *92*(2), 181-193.

Bertram, S. (2003). Late Quaternary sand ramps in south-western Namibia-Nature, origin and palaeoclimatological significance.

Betancourt, J. L. (1990). Late quaternary biogeography of the Colorado Plateau. *Packrat middens: the last*, *40*(000), 259-292.

Birkeland, P. W., Machette, M. N., & Haller, K. M. (1991). *Soils as a tool for applied Quaternary geology* (No. 3). Utah Geological Survey.

Blott, S. J., & Pye, K. (2001). GRADISTAT: a grain size distribution and statistics package for the analysis of unconsolidated sediments. *Earth surface processes and Landforms*, *26*(11), 1237-1248.

Bogle, R., Redsteer, M. H., & Vogel, J. (2015). Field measurement and analysis of climatic factors affecting dune mobility near Grand Falls on the Navajo Nation, southwestern United States. *Geomorphology*, *228*, 41-51.

Bowers, J. E. (1984). Plant geography of southwestern sand dunes.

Brumbaugh, D. S. (2008). Seismicity and active faulting of the Kanab-Fredonia area of the southern Colorado Plateau. *Journal of Geophysical Research: Solid Earth*, *113*(B5).

Chase, B. M., & Thomas, D. S. (2006). Late Quaternary dune accumulation along the western margin of South Africa: distinguishing forcing mechanisms through the analysis of migratory dune forms. *Earth and Planetary Science Letters*, *251*(3-4), 318-333.

Doelling, H. H., Davis, F. D., & Brandt, C. J. (1989). *The geology of Kane County, Utah: Geology, mineral resources, geologic hazards* (Vol. 124). Utah Geological Survey.

Draut, A. E., Redsteer, M. H., & Amoroso, L. (2012). *Vegetation, Substrate, and Eolian Sediment Transport at Teesto Wash, Navajo Nation, 2009-2012*. US Department of the Interior, US Geological Survey.

Duller, G. A. (2008). Luminescence Dating: guidelines on using luminescence dating in archaeology.

Dumitru, T. A., Duddy, I. R., and Green, P. F. (1994). Mesozoic-Cenozoic burial, uplift, and erosion history of the west-central Colorado Plateau: *Geology*, v. 22, p. 499-502.

Ellwein, A. L., Mahan, S. A., & McFadden, L. D. (2015). Impacts of climate change on the formation and stability of late Quaternary sand sheets and falling dunes, Black Mesa region, southern Colorado Plateau, USA. *Quaternary international*, *362*, 87-107.

Ewing, R. C., & Kocurek, G. (2010). Aeolian dune-field pattern boundary conditions. *Geomorphology*, *114*(3), 175-187.

Folk, R. L., & Ward, W. C. (1957). Brazos River bar [Texas]; a study in the significance of grain size parameters. *Journal of Sedimentary Research*, *27*(1), 3-26.

Ford, R. L., Gillman, S. L., Wilkins, D. E., Clement, W. P., & Nicoll, K. (2010). Geology and Geomorphology of Coral Pink Sand Dunes State Park, Utah. *Geology of Utah's Parks and Monuments, Utah Geological Association*, 379-406.

Forman, S. L., Spaeth, M., Marín, L., Pierson, J., Gómez, J., Bunch, F., & Valdez, A. (2006). Episodic Late Holocene dune movements on the sand-sheet area, Great Sand Dunes National Park and Preserve, San Luis Valley, Colorado, USA. *Quaternary Research*, *66*(1), 97-108.

Galbraith, R. F. (1988). Graphical display of estimates having differing standard errors. Technometrics, 30(3), 271-281.

Galbraith, R. F., & Roberts, R. G. (2012). Statistical aspects of equivalent dose and error calculation and display in OSL dating: an overview and some recommendations. *Quaternary Geochronology*, *11*, 1-27.

Godfrey-Smith, D. I., Huntley, D. J., & Chen, W. H. (1988). Optical dating studies of quartz and feldspar sediment extracts. *Quaternary Science Reviews*, *7*(3-4), 373-380.

Goldschmidt, V. M. (1954). *Geochemistry* (Vol. 78, No. 2, p. 156). LWW.

Gowan, C., & Knisley, C. B. (2014). Distribution, abundance and conservation of the highly endemic Coral Pink Sand Dunes tiger beetle, Cicindela albissima Rumpp. *Biodiversity*, *15*(2-3), 119-129.

Gregory, H. E. (1950). *Geology and geography of the Zion Park region, Utah and Arizona* (No. 220).

Guérin, G., Mercier, N., Adamiec, G. (2011). Dose-rate conversion factors: update: Ancient TL 29, 5-8.

Hack, J. T. (1941). Dunes of the western Navajo country. *Geographical Review*, *31*(2), 240-263.

Halfen, A. F., Lancaster, N., & Wolfe, S. (2016). Interpretations and common challenges of aeolian records from North American dune fields. *Quaternary international*, *410*, 75-95.

Hao, Q., Guo, Z., Qiao, Y., Xu, B., & Oldfield, F. (2010). Geochemical evidence for the provenance of middle Pleistocene loess deposits in southern China. *Quaternary Science Reviews*, *29*(23-24), 3317-3326.

Hayden, J.M. (2013). Geologic Map of the Yellowjacket Canyon Quadrangle, Kane County, Utah, and Mohave County, Arizona: Utah Geological Survey, Map 256DM, doi: 10.1029/2007JB005278.

Holland, H. D. (1978). The chemistry of the atmosphere and oceans-(v. 1).

Huang, J., Yu, H., Guan, X., Wang, G. and Guo, R. (2016). Accelerated dryland expansion under climate change. *Nature Climate Change*, *6*(2), p.166.

Huntley, D. J., Godfrey-Smith, D. I., & Thewalt, M. L. (1985). Optical dating of sediments. *Nature*, *313*(5998), 105.

Jewell, P. W., & Nicoll, K. (2011). Wind regimes and aeolian transport in the Great Basin, USA. *Geomorphology*, *129*(1-2), 1-13.

Kerr, R. A. (2008). Climate change hot spots mapped across the United States.

Knisley, C. B., & Hill, J. M. (2001). Biology and conservation of the Coral Pink Sand Dunes tiger beetle, Cicindela limbata albissima Rumpp. *Western North American Naturalist, 61*(4), 381-394.

Kocurek, G., & Lancaster, N. (1999). Aeolian system sediment state: theory and Mojave Desert Kelso dune field example. *Sedimentology*, *46*(3), 505-515.

Kumar, A., Srivastava, P., & Meena, N. K. (2017). Late Pleistocene aeolian activity in the cold desert of Ladakh: a record from sand ramps. *Quaternary International, 443*, 13-28.

Lachniet, M., Asmerom, Y., Polyak, V., & Denniston, R. (2017). Arctic cryosphere and Milankovitch forcing of Great Basin paleoclimate. Scientific reports, 7(1), 12955.

Lancaster, N. (2008). Desert dune dynamics and development: insights from luminescence dating. *Boreas, 37*(4), 559-573.

Lancaster, N., & Tchakerian, V. P. (1996). Geomorphology and sediments of sand ramps in the Mojave Desert. *Geomorphology*, *17*(1-3), 151-165.

Lancaster, N., Wolfe, S., Thomas, D., Bristow, C., Bubenzer, O., Burrough, S., ... & Singhvi, A. (2016). The INQUA dunes atlas chronologic database. *Quaternary international, 410*, 3-10.

Lomax, J., Hilgers, A., Twidale, C. R., Bourne, J. A., & Radtke, U. (2007). Treatment of broad palaeodose distributions in OSL dating of dune sands from the western Murray Basin, South Australia. *Quaternary Geochronology*, *2*(1-4), 51-56.

Lund, W. R., Knudsen, T. R., & Vice, G. S. (2008). Paleoseismic reconnaissance of the Sevier fault, Kane and Garfield Counties, Utah: Utah Geological Survey Special Study 122, 31 p.

Mayer, J. H., & Mahan, S. A. (2004). Late Quaternary stratigraphy and geochronology of the western Killpecker Dunes, Wyoming, USA. *Quaternary Research, 61*(1), 72-84.

Mayya, Y. S., Morthekai, P., Murari, M. K., & Singhvi, A. K. (2006). Towards quantifying beta microdosimetric effects in single-grain quartz dose distribution. *Radiation Measurements*, *41*(7-8), 1032-1039.

Muhs, D. R., Bettis III, E. A., Aleinikoff, J. N., McGeehin, J. P., Beann, J., Skipp, G., ... & Benton, R. (2008). Origin and paleoclimatic significance of late Quaternary loess in Nebraska: evidence from stratigraphy, chronology, sedimentology, and geochemistry. *Geological Society of America Bulletin*, *120*(11-12), 1378-1407.

Muhs, D. R. (2017). Evaluation of simple geochemical indicators of aeolian sand provenance: Late Quaternary dune fields of North America revisited. *Quaternary Science Reviews*, *171*, 260-296.

Munson, S. M., Belnap, J., & Okin, G. S. (2011). Responses of wind erosion to climate-induced vegetation changes on the Colorado Plateau. *Proceedings of the National Academy of Sciences*, *108*(10), 3854-3859.

Murray, A. S., & Wintle, A. G. (2000). Luminescence dating of quartz using an improved single-aliquot regenerative-dose protocol. *Radiation measurements*, *32*(1), 57-73.

Nelson, M. S., Gray, H. J., Johnson, J. A., Rittenour, T. M., Feathers, J. K., & Mahan, S. A. (2015). User guide for luminescence sampling in archaeological and geological contexts. *Advances in Archaeological Practice*, *3*(2), 166-177.

Pelletier, J. D., Brad Murray, A., Pierce, J. L., Bierman, P. R., Breshears, D. D., Crosby, B. T., ... & Lancaster, N. (2015). Forecasting the response of Earth's surface to future climatic and land use changes: A review of methods and research needs. *Earth's Future*, *3*(7), 220-251.

Parsons, T. (1995). The Basin and Range Province, in Olsen, K. H., editor, Continental rifts: evolution, structure, tectonics, *Dev. Geotect.*, v. 25, ElSevier, p. 277-324.

Prăvălie, R. (2016). Drylands extent and environmental issues. A global approach. *Earth-Science Reviews*, *161*, 259-278.

Prescott, J. R., & Hutton, J. T. (1994). Cosmic ray contributions to dose rates for luminescence and ESR dating: large depths and long-term time variations. *Radiation measurements*, *23*(2-3), 497-500.

Redsteer, M. H., Bogle, R. C., & Vogel, J. M. (2011). *Monitoring and analysis of sand dune movement and growth on the Navajo Nation, southwestern United States*. US Department of the Interior, US Geological Survey.

Reheis, M.C., Reynolds, R.L., Goldstein, H., Roberts, H.M., Yount, J.C., Axford, Y., Cummings, L.S. and Shearin, N. (2005). Late Quaternary eolian and alluvial response to paleoclimate, Canyonlands, southeastern Utah. *Geological Society of America Bulletin*, *117*(7-8), pp.1051-1069.

Rowell, A. L., Thomas, D. S., Bailey, R. M., & Holmes, P. J. (2018). Sand ramps as palaeoenvironmental archives: Integrating general principles and regional contexts through reanalysis of the Klipkraal Sands, South Africa. *Geomorphology*, *311*, 103-113.

Rowley, P. D., Anderson, J. J., Williams, P. L., and Fleck, R. J. (1978). Age of structural differentiation between the Colorado Plateaus and Basin and Range provinces, southwestern Utah: *Geology*, v. 6, p. 51-55.

Rozar, E.J. (2015). Defining Antecedent Topography at Coral Pink Sand Dunes, Kane County, Utah: The Influence of Structural Controls on Dune-Field Boundary Conditions and Holocene Landscape Evolution, Boise State University Theses and Dissertations, paper 987.

Singhvi, A. K., & Porat, N. (2008). Impact of luminescence dating on geomorphological and palaeoclimate research in drylands. *Boreas*, *37*(4), 536-558.

Stokes, S. and Breed, C.S. (1993). A chronostratigraphic re-evaluation of the Tusayan Dunes, Moenkopi Plateau and southern Ward Terrace, northeastern Arizona. *Geological Society, London, Special Publications, 72*(1), pp.75-90.

Taylor, S. R., & McLennan, S. M. (1985). The continental crust: its composition and evolution.

Telfer, M. W., Mills, S. C., & Mather, A. E. (2014). Extensive quaternary aeolian deposits in the Drakensberg foothills, Rooiberge, South Africa. *Geomorphology*, *219*, 161-175.

Thomas, D. S., & Burrough, S. L. (2012). Interpreting geoproxies of late Quaternary climate change in African drylands: implications for understanding environmental change and early human behaviour. *Quaternary International*, *253*, 5-17.

Wannamaker, P. E., Bartley, J. M., Sheehan, A. F., Jones, C. H., Lowry, A. R., Dumitru, T. A., . . . Wolfe, J. A. (2001). Great Basin-Colorado Plateau transition in central Utah: An interface between active extension and stable interior, 38 p.

Wells, S. G., McFadden, L. D., & Schultz, J. D. (1990). Eolian landscape evolution and soil formation in the Chaco dune field, southern Colorado Plateau, New Mexico. *Geomorphology*, *3*(3-4), 517-546.

Wentworth, C. K. (1922). A scale of grade and class terms for clastic sediments. *The journal of geology*, *30*(5), 377-392.

Western Regional Climate Center, www.wrcc.dri.edu/ (Accessed July 2018, monthly climate summary record from December 1899 to June 2016)

Wilkins, D.E., Ford, R.L., Clement, W.P., and Nicoll, K. (2005). Little Ice Age behavior of the Coral Pink Sand Dunes, Kane County, Utah, Abstracts with Programs - GSA, v. 37, p. 426.

Wilkins, D., Ford, R. L., Clement, W., & Nicoll, K. (2007). Multiproxy evidence for late Holocene climate change. In *Coral Pink Sand Dunes, Utah (abstract): Association of American Geographers 2007 Annual Meeting (San Francisco, CA) Online Program*.

Wilkins, D. E., & Ford, R. L. (2007). Nearest neighbor methods applied to dune field organization: the Coral Pink Sand Dunes, Kane County, Utah, USA. *Geomorphology*, *83*(1-2), 48-57.

CHAPTER 2: SAND RAMPS RECORD LATE PLEISTOCENE AEOLIAN ACTIVITY DURING GLACIAL/INTERGLACIAL TRANSITIONS, SOUTHWESTERN USA

Here the CPSD aeolian chronology is compared to regional dune chronologies, geomorphic records, and paleoclimate proxy records from similar latitudes or elevations to understand how the landscapes of the Colorado Plateau were influenced by past climate change. Placing the CPSD chronology within the context of regional landscape and climate proxies creates a more robust record of landscape activity on the Colorado Plateau, and allows interpretations beyond the local geomorphic system. Synchronous activity in individual dune fields across a region can indicate a common response to regional climate forcings. This chapter is written as a manuscript to be submitted as a Brief Research Report to Frontiers in Earth Science - Quaternary Science, Geomorphology and Paleoenvironment Section.

2.1 Abstract

This study provides new optically stimulated luminescence (OSL) age data for aeolian activity preserved within sand ramps adjoining the Coral Pink Sand Dunes (CPSD), Utah. While many aeolian features are prone to preservation bias in landscape studies, sand ramps are topographically-controlled features that can preserve long records of landscape change in drylands. Topographic and structural (i.e., fault scarp) controls present in the CPSD sand ramp system have preserved aeolian deposits from the late Pleistocene. By comparing the ages from our sampled aeolian units to climate proxies,

we show that aeolian activity during the late Pleistocene-Holocene transition (MIS 2/1; OSL ~12.5 ka) occurred under conditions that were relatively wetter and cooler than present. Dune activity during the MIS 6 and MIS 5 (OSL ~145 ka to OSL ~118 ka) spans a range of climate conditions during a period of rapid and abrupt change. Rather than a response to any specific climate regime, late Pleistocene aeolian deposits may record changes in sediment supply under relatively wet and variable conditions.

2.2 Introduction

Projected climate change is expected to have large impacts on arid regions of the world (e.g., Huang, Yu, Guan, Xu, & Oldfield, 2016) and it is becoming increasingly important to understand how these sensitive landscapes respond to change. Inland, continental dune fields respond to changes in climate and the surrounding environment and are an important source for understanding interactions between Earth's surface, atmosphere, and biosphere in drylands (Lancaster, 2008). The Colorado Plateau physiographic province is located in the dry interior of the southwestern United States; low effective moisture, strong winds, and variable climate limit perennial vegetation cover, making its landscapes highly susceptible to wind erosion (Redsteer, Bogle, & Vogel, 2011). Reconstructing past phases of dune activity can help to quantify the magnitude, frequency, and thresholds of activity and help to understand how wind has shaped these landscapes in the past.

The majority of aeolian features on the Colorado Plateau were formed during the late Pleistocene, and have since experienced localized reactivation of previously stabilized deposits throughout the Holocene in response to drought conditions (Wells, McFadden, & Schultz, 1990; Reheis et al., 2005; Ellwein, Mahan, &, McFadden, 2015).

Reactivation of dunes results in a preservation bias toward younger deposits (Lancaster et al., 2016). While many aeolian features (e.g., migrating dunes, sand sheets) have low preservation potential, sand ramps are protected by topography and therefore have the potential to preserve longer records of aeolian activity (e.g., Kumar, Srivastava, & Meena, 2017). Targeting geomorphic settings that are conducive to preserving older records is critical to reconstructing longer and more complete records of landscape change.

Here we present new optically stimulated luminescence (OSL) ages of aeolian deposits preserved in sand ramps located adjacent to the Coral Pink Sand Dunes (CPSD), a fault-bounded dune field located on the northern Colorado Plateau (Figure 2.1). Previous OSL work in the active region of the CPSD dune field identifies three distinct phases of late Holocene aeolian activity during periods of regional drought (Wilkins, Ford, Clement, & Nicoll, 2005) that correspond to timing of dune activity recorded in other dune fields across the Colorado Plateau (Wells, McFadden, & Schultz, 1990; Stokes & Breed, 1993). CPSD dunes stabilized at the same time that nearby arroyos were aggrading (Hereford, 2002; Summa-Nelson & Rittenour, 2011; Townsend, Nelson, Rittenour, & Pederson, 2019) with the onset of relatively cooler and wetter conditions during the Little Ice Age (1440-1860 CE; Grove, 1988). While the active dune field records recent reactivation of dune deposits throughout the late Holocene, the CPSD sand ramps have captured and preserved past periods of aeolian deposition from as early as 150 ka. We compare this extended chronology to other dune chronologies, records of deposition in nearby fluvial and alluvial systems, and paleoclimate reconstructions to identify possible drivers of dune activity.

2.2.1 Study Area

The Coral Pink Sand Dunes (CPSD) are a 14 km^2 dune field located approximately 15 kilometers west of Kanab, Utah on the Vermillion Cliffs of the Grand Staircase on the northern Colorado Plateau (Figure 2.1). The dune field is located within a high elevation, semi-arid steppe environment and ranges in elevation from 1,700 to 2,000 meters. Modern average annual minimum and maximum temperatures are 4°C and 21°C, respectively. Precipitation occurs predominantly during the winter and summer while spring and fall are typically dry. Total annual precipitation is 35 cm and total snowfall is 57 cm (Western Regional Climate Center accessed July 2018). The primary bedrock unit exposed in the dune field is Jurassic Navajo sandstone, a high-angle cross-bedded aeolian unit. The Sevier Normal Fault divides the CPSD into two distinct upper (northern) and lower (southern) fields, and the eastern edge of the southern dune field is bound by the steeply dipping faultline scarp (Hayden, 2013). The lower dune field exists within a structurally controlled graben (Sand Canyon) bound by a series of shallow, east-dipping antithetic faults running parallel to the regional Sevier fault (Rozar, 2015). The dune field is a depositional sink for aeolian, alluvial, and fluvial sediments derived both locally and externally. From south to north, the dune field transitions from stabilized sand sheets to partially stabilized dunes and eventually into a series of actively migrating dune forms in its northern, active core (Ford, Gillman, Wilkins, Clement, & Nicoll, 2010). Large sand ramps, the focus of this study, are situated along the base of the Sevier fault scarp and are separated from the active dune field by Sand Canyon Wash, an incised ephemeral channel with several large tributaries that flows south along the eastern margin of the lower dune field.

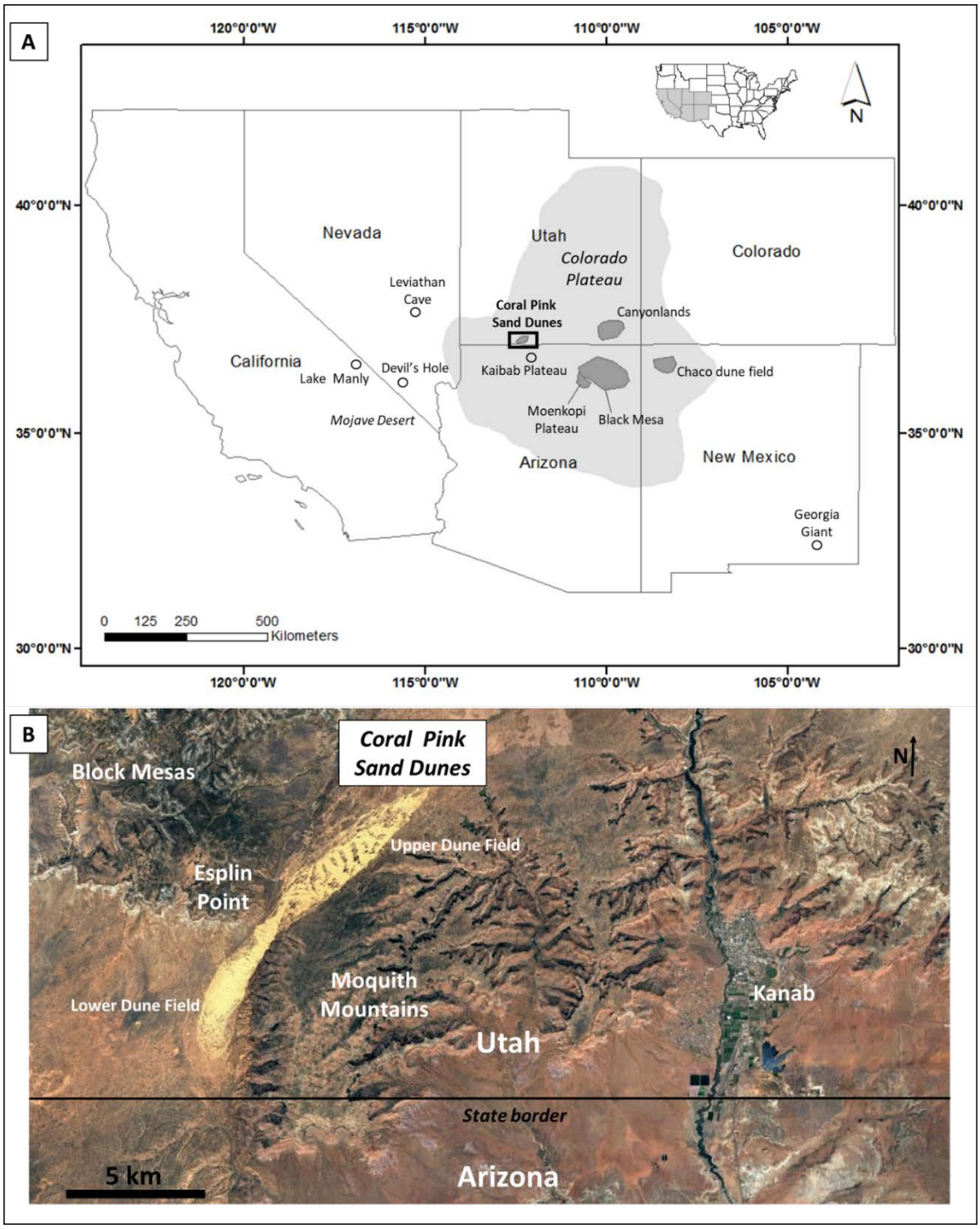

Figure 2.1 The Coral Pink Sand Dunes (CPSD) are located in southern Utah on the Colorado Plateau. The upper map shows other dune fields and locations of paleoclimate records referenced in the text.

2.3 Methods

2.3.1 Stratigraphy

Sand ramp stratigraphy is described from natural exposures where ephemeral fluvial channels incised through the sand ramps. Exposures were cleared with a shovel and each stratigraphic unit is described noting the texture, composition, bedding structure, and color. When applicable, soil characteristics are described according to Birkeland, Machette, & Haller (1991). Units were characterized as aeolian, fluvial, or alluvial based on grain size, sorting, and primary bedding structures. We identified aeolian units based on observations of homogenous, well-sorted sand units with primary bedding structures. Five aeolian units were sampled and analyzed using optically stimulated luminescence (OSL) (see sample locations map, Figure 2.2).

2.3.2 Geochronology

Luminescence dating estimates the last time sediment was exposed to sunlight by directly dating mineral grains (Huntley, Godfrey-Smith, & Thewalt, 1985), providing a way to date past periods of aeolian activity (Duller, 2008). Luminescence dating works on the premise that some mineral grains, such as quartz and feldspar, are able to store energy within their crystal lattice. Exposure to sunlight during transport removes stored energy, bleaching the luminescence signal to zero. After burial, grains are subject to ionizing radiation from surrounding sediment and cosmic radiation that rebuild the luminescence signal. Luminescence dating measures the signal of a buried grain to determine when it was last exposed to sunlight and an OSL age is estimated by dividing the equivalent dose (D_E) (units of Grays) of radiation the sediment was exposed to during burial by the environmental dose rate (D_R) (units of Grays per ka) of the surrounding

sediment to yield an age (ka). The D_E is calculated from the amount of laboratory radiation needed to induce a luminescence signal equal to the natural luminescence signal of the sample, which is proportional to the amount of radiation the sample received during burial. The D_R of the surrounding sediment is calculated from concentrations of radioisotopes from surrounding sediment and cosmic radiation.

OSL samples were taken by pounding an opaque metal tube horizontally into the outcrop with a rubber mallet. Samples were prepared at Utah State University Luminescence Laboratory (USULL) under dim, amber light. Samples were wet sieved to isolate the desired target grain size fraction of 90 to 150 µm. Quartz grains were isolated with sodium polytungstate with a density of 2.7 g/cm^3. Samples were treated with hydrofluoric acid to remove residual feldspar, hydrochloric acid to remove carbonates, and bleach to remove organic material. Optical measurements were made on a Risø TL/OSL DA-20 reader at USULL. Luminescence signal was stimulated with blue-green (470 nm wavelength) light emitting diodes at 90% power at 125ºC for 40 seconds. The resulting luminescence signal was filtered with a UV filter (280-380 nm). For each sample, D_E was estimated using the single-aliquot regenerative (SAR) protocol for quartz sand (Wintle & Murray, 2000) and then calculated based on the Central Age Model by Galbraith & Roberts (2012). Standardized D_E estimates and standard error for each aliquot are displayed on radial plots (Supplementary Material Figure 1).

For each OSL sample, one homogenized environmental dose rate (D_R) sample was taken from a 15 cm radius surrounding the D_E sample location. An additional sample was taken to measure in-situ water content. The D_R samples were analyzed using inductively coupled plasma mass spectrometry (ICP-MS) and inductively coupled plasma

atomic emission spectroscopy (ICP-AES) to determine radioisotope elemental concentrations of U, Th, K, and Rb. D_R was derived from radioisotope concentrations converted with factors from Guérin et al. (2011), the contribution of cosmic dose rate, which is estimated based on altitude, latitude, and depth below surface of the sample (Prescott & Hutton, 1994) and corrected for water content. Dose rate information is included in Supplementary Material Table 1.

.

2.4 Results

The CPSD sand ramps are composed primarily of alluvial and fluvial sediments interbedded with aeolian units. Five aeolian units (CPSD-3, 4, 9, 20, and 22) were identified in natural exposures within the sand ramps and dated with OSL (Figure 2.2). All aeolian units are unconsolidated, moderately well-sorted to moderately sorted medium- to fine-grained sand with some silt and clay (Table 1) and were capped and stabilized by alluvial or fluvial deposits (Figure 2.2). Detailed stratigraphic descriptions are available in Supplementary Material Figure 2. Topographic and structural (i.e., fault scarp) controls present in the CPSD sand ramp system have preserved aeolian deposits as early as ~150 ka to as late as ~12.5 ka (Table 1).

CPSD sand ramps were actively forming along the eastern margin of the lower dune field from ~150 ka until at least 12.5 ka. During this time hillslope material from the Moquith Mountains deposited directly onto the active dune field and preserved marginal dunes (CPSD-4, 9, 20, 22). Sand Wash incised sometime since 12.5 ka (CPSD-4, OSL 12.40 ± 1.65 ka) and dissected the sand ramp system from the main dune field. Incision of Sand Canyon Wash channel produced an irreversible change in the morphology of the sand ramps; the physical isolation of the sand ramps from the main dune field effectively separated it from its aeolian sediment source. Rather than migrate directly onto the sand ramps, aeolian sediments are now deposited into Sand Canyon Wash channel, where it is stored until it is mobilized by ephemeral flows and ultimately removed from the CPSD system. The thick hillslope deposits have stabilized the surface of the sand ramps, allowing vegetation to establish.

Table 2.1 OSL age estimates and sediment characteristics.

	Aeolian				
Site ID	**CPSD-3**	**CPSD-4**	**CPSD-9**	**CPSD-20**	**CPSD-22**
USU sample ID	**USU-2593**	**USU-2592**	**USU-2594**	**USU-2756**	**USU-2758**
OSL measurements (provided by USULL)					
# aliquots[1]	17 (26)	18 (27)	14 (21)	19 (26)	18 (22)
D_R (Gy/ka)	1.04 ± 0.05	1.59 ± 0.07	0.88 ± 0.05	0.74 ± 0.04	1.21 ± 0.06
D_E[2] **± 2σ (Gy)**	118.98 ± 17.56	19.74 ± 1.76	125.69 ± 12.92	90.46 ± 10.08	180.76 ± 16.05
OD[3] **(%)**	25.3 ± 6.1	13.2 ± 4.3	13.8 ± 4.7	20.4 ± 4.6	16.3 ± 3.6
OSL age± 2σ (ka)[4]	**114.7 ± 20.6**	**12.40 ± 1.65**	**142.7 ± 20.4**	**123.0 ± 18.6**	**149.8 ± 20.0**
Deposit characteristics					
Dry Color[5]	5YR 5/6	5YR 6/8	5YR 5/8	5YR 6/8	5YR 6/8
Wet Color[5]	2.5YR 4/8	5YR 6/8	5YR 5/6	5YR 5/8	5YR 5/8
% Sand[6]	100	98.2	96.3	100	98
% Silt[6]	0	1.8	3.6	0	2
% Clay[6]	0	0	0.1	0	0

[1] Age analysis using the single-aliquot regenerative-dose procedure of Wintle & Murray (2000) on 2mm small-aliquots of quartz sand. Number of aliquots used in age calculation and number of aliquots analyzed in parentheses.
[2] Equivalent dose (D_E) calculated using the Central Age Model (CAM) of Galbraith & Roberts (2012).
[3] Overdispersion represents variance in DE data beyond measurement uncertainties, value >20% may indicate significant scatter due to depositional or post-depositional processes.
[4] Final age estimates are reported at two sigma standard deviation of the age uncertainty D_E measurements.
[5] Color determined with Munsell Color Chart.
[6] Grain size analyses by laser light diffraction and results summarized with GRADISTAT.

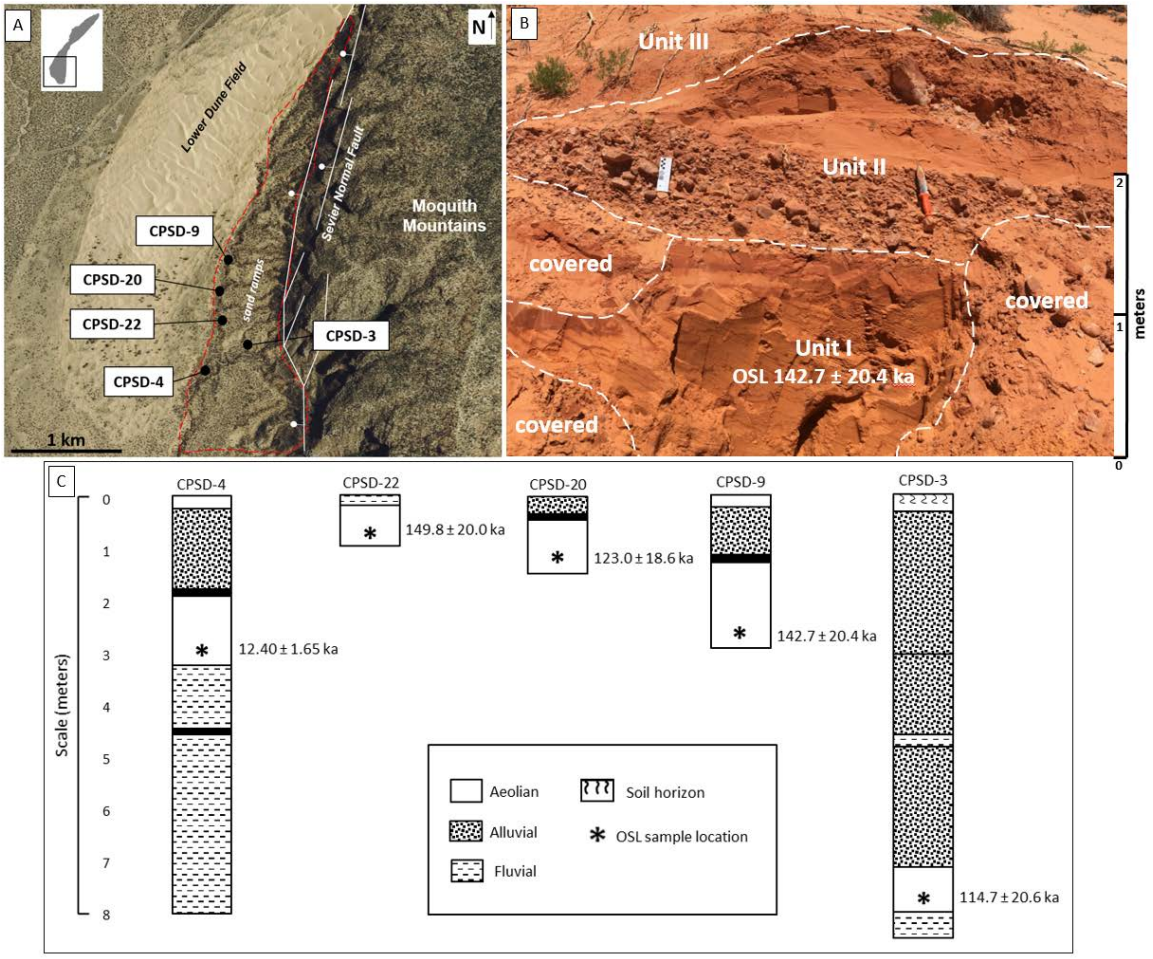

Figure 2.2 A) The Sevier fault normal fault runs through the CPSD, dividing the dune field into two separate dune fields. This study focuses on the sand ramps along the base of the Sevier fault normal fault scarp. Five aeolian units are identified in natural exposures within the sand ramps (CPSD-3, 4, 9, 20, 22). B) An example of an aeolian unit preserved within the sand ramps by overlaying fluvial and alluvial deposits. CPSD-9 is located in the main channel of Sand Wash. Unit I, an aeolian unit dated at OSL 142.7 ± 20.4 ka, is capped by Unit II, a fluvial deposit. C) Simplified chronostratigraphic profiles containing OSL-dated aeolian units. Sand ramps stratigraphy is primarily fluvial and alluvial deposits interbedded with aeolian units. All OSL-dated aeolian units are capped and preserved by fluvial or alluvial deposits.

2.5 Discussion

The CPSD sand ramps are primarily alluvial and fluvial depositional features, but have captured and preserved past periods of aeolian deposition. In addition to the structural control imposed by the Sevier fault scarp, overlaying hillslope deposits have also helped to preserve aeolian deposits from the end of the last glacial (MIS 6) through MIS 5d/e (OSL ~145 ka to OSL ~118 ka) and during the late Pleistocene-Holocene (LPH) transition (OSL ~12.5 ka). The aeolian chronology preserved in the CPSD sand ramps records activity during both glacial and interglacial climates, with ages that cluster around major transitions from glacial to interglacial conditions (Figure 2.3). The CPSD sand ramps have persisted during subsequent periods of climate change showing that these landforms are stable. Here the CPSD aeolian chronology is compared to regional dune chronologies, geomorphic records, and paleoclimate reconstructions to identify past drivers of activity.

Aeolian activity recorded in the CPSD sand ramps at 12.5 ka occurred under relatively wet and cool conditions compared to present, but during a time of major climate change during a transition from glacial to interglacial conditions (Figure 2.3). The late Pleistocene-Holocene transition (MIS 2/1) is characterized by the transition from the cooler and wetter Pleistocene climates into the warmer and drier Holocene conditions, but was briefly interrupted by the Younger Dryas, a cool and dry period that lasted from 12.9 to 11.7 ka (Rasmussen et al., 2006). Strengthening of the summer monsoon resulted in increased summer precipitation and effectively wetter conditions than present across the southwestern United States (U.S.) at this time (Betancourt, Van Devender, & Martin, 1990; Polyak, Rasmussen, & Asmerom, 2004). On the Kaibab Plateau, located

approximately 15 kilometers southeast from the study site, vegetation indices record major shifts in plant species to higher elevations with the onset of warmer and drier conditions from 15 to 9 ka, but conditions were still relatively cool and wet at 12 ka (Weng & Jackson, 1999). During this time, pluvial lakes across the Great Basin and southern North America experience their last high stands, and afterward began to decrease and never return to fullness (e.g., Lake Mojave, California, Wells et al., 2003; Lake Lahontan, Nevada and Lake Estancia, New Mexico, Lyle et al., 2012; Baldwin Lake, California, Glover et al., 2017). While these pluvial lakes existed at lower elevations than the study site, the Colorado Plateau generally receives more precipitation than the lower elevation regions of the Great Basin and southwest deserts. As pluvial lakes desiccated, alluvial fans across the southwestern U.S. were aggrading in response to changing conditions (e.g., Sohn, Mahan, Knott, & Bowman, 2007).

CPSD aeolian activity during late MIS 6 and MIS 5e/5d occurred under a range of climate conditions, including large changes in regional precipitation and temperature that resulted in major changes in hydrologic systems across the southwestern U.S. (Figure 2.3). The southward expansion of the Laurentide ice sheet during MIS 6 pushed the polar jet stream south, resulting in increased winter precipitation and considerably wetter and colder conditions in the southwestern U.S. (Asmerom, Polyak, & Burns, 2010). Groundwater discharge deposits in the Mojave Desert of southeastern California indicate a high water table and wetland environment from 185 to 140 ka (Mahan, Miller, Menges, & Yount, 2007). Lake Manly in Death Valley, California sustained perennial lakes through MIS 6 until 120 ka, followed by drier conditions that continued until 100 ka (Lowenstein et al., 1999). Speleothem records from New Mexico show a rapid shift in

temperature and decrease in precipitation during MIS 5e, before returning to relatively wetter and colder conditions in MIS 5d (Brook, Ellwood, Railsback, & Cowart, 2006).

CPSD dune activity at 12.5 ka coincides with activity in other dune fields across the Colorado Plateau (Wells et al., 1990; Reheis et al., 2005; Ellwein, Mahan, &, McFadden, 2015) (Figure 2.3). Synchronous, geographically-widespread dune activity may indicate a regional-scale response to changing climate and environmental conditions during the late Pleistocene-Holocene transition. However, earlier records of dune activity throughout the late Pleistocene are not synchronous between dune fields; CPSD dune activity during MIS 6 and MIS 5e/5d predate other dune records on the Colorado Plateau (Figure 2.3). The current chronology for the Colorado Plateau records asynchronous periods of aeolian activity throughout the late Pleistocene, including late MIS 5, MIS 3, and MIS 2 under a range of climate conditions (Wells, McFadden, & Schultz, 1990; Reheis et al., 2005; Manning, 2010; Ellwein, Mahan, &, McFadden, 2015).

Isolated records of activity from different dune fields across the Colorado Plateau under a range of climate conditions could be due to one or a combination of the following: 1) presevation bias that favors more recent activity, 2) sampling bias, which could be rectified by more sampling of stabilized aeolian deposits, or, 3) indicate that activity is driven by local environmental factors, rather than regional forcings. Activity driven by local conditions could be attributed to changes in sediment supply in response to changes in hydrologic or geomorphic conditions. Dune activity in supply-limited dune fields has been attributed to changes in nearby fluvial or lacustrine environments, which provide a source of sediment to aeolian systems (e.g., Tchakerian & Lancaster, 2002; Draut, Redsteer, & Amoroso, 2012; Yu, ZhongPing, Ping, Tong, & QuiFang, 2015). Work in

nearby dune fields show that late Pleistocene dune activity in this region corresponds to periods of high sediment supply in nearby fluvial and alluvial systems. Ellwein, Mahan, &, McFadden (2015) suggest that late Pleistocene dune activity on the Black Mesa region of the Colorado Plateau during MIS 3/2 (30 to 16 ka) may have been driven by high sediment supply in the Little Colorado River under relatively wet and variable conditions. Coeval alluvial and aeolian activity during the late Pleistocene-Holocene transition in the Canyonlands region of Utah is attributed to increased sediment supply under changing climate conditions (Reheis et al., 2005). Within the CPSD, hillslope deposits could have supplied a local source of aeolian sediment to the sand ramps. The sand ramp stratigraphy is composed of interfingered colluvial, alluvial, fluvial, and aeolian sediments (Figure 2.2), indicating coeval aggradation of these different deposit types. CPSD dune geochemistry is distinct from nearby dune fields, indicating that sediments are sourced locally.

Hillslope sediment accumulates under cooler and wetter glacial climates, which promote increased vegetation cover and bedrock weathering. Erosion of accumulated sediment occurs during transitions from glacial climates to relatively warmer and drier interglacial climates because of increased precipitation intensity and streamflow (Bull, 1991). For example, as alluvial fans aggraded during the late Pleistocene-Holocene transition sediment loads in ephemeral drainages increased (Sohn, Mahan, Knott, & Bowman, 2007). Late Pleistocene aeolian activity on the Colorado Plateau adds to this story, showing that increased fluvial sediment loads during glacial-interglacial climate change provided sediment to be entrained by wind and leading to the formation of aeolian features in this region. While actively migrating dune fields record recent phases of

reactivation, topographically-controlled aeolian deposits are not prone to reactivation and therefore preserve a record of initial sand emplacement. Additional work reconstructing aeolian activity from topographically-controlled deposits could help to better understand sediment cycling between alluvial, fluvial, and aeolian systems in drylands.

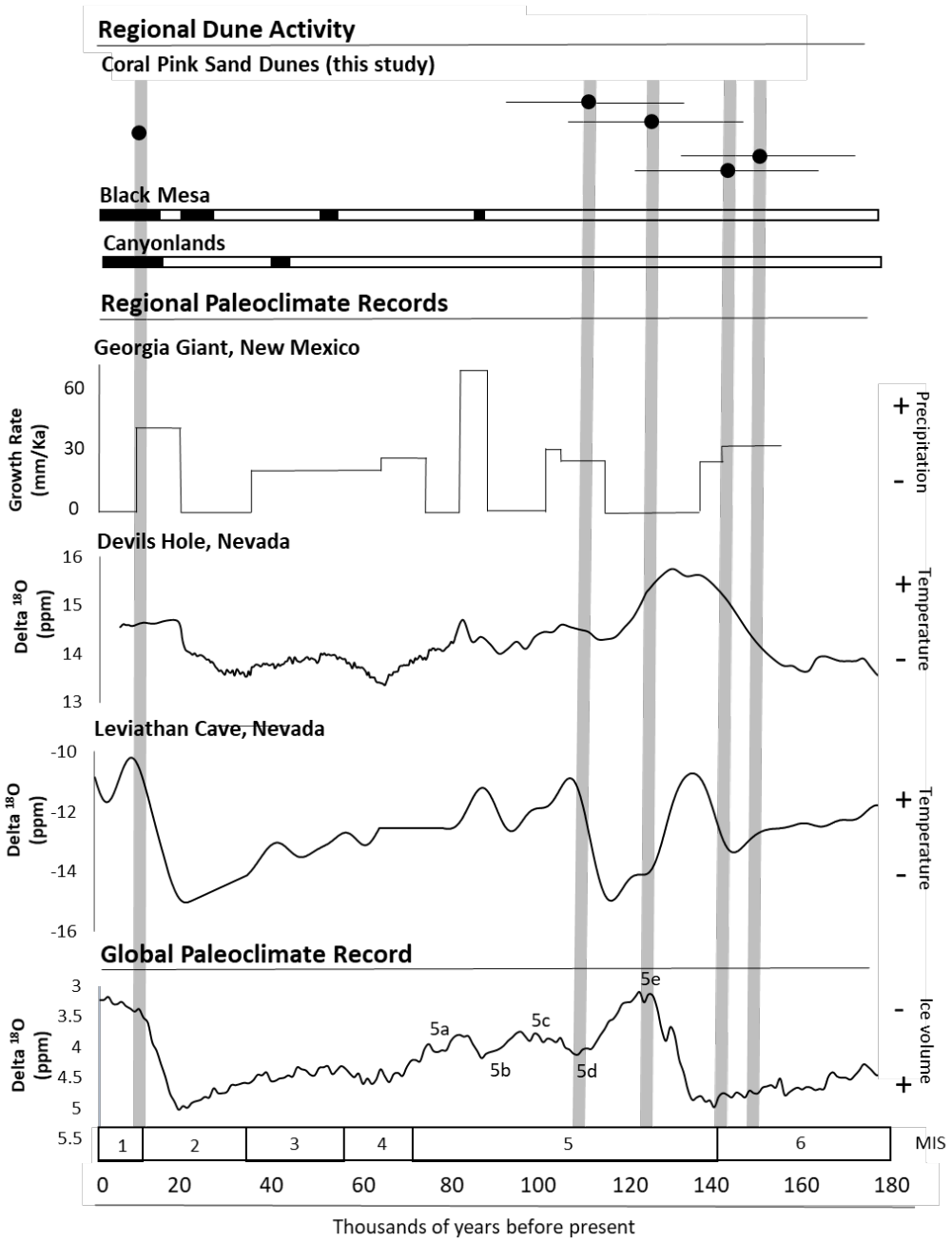

Figure 2.3. Timing of aeolian activity reconstructed from CPSD sand ramps compared to other dune chronologies from Colorado Plateau, paleoclimate reconstructions form the southwestern United States, and global climate records. CPSD dune activity is shown as five OSL age estimates with error bars (2 sigma standard error) presented in Table 1. Black Mesa aeolian activity summarized from various OSL dune chronologies: 92 ka in Tsegi Canyon, 56-50 ka in Tsegi Canyon and Canyon de Chelly (Manning, 2010); 33-20 ka and 17-11 ka from various locations (Ellwein, Mahan, &, McFadden, 2015); 46 ka, 40 ka, 17-12 ka in Canyonlands region of Utah (Reheis et al., 2005). Regional paleoclimate records include speleothem records from: Georgia Giant (Brook et al, 2006); Devils Hole (Landwehr, Sharp, Coplen, Ludwig, & Winograd, 2011); Leviathan Cave (Lachniet, Asmerom, Polyak, & Denniston, 2017). The global paleoclimate record is from LR04, a combined proxy for both global ice volume and ocean temperature derived from 57 globally distributed sites (Leisicki and Raymo, 2005).

2.6 Supplemental Material

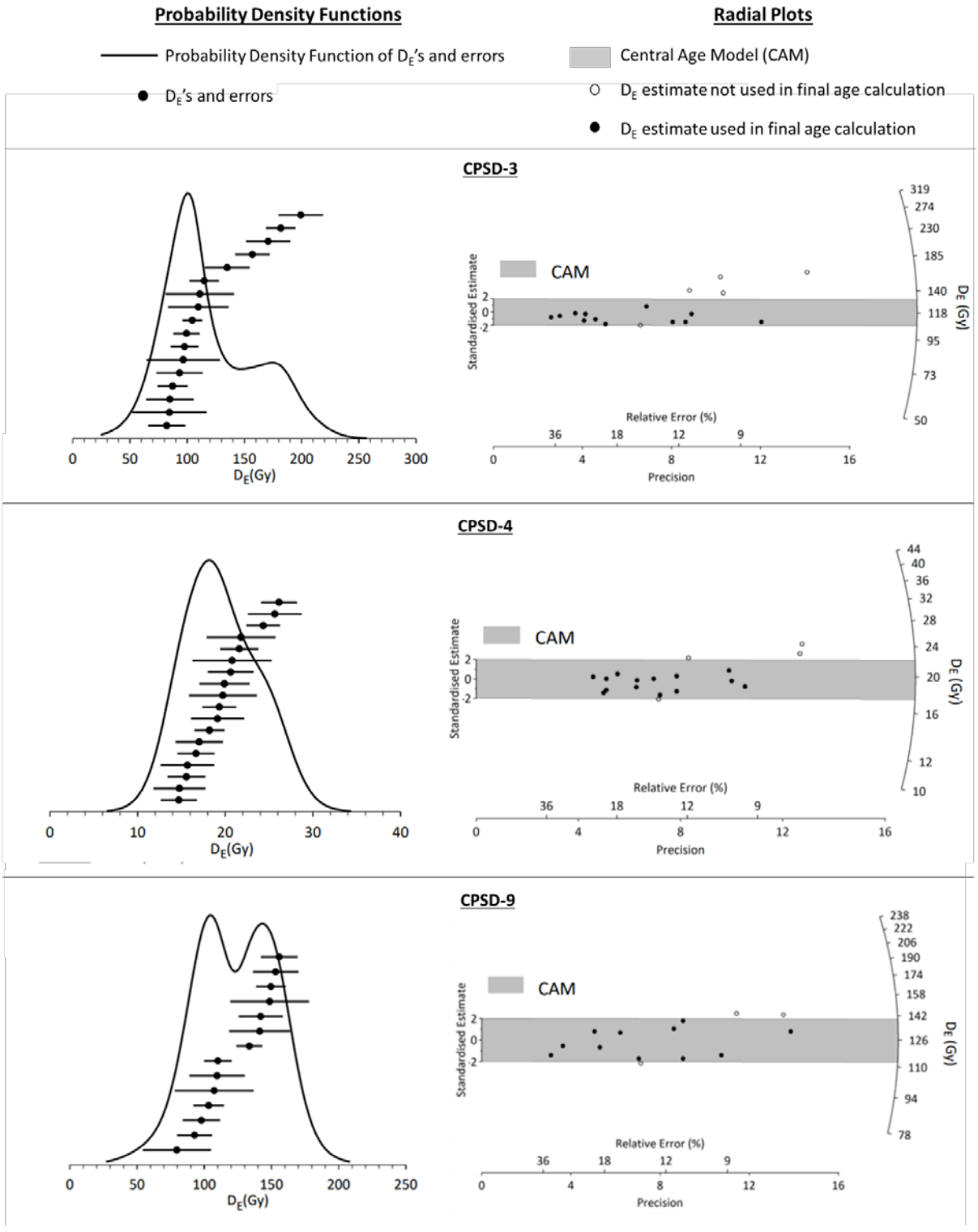

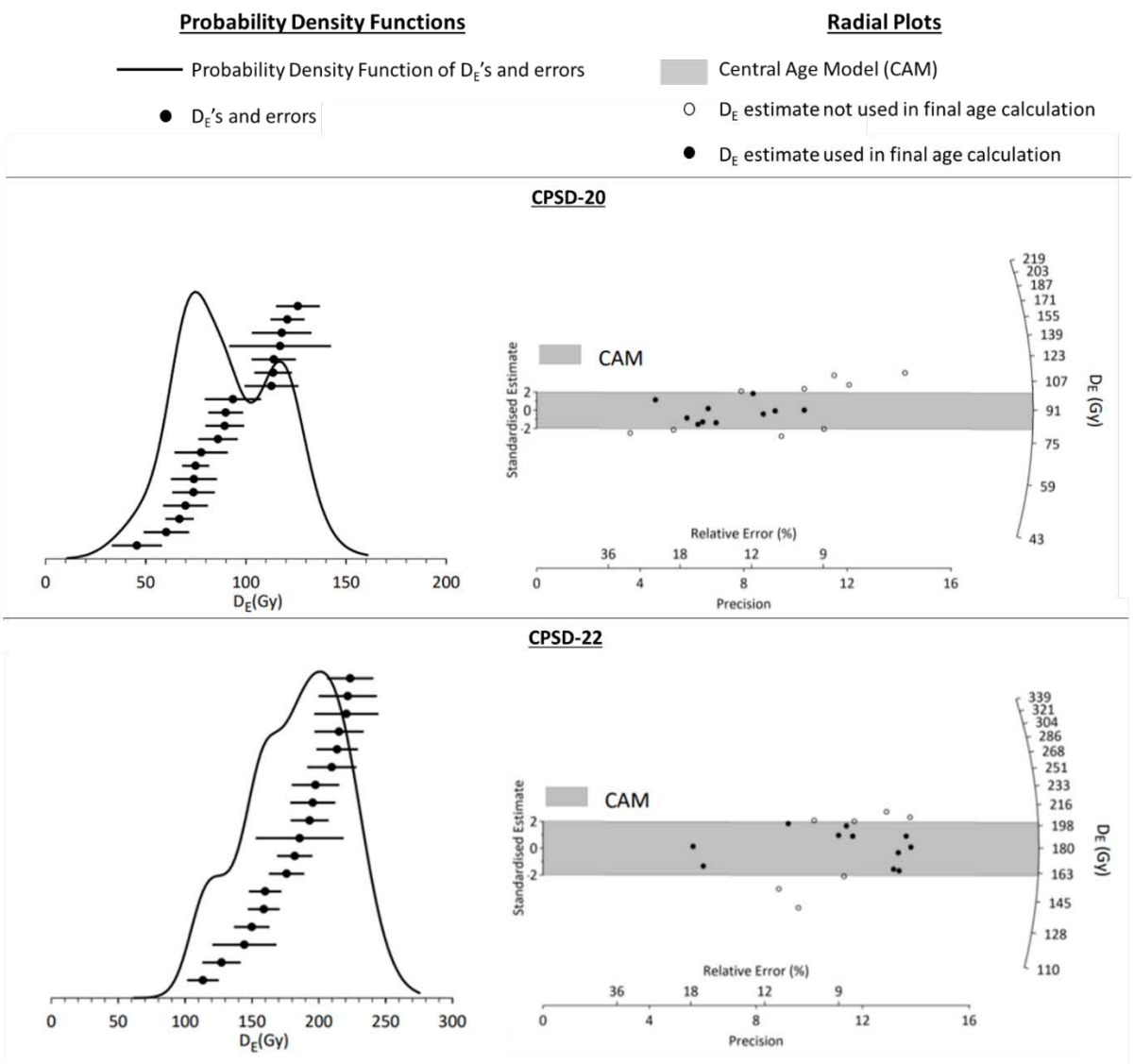

Supplementary Figure 1 D_E Probability Density Functions and Radial Plots

D_E is calculated based on the Central Age Model by Galbraith & Roberts (2012) using a minimum of 20 aliquots per sample. Standardized D_E estimates and standard error for each aliquot are displayed on radial plots. Differences in D_E measurements between aliquots of a single sample are caused by instrument error and natural sources of variability. Incomplete bleaching of grains, post-depositional mixing of grains, or in-situ dose heterogeneity during burial can cause natural sources of variability (Mayya, Morthekai, Murari, & Singhvi, 2006; Lomax, Hilgers, Twidale, Bourne, & Radtke, 2007). Test doses were applied after every SAR step and aliquots with high test dose scatter were rejected from final D_E calculation.

Supplemental Table 1 Environmental dose rate calculation

D_R is derived from concentrations of radioisotopes (K, Rb, Th, U) converted with factors from Guérin et al. (2011) and cosmic dose rate, which is estimated based on altitude, latitude, and depth below surface of the sample (Prescott & Hutton, 1994; Hutton 1994). The D_R estimate is corrected for water content because pore moisture attenuates the rate at which radioactive decay move through sediment.

Site ID	Grain size fraction (um)	In-situ H_2O (%)[1]	K (%)[2]	Rb (ppm)[2]	Th (ppm)[2]	U (ppm)[2]	Cosmic dose rate (Gy/ka)
Site 3	150-250	1.7	0.85±0.02	26.0±1.0	0.8±0.2	0.2±0.1	0.15±0.01
Site 4	150-250	3.9	1.34±0.03	39.4±1.6	1.0±0.2	0.3±0.1	0.21±0.02
Site 9	150-250	3.7	0.58±0.01	19.0±0.8	0.9±0.2	0.3±-0.1	0.22±0.02
Site 20	150-250	0.3	0.44±0.01	13.3±0.5	0.6±0.2	0.2±0.1	0.24±0.02
Site 22	150-250	1.6	0.92±0.02	29.1±1.2	1.0±0.2	0.2±0.1	0.24±0.02

[1] Measured in-situ water content. Assumed 5.0% for all samples as moisture content over burial history.
[2] Radioelemental concentrations determined by ALS Chemex using ICP-MS and ICP-AES techniques.

Supplemental Table 2 Stratigraphy

General description of stratigraphy of entire vertical profile at each site where an OSL sample was taken. Units are numbered from bottom-most exposed unit and divided based on differences in composition, bedding styles, and structures.

Unit	Depth (m)	Description (composition and bedding style/structures)	Depositional Environment
CPSD-3; Located in a main tributary east of Sand Canyon Wash (37.01899, -112.71660, elev 1768 m)			
VII	0.7	Weakly developed soil in sand and silt; Av horizon, capped with biogenic crust	Aeolian
VI	3.3	Angular, unsorted, boulders up to 1 meter diameter, clast supported, Stage 1 pedogenic carbonate	Colluvial
V	4.9	Angular, unsorted clast supported gravel	Colluvial
IV	5.1	Gravel lenses in sand	Fluvial
III	7.1	Angular unsorted sand to boulders, clast supported, interbedded with layers of sand and gravel	Alluvial
II	**7.8**	**High angle bedding, unconsolidated sand, dip direction 090°, dip angle 18°, no reaction to HCl**	**Aeolian***
I	8.1+	Gravel lenses interbedded in sand	Fluvial
CPSD-4; Located in Sand Canyon Wash main channel (37.01822, -112.72327, elev. 1729 m)			
IV	0.05	Modern dune sand	Aeolian
III	2.0	Imbricated sub-rounded to angular unsorted sand to boulder clasts (sheet flood couplets) with thin pedogenic carbonate coating, bottom of unit has a layer of red sand hardened with secondary silica precipitate	Alluvial
II	**3.0**	**High angle bedding, unconsolidated sand, dip angle 25°, no reaction to HCl**	**Aeolian***
I	7.0+	Sand interbedded with gravel lenses and fine grained mud layers	Fluvial
CPSD-9; Located in Sand Canyon Wash main channel (37.02726, -112.71993, elev 1755 m)			
III	0.05	Modern dune sand	Aeolian
II	1.3	Imbricated clast supported large cobbles and boulders interbedded with sand and gravel lenses, bottom of unit has a layer of red sand hardened with secondary silica precipitate	Alluvial

I	**2.8+**	**High angle bedding, unconsolidated sand, dip angle 25°, No reaction to HCl**	**Aeolian***
CPSD-20; Located in Sand Canyon Wash main channel (37.02526, -112.72074, elev 1752 m)			
II	0.15	Unsorted 50 % sand 50% pebbles with some pedogenic carbonate coating, but not cemented and no ped structure	Alluvial
I	**1.25+**	**High angle bedding, unconsolidated sand, dip direction 330°, dip angle 22°, no reaction to HCl**	**Aeolian***
CPSD-22; Located in Sand Canyon Wash main channel (37.02224, -112.72120, elev 1743 m)			
II	0.1	Unsorted, imbricated gravel with pedogenic carbonate coating	Fluvial
I	**1.0+**	**High angle bedding, unconsolidated sand, dip direction 155°, dip angle 25°**	**Aeolian***

*OSL sample taken from this unit

References

Asmerom, Y., Polyak, V. J., & Burns, S. J. (2010). Variable winter moisture in the southwestern United States linked to rapid glacial climate shifts. *Nature Geoscience*, *3*(2), 114.

Betancourt, J. L., Van Devender, T. R., & Martin, P. S. (Eds.). (1990). *Packrat middens: the last 40,000 years of biotic change*. University of Arizona Press.

Birkeland, P. W., Machette, M. N., & Haller, K. M. (1991). *Soils as a tool for applied Quaternary geology* (No. 3). Utah Geological Survey.

Brook, G. A., Ellwood, B. B., Railsback, L. B., & Cowart, J. B. (2006). A 164 ka record of environmental change in the American Southwest from a Carlsbad Cavern speleothem. *Palaeogeography, Palaeoclimatology, Palaeoecology*, *237*(2-4), 483-507.

Bull, W. B. (1991). Geomorphic responses to climatic change.

Color, B. M. (2009). *Munsell soil-color charts: with genuine Munsell® color chips*. Munsell.

Draut, A. E., Redsteer, M. H., & Amoroso, L. (2012). *Vegetation, Substrate, and Eolian Sediment Transport at Teesto Wash, Navajo Nation, 2009-2012*. US Department of the Interior, US Geological Survey.

Duller, G. A. (2008). Luminescence Dating: guidelines on using luminescence dating in archaeology.

Ellwein, A. L., Mahan, S. A., & McFadden, L. D. (2015). Impacts of climate change on the formation and stability of late Quaternary sand sheets and falling dunes, Black Mesa region, southern Colorado Plateau, USA. *Quaternary international*, *362*, 87-107.

Ford, R. L., Gillman, S. L., Wilkins, D. E., Clement, W. P., & Nicoll, K. (2010). Geology and Geomorphology of Coral Pink Sand Dunes State Park, Utah. *Geology of Utah's Parks and Monuments, Utah Geological Association*, 379-406.

Galbraith, R. F., & Roberts, R. G. (2012). Statistical aspects of equivalent dose and error calculation and display in OSL dating: an overview and some recommendations. *Quaternary Geochronology*, *11*, 1-27.

Glover, K. C., MacDonald, G. M., Kirby, M. E., Rhodes, E. J., Stevens, L., Silveira, E., ... & Lydon, S. (2017). Evidence for orbital and North Atlantic climate forcing in alpine Southern California between 125 and 10 ka from multi-proxy analyses of Baldwin Lake. Quaternary Science Reviews, 167, 47-62.

Grove, J.M. (1988). The Little Ice Age: New York, Methuen, 498 p.

Guérin, G., Mercier, N., Adamiec, G. (2011). Dose-rate conversion factors: update: Ancient TL 29, 5-8.

Hayden, J.M. (2013). Geologic Map of the Yellowjacket Canyon Quadrangle, Kane County, Utah, and Mohave County, Arizona: Utah Geological Survey, Map 256DM, doi: 10.1029/2007JB005278.

Hereford, R. (2002). Valley-fill alluviation during the Little Ice Age (ca. AD 1400–1880), Paria River basin and southern Colorado Plateau, United States. *Geological Society of America Bulletin*, *114*(12), 1550-1563.

Huang, J., Yu, H., Guan, X., Wang, G. and Guo, R. (2016). Accelerated dryland expansion under climate change. *Nature Climate Change*, *6*(2), p.166.

Huntley, D. J., Godfrey-Smith, D. I., & Thewalt, M. L. (1985). Optical dating of sediments. *Nature*, *313*(5998), 105.

Kumar, A., Srivastava, P., & Meena, N. K. (2017). Late Pleistocene aeolian activity in the cold desert of Ladakh: a record from sand ramps. *Quaternary International*, *443*, 13-28.

Lachniet, M., Asmerom, Y., Polyak, V., & Denniston, R. (2017). Arctic cryosphere and Milankovitch forcing of Great Basin paleoclimate. Scientific reports, 7(1), 12955.

Lancaster, N. (2008). Desert dune dynamics and development: insights from luminescence dating. *Boreas*, *37*(4), 559-573.

Lancaster, N., Wolfe, S., Thomas, D., Bristow, C., Bubenzer, O., Burrough, S., ... & Singhvi, A. (2016). The INQUA dunes atlas chronologic database. *Quaternary international*, *410*, 3-10.

Landwehr, J.M., W.D. Sharp, T.B. Coplen, K.R. Ludwig, and I.J. Winograd. (2011). The chronology for the d18O record from Devils Hole, Nevada, extended into the mid-Holocene. U.S. Geological Survey Open-File Report 2011-1082, 5 p. http://pubs.usgs.gov/of/2011/1082/ accessed May 7, 2018

Liesicki, L.E. and M.E. Raymo. (2005). LR04 Global Pliocene-Pleistocene Benthic d18O Stack. IGBP PAGES/World Data Center for Paleoclimatology Data Contribution Series #2005-008. NOAA/NGDC Paleoclimatology Program, Boulder CO, USA.

Lowenstein, T. K., Li, J., Brown, C., Roberts, S. M., Ku, T. L., Luo, S., & Yang, W. (1999). 200 ky paleoclimate record from Death Valley salt core. *Geology*, *27*(1), 3-6.

Lyle, M., Heusser, L., Ravelo, C., Yamamoto, M., Barron, J., Diffenbaugh, N. S., ... & Andreasen, D. (2012). Out of the tropics: the Pacific, Great Basin Lakes, and Late Pleistocene water cycle in the western United States. *Science*, *337*(6102), 1629-1633.

Mahan, S. A., Miller, D. M., Menges, C. M., & Yount, J. C. (2007). Late Quaternary stratigraphy and luminescence geochronology of the northeastern Mojave Desert. *Quaternary International*, *166*(1), 61-78.

Manning, J.C. (2010). *Falling Dunes of Northeastern Arizona: An Evaluation of Quaternary Aeolian History Using Optically Stimulated Luminescence.*

Polyak, V. J., Rasmussen, J. B., & Asmerom, Y. (2004). Prolonged wet period in the southwestern United States through the Younger Dryas. *Geology*, *32*(1), 5-8.

Prescott, J. R., & Hutton, J. T. (1994). Cosmic ray contributions to dose rates for luminescence and ESR dating: large depths and long-term time variations. *Radiation measurements*, *23*(2-3), 497-500.

Rasmussen, S. O., Andersen, K. K., Svensson, A. M., Steffensen, J. P., Vinther, B. M.,

Clausen, H. B., ... & Bigler, M. (2006). A new Greenland ice core chronology for the last glacial termination. *Journal of Geophysical Research: Atmospheres*, *111*(D6).

Redsteer, M. H., Bogle, R. C., & Vogel, J. M. (2011). *Monitoring and analysis of sand dune movement and growth on the Navajo Nation, southwestern United States*. US Department of the Interior, US Geological Survey.

Reheis, M.C., Reynolds, R.L., Goldstein, H., Roberts, H.M., Yount, J.C., Axford, Y., Cummings, L.S. and Shearin, N. (2005). Late Quaternary eolian and alluvial response to paleoclimate, Canyonlands, southeastern Utah. *Geological Society of America Bulletin*, *117*(7-8), pp.1051-1069.

Rozar, E.J. (2015). Defining Antecedent Topography at Coral Pink Sand Dunes, Kane County, Utah: The Influence of Structural Controls on Dune-Field Boundary Conditions and Holocene Landscape Evolution, Boise State University Theses and Dissertations, paper 987. http://scholarworks.boisestate.edu/td/987

Sohn, M. F., Mahan, S. A., Knott, J. R., & Bowman, D. D. (2007). Luminescence ages for alluvial-fan deposits in Southern Death Valley: Implications for climate-driven sedimentation along a tectonically active mountain front. *Quaternary International*, *166*(1), 49-60.

Stokes, S. and Breed, C.S. (1993). A chronostratigraphic re-evaluation of the Tusayan Dunes, Moenkopi Plateau and southern Ward Terrace, northeastern Arizona. *Geological Society, London, Special Publications*, *72*(1), pp.75-90.

Summa-Nelson, M.C., and Rittenour, T.M. (2011). Investigating arroyo cut-fill cycles and their link to Holocene climate change along Kanab Creek, southern Utah: Abstracts with Programs - Geological Society of America, v. 43, no. 4.

Tchakerian, V. P., & Lancaster, N. (2002). Late Quaternary arid/humid cycles in the Mojave Desert and western Great Basin of North America. *Quaternary Science Reviews*, *21*(7), 799-810.

Townsend, K., Nelson, M.S., Rittenour, T.M., Pederson, J.L. (2019). Anatomy and evolution of a dynamic arroyo system, Kanab Creek, southern Utah, USA. *Geological Society of America Bulletin*, 131 (11-12): 2094-2109.

Wells, S. G., McFadden, L. D., & Schultz, J. D. (1990). Eolian landscape evolution and soil formation in the Chaco dune field, southern Colorado Plateau, New Mexico. *Geomorphology*, *3*(3-4), 517-546.

Wells, S. G., Brown, W. J., Enzel, Y., Anderson, R. Y., McFadden, L. D., & Lancaster, N. (2003). Late Quaternary geology and paleohydrology of pluvial Lake Mojave, southern California. Special Papers-Geological Society of America, 79-114.

Weng, C., & Jackson, S. T. (1999). Late Glacial and Holocene vegetation history and paleoclimate of the Kaibab Plateau, Arizona. *Palaeogeography, Palaeoclimatology, Palaeoecology*, *153*(1-4), 179-201.

Western Regional Climate Center, www.wrcc.dri.edu/ (Accessed July 2018, monthly climate summary record from December 1899 to June 2016)

Wilkins, D.E., Ford, R.L., Clement, W.P., and Nicoll, K. (2005). Little Ice Age behavior of the Coral Pink Sand Dunes, Kane County, Utah, Abstracts with Programs - GSA, v. 37, p. 426.

Wintle, A. G., & Murray, A. S. (2000). Quartz OSL: effects of thermal treatment and their relevance to laboratory dating procedures. *Radiation Measurements*, *32*(5-6), 387-400.

Yu, LuPeng, ZhongPing Lai, Ping An, Tong Pan, and QiuFang Chang. "Aeolian sediments evolution controlled by fluvial processes, climate change and human activities since LGM in the Qaidam Basin, Qinghai-Tibetan Plateau." *Quaternary International* 372 (2015): 23-32.

CHAPTER 3: SUMMARY AND FUTURE WORK

Sand ramp investigations are useful for extending records of landscape change. Targeted sampling of topographically-controlled aeolian deposits helps to increase the availability of older records, which is necessary to understand how landscapes have responded to past climate change events. The CPSD sand ramps are primarily alluvial and fluvial depositional features, but have also preserved past periods of aeolian deposition as far as 150 ka. The CPSD sand ramps formed from ~150 ka to at least 12.5 ka, filling accommodation space at the base of the Sevier fault scarp.

Topographically-controlled aeolian deposits are not prone to reactivation and therefore preserve a record of initial sand emplacement, whereas actively migrating dune fields and sand sheets record recent phases of reactivation (Reheis et al., 2005; Ellwein, Mahan, &, McFadden, 2015). The different geomorphic settings within the CPSD dune field show two very different records of activity: 1) topographically-controlled deposits in the sand ramps suggest a supply-limited system during the late Pleistocene; 2) the active dune field records more recent reactivation of dune deposits in response to late Holocene episodes of aridity.

This study provides the first evidence of aeolian activity during the last major glacial (MIS 6) on the Colorado Plateau and an opportunity to investigate hypotheses of landscape change during glacial-interglacial climate change. Aeolian activity during the late Pleistocene-Holocene transition (MIS 2/1; OSL ~12.5 ka) occurred under conditions that were relatively wetter and cooler than present. Dune activity during the MIS 6 and

MIS 5 (OSL ~145 ka to OSL ~118 ka) spans a range of climate conditions during a period of rapid and abrupt change. CPSD dune geochemistry is distinct from nearby dune fields, indicating that sediments are sourced locally, rather than transported long distances. Rather than a response to any specific climate regime, late Pleistocene aeolian deposits may record local changes in sediment supply.

Considerations for future work include additional OSL work in the sand ramps and lower dune field. Additional work investigating the geochemistry of the dune deposits could compare dune sediments to proposed sources upwind (i.e., fluvial and alluvial washes and bedrock samples from different exposed units). Geochemical investigations in this study are preliminary and based on available data from OSL environmental dose rate measurements. Additional geochemical studies should include full analyses of major element, trace elements, and REEs used in other aeolian provenance studies (e.g., Muhs et al., 2008; Hao, Guo, Qiao, Xu, & Oldfield, 2010; Muhs, 2017).

References

Ellwein, A. L., Mahan, S. A., & McFadden, L. D. (2015). Impacts of climate change on the formation and stability of late Quaternary sand sheets and falling dunes, Black Mesa region, southern Colorado Plateau, USA. *Quaternary international*, *362*, 87-107.

Hao, Q., Guo, Z., Qiao, Y., Xu, B., & Oldfield, F. (2010). Geochemical evidence for the provenance of middle Pleistocene loess deposits in southern China. *Quaternary Science Reviews*, *29*(23-24), 3317-3326.

Muhs, D. R., Bettis III, E. A., Aleinikoff, J. N., McGeehin, J. P., Beann, J., Skipp, G., ... & Benton, R. (2008). Origin and paleoclimatic significance of late Quaternary

loess in Nebraska: evidence from stratigraphy, chronology, sedimentology, and geochemistry. *Geological Society of America Bulletin*, *120*(11-12), 1378-1407.

Muhs, D. R. (2017). Evaluation of simple geochemical indicators of aeolian sand provenance: Late Quaternary dune fields of North America revisited. *Quaternary Science Reviews*, *171*, 260-296.

Reheis, M.C., Reynolds, R.L., Goldstein, H., Roberts, H.M., Yount, J.C., Axford, Y., Cummings, L.S. and Shearin, N. (2005). Late Quaternary eolian and alluvial response to paleoclimate, Canyonlands, southeastern Utah. *Geological Society of America Bulletin*, *117*(7-8), pp.1051-1069.

APPENDIX A

Grain Size Distributions

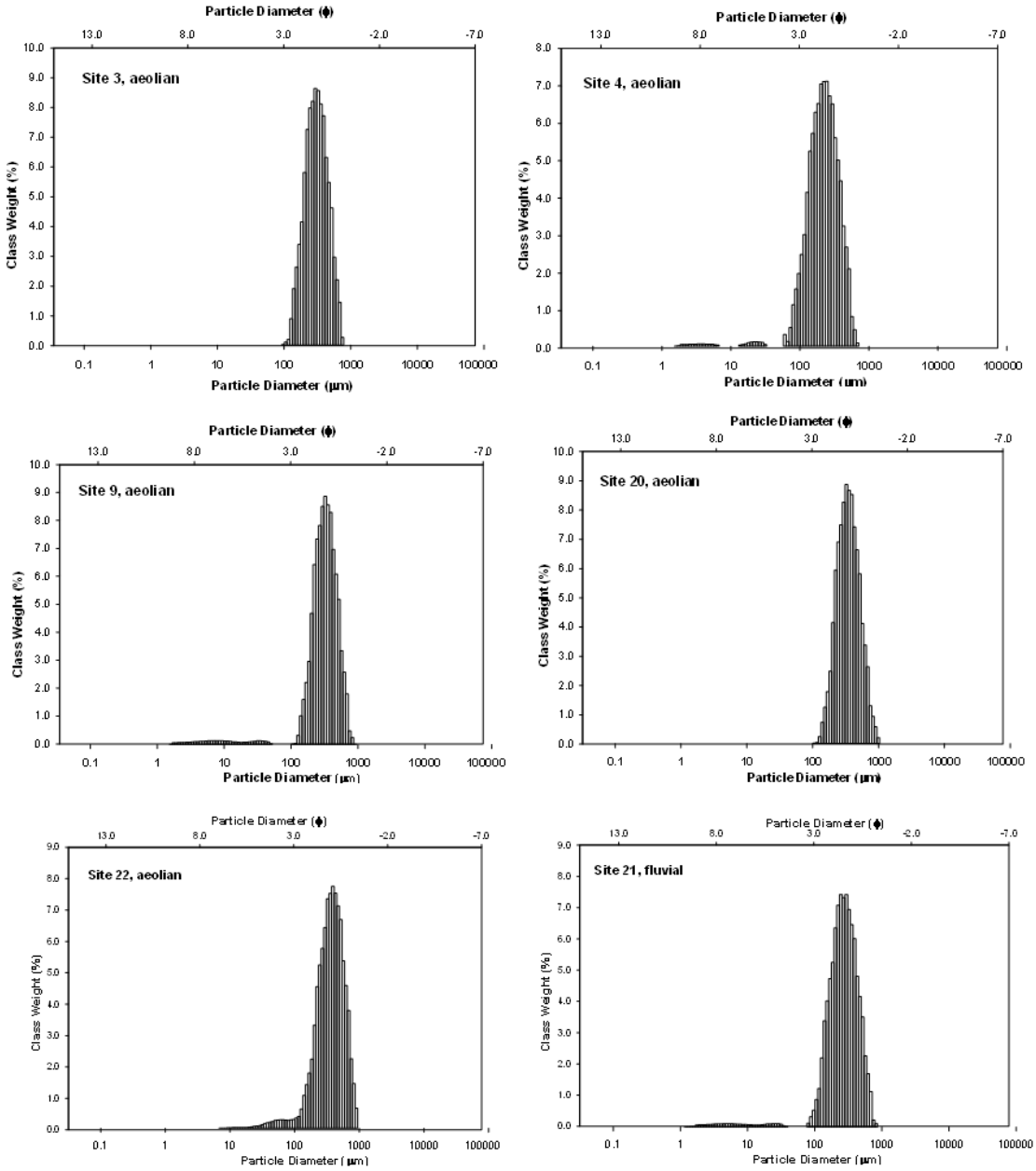

Figure A.1. Grain size distributions of all samples dated by OSL (five aeolian and one fluvial). All sites are primarily sand sized sediment and CPSD- 4, 9, 21, 22, also have a small silt fraction. All sites interpreted in the field to be aeolian units (CPSD-3, 4, 20, 22) have unimodal distributions and the fluvial deposit (CPSD-21) was analyzed for comparison, has a bi-modal distribution, supporting field observations and depositional environment interpretations.

Table A.1. Grain size distribution raw data

	Site 3 aeolian	Site 4 aeolian	Site 9 aeolian	Site 20 aeolian	Site 21 fluvial	Site 22 aeolian
% GRAVEL:	0.0%	0.0%	0.0%	0.0%	0.0%	0.0%
% SAND:	100.0%	98.2%	96.3%	100.0%	97.2%	98.0%
% MUD:	0.0%	1.8%	3.7%	0.0%	2.8%	2.0%
% V COARSE GRAVEL:	0.0%	0.0%	0.0%	0.0%	0.0%	0.0%
% COARSE GRAVEL:	0.0%	0.0%	0.0%	0.0%	0.0%	0.0%
% MEDIUM GRAVEL:	0.0%	0.0%	0.0%	0.0%	0.0%	0.0%
% FINE GRAVEL:	0.0%	0.0%	0.0%	0.0%	0.0%	0.0%
% V FINE GRAVEL:	0.0%	0.0%	0.0%	0.0%	0.0%	0.0%
% V COARSE SAND:	0.0%	0.0%	0.0%	0.1%	0.0%	0.0%
% COARSE SAND:	11.0%	3.1%	13.1%	18.3%	8.6%	24.2%
% MEDIUM SAND:	56.7%	36.8%	58.5%	59.7%	46.6%	52.8%
% FINE SAND:	31.8%	46.3%	24.6%	21.7%	38.3%	18.7%
% V FINE SAND:	0.5%	12.0%	0.1%	0.1%	3.7%	2.3%
% V COARSE SILT:	0.0%	0.3%	0.6%	0.0%	0.1%	1.6%
% COARSE SILT:	0.0%	0.7%	0.7%	0.0%	0.7%	0.4%
% MEDIUM SILT:	0.0%	0.1%	0.9%	0.0%	0.5%	0.1%
% FINE SILT:	0.0%	0.3%	0.9%	0.0%	0.7%	0.0%
% V FINE SILT:	0.0%	0.4%	0.6%	0.0%	0.6%	0.0%
% CLAY:	0.0%	0.0%	0.1%	0.0%	0.1%	0.0%
MODE 1 (μm):	295.9	245.5	324.7	324.7	245.5	391.4
MODE 2 (μm):	na	na	na	na	295.9	na
MODE 1 (ϕ):	1.759	2.028	1.624	1.624	2.028	1.355
MODE 2 (ϕ):	na	na	na	na	1.759	na
D10 (μm):	180.1	112.5	182.8	209.2	140.6	183.8
D50 (μm):	303.8	219.4	319.3	343.7	266.6	363.6
D90 (μm):	509.7	404.2	528.2	583.7	483.7	629.8
(D90 / D10) (μm):	2.831	3.592	2.889	2.790	3.440	3.426
(D90 - D10) (μm):	329.7	291.6	345.3	374.4	343.1	446.0
(D75 / D25) (μm):	1.756	1.996	1.756	1.751	1.931	1.912
(D75 - D25) (μm):	173.3	153.4	181.0	195.5	178.2	235.7
D10 (ϕ):	0.972	1.307	0.921	0.777	1.048	0.667
D50 (ϕ):	1.719	2.188	1.647	1.541	1.907	1.460
D90 (ϕ):	2.474	3.152	2.451	2.257	2.830	2.443
(D90 / D10) (□):	2.544	2.411	2.662	2.905	2.701	3.663
(D90 - D10) (ϕ):	1.501	1.845	1.530	1.480	1.782	1.776
(D75 / D25) (ϕ):	1.619	1.586	1.650	1.713	1.661	1.919
(D75 - D25) (ϕ):	0.812	0.997	0.812	0.808	0.949	0.935

Table A.2. Grain size distribution statistics calculated in GRADISTAT (Blott & Pye, 2001) according to Folk & Ward (1957) methods and moments methods.

		Site 3, aeolian	Site 4, aeolian	Site 9, aeolian	Site 20, aeolian	Site 21, fluvial	Site 22, aeolian
	SAMPLE TYPE:	Unimodal, Moderately Well Sorted	Unimodal, Moderately Sorted	Unimodal, Moderately Well Sorted	Unimodal, Moderately Well Sorted	Bimodal, Moderately Well Sorted	Unimodal, Moderately Sorted
	TEXTURE	Sand	Sand	Sand	Sand	Sand	Sand
	SEDIMENT NAME:	Moderately Well Sorted Medium Sand	Moderately Sorted Fine Sand	Moderately Well Sorted Medium Sand	Moderately Well Sorted Medium Sand	Moderately Well Sorted Medium Sand	Moderately Sorted Medium Sand
METHOD OF MOMENTS Arithmetic (μm)	MEAN	327.0	240.6	336.1	373.9	289.9	385.5
	SORTING	127.3	115.7	142.8	151.2	138.2	173.9
	SKEWNESS	0.768	0.766	0.374	1.026	0.681	0.489
	KURTOSIS	3.144	3.365	3.435	4.076	3.467	2.967
METHOD OF MOMENTS Geometric (μm)	MEAN	303.2	209.0	285.7	345.8	245.0	339.3
	SORTING	1.475	1.849	2.168	1.480	2.103	1.754
	SKEWNESS	-0.050	-2.447	-3.613	0.057	-3.223	-1.519
	KURTOSIS	2.429	16.82	19.53	2.606	18.53	7.549
METHOD OF MOMENTS Logarithmic (ϕ)	MEAN	1.722	2.258	1.808	1.532	2.029	1.559
	SORTING	0.560	0.887	1.116	0.566	1.073	0.811
	SKEWNESS	0.050	2.447	3.613	-0.057	3.223	1.519
	KURTOSIS	2.429	16.82	19.53	2.606	18.53	7.549
FOLK AND WARD METHOD (μm)	MEAN	304.3	217.9	317.7	345.4	264.3	355.3
	SORTING	1.494	1.645	1.520	1.491	1.619	1.625
	SKEWNESS	-0.006	-0.046	-0.064	0.023	-0.051	-0.133
	KURTOSIS	0.947	0.967	1.029	0.950	0.984	1.040
FOLK AND	MEAN	1.716	2.198	1.654	1.534	1.920	1.493

WARD METHOD (ϕ)	SORTING	0.579	0.718	0.604	0.576	0.695	0.701
	SKEWNESS	0.006	0.046	0.064	-0.023	0.051	0.133
	KURTOSIS	0.947	0.967	1.029	0.950	0.984	1.040
FOLK AND WARD METHOD (Description)	MEAN:	Medium Sand	Fine Sand	Medium Sand	Medium Sand	Medium Sand	Medium Sand
	SORTING:	Moderately Well Sorted	Moderately Sorted	Moderately Well Sorted	Moderately Well Sorted	Moderately Well Sorted	Moderately Sorted
	SKEWNESS:	Symmetrical	Symmetrical	Symmetrical	Symmetrical	Symmetrical	Fine Skewed
	KURTOSIS	Mesokurtic	Mesokurtic	Mesokurtic	Mesokurtic	Mesokurtic	Mesokurtic